A Nonlinear Finite Element Model of the Human Eye to Investigate Ocular Injuries From Night Vision Goggles

Erik D. Power

Thesis submitted to the Faculty of the
Virginia Polytechnic Institute and State University
in partial fulfillment of the requirements for the degree of

Master of Science
in
Mechanical Engineering

Stefan M. Duma, Chair
Robert L. West
Ian P. Herring
Tyler A. Kress

April 26, 2001
Blacksburg, Virginia

Keywords: Eye, Airbag, Model, Goggles

A Nonlinear Finite Element Model of the Human Eye to Investigate Ocular Injuries From Night Vision Goggles

Erik D. Power

(ABSTRACT)

Airbags have been saving lives in automobile crashes for many years and are now being used in helicopters. The purpose of this study was to investigate the potential for ocular injuries to helicopter pilots wearing night vision goggles when the airbag is deployed. A nonlinear finite element model of the human eye was constructed. Ocular structures never before included in finite element models of the eye, such as the fatty tissue, extraocular muscles, and bony orbit were included in this model. In addition, this model includes material properties up to rupture making the eye suitable for large deformation applications.

The model was imported into Madymo and used to determine the worst-case position of a helicopter pilot wearing night vision goggles. This was evaluated as the greatest Von Mises stress in the eye when the airbag is deployed. The worst-case position was achieved by minimizing the distance between the eyes and goggles, having the occupant look directly into the airbag, and making initial contact with the airbag halfway through its full deployment. By removing the extraocular muscles, the stress sustained by the eye decreased. Simulations with both the goggles remaining fastened and breaking away from the aviator helmet were performed. Finally, placing a protective lens in front of the eyes was found to reduce the stress to the eye but increase the force experienced by the surrounding orbital bones.

The finite element model of the eye proved effective at evaluating the experimental boundary conditions, and could be used in the future to evaluate impact loading on eyes that have been surgically corrected and to model the geometry of the orbital bones.

Disclaimer

Mention of company names or products does not constitute endorsement in any way by the Virginia Polytechnic Institute and State University.

Acknowledgements

This research would not have been possible without the support and encouragement of the faculty and staff at Virginia Tech. Primarily, I would like to thank my advisor, Dr. Stefan M. Duma, for providing academic guidance throughout the year. I also thank Dr. Robert L. West for his finite element input, and Dr. Ian P. Herring, Dr. Tyler A. Kress, and Joel D. Stitzel for reviewing my thesis. Additionally, I appreciate all the Madymo technical support provided by Steve Lynn and Rob Marshall. Above all, thanks to God, my friends, and family for their support. Through the combined efforts of all involved, I believe this work contributes significantly to the understanding of ocular injuries from night vision goggles.

Table of Contents

List of Figures

List of Tables

Chapter 1
Introduction

Airbags have been saving lives in automobile crashes for many years and are now being used in helicopters. A military study found that most pilot fatalities could have been avoided if airbags were deployed during the accident. The pilots are able to control the pitch of the blades enabling the helicopter to auto-rotate and land with only minimal structural damage, rather than falling straight down if the engine loses power for any reason. Moreover, most crashes occur at low altitude from collisions with trees or wires. Impacts such as this are where an airbag becomes effective in reducing fatal injuries sustained by the occupant. The economic costs associated with a trained pilot no longer being able to serve in the military due to injuries can be enormous.

With advancements in technology, soldiers are now being equipped with more sophisticated equipment. One example is that helicopter pilots now wear night vision goggles (NVGs) to facilitate distinguishing images at night. Although the use of airbags in helicopters may reduce the number of fatalities to helicopter pilots, the scenario with the pilot wearing night vision goggles when the airbag is deployed raises new injury concerns. Such a scenario may place helicopter pilots at a high risk for ocular injuries. If serious enough, an ocular injury could make a pilot no longer able to serve in the military. The purpose of this study was to investigate the potential for ocular injuries to helicopter pilots wearing night vision goggles when the airbag is deployed.
The primary objective was to determine a worst-case position for future laboratory experiments.

In order to investigate this, a nonlinear finite element (FE) model of the human eye was constructed. Material and geometric properties were gathered from the literature wherever possible, and reasonable approximations were made whenever not available. Ocular structures never before included in FE models of the eye, such as the fatty tissue,

extraocular muscles, and bony orbit were included in this study. This model was then imported into Madymo (TNO, Troy, MI) to simulate the helicopter airbag deployments. A 50^{th} percentile male hybrid III dummy was used to model the helicopter pilot. Night vision goggles were obtained from the Army, their dimensions measured, and modeled in Madymo. A parametric study was conducted that determined the worst-case position and orientation of a helicopter pilot wearing NVGs to be in when the airbag is deployed. The worst-case position was established as that which induced the greatest Von Mises stress to the finite element eye model. This position was then recommended for future laboratory testing. The advantage of this approach is that the model can be used to investigate experimental parameters prior to the very expensive laboratory testing.

In addition to determining the worst-case position, several secondary objectives were investigated.

- First, simulations were performed with and without the fatty tissue to evaluate the effect of the tissue.
- Second, simulations with and without the extraocular muscles were performed to evaluate the effect of the muscles.
- Third, simulations with the night vision goggles both remaining fastened to and breaking away from the aviator helmet were conducted.
- Fourth, the effect of increasing the goggle mass was investigated. Additional mass was added to the goggles to account for load cells used in experiments.
- Fifth, the effectiveness of having the pilot wear eye protection was investigated. A protective lens was placed in between the goggles and the pilot's eyes. Stress induced to the eye and contact forces to surrounding orbital bones were compared with and without the protective lens in place.

Chapter 2
Literature Review

2.1 Eye and Orbital Anatomy

In order to provide an understanding of the terminology used throughout this study, a review of the relevant anatomy is provided. More specifically, a review of the human eye, bony orbit, and extraocular muscles is given.

The eyeball is formed by two spherical bodies of different sizes that are attached to each other (Figure 2.1). The anterior body is the smaller of the two, consisting of the clear cornea and the water-like fluid within the anterior chamber, called aqueous humor.

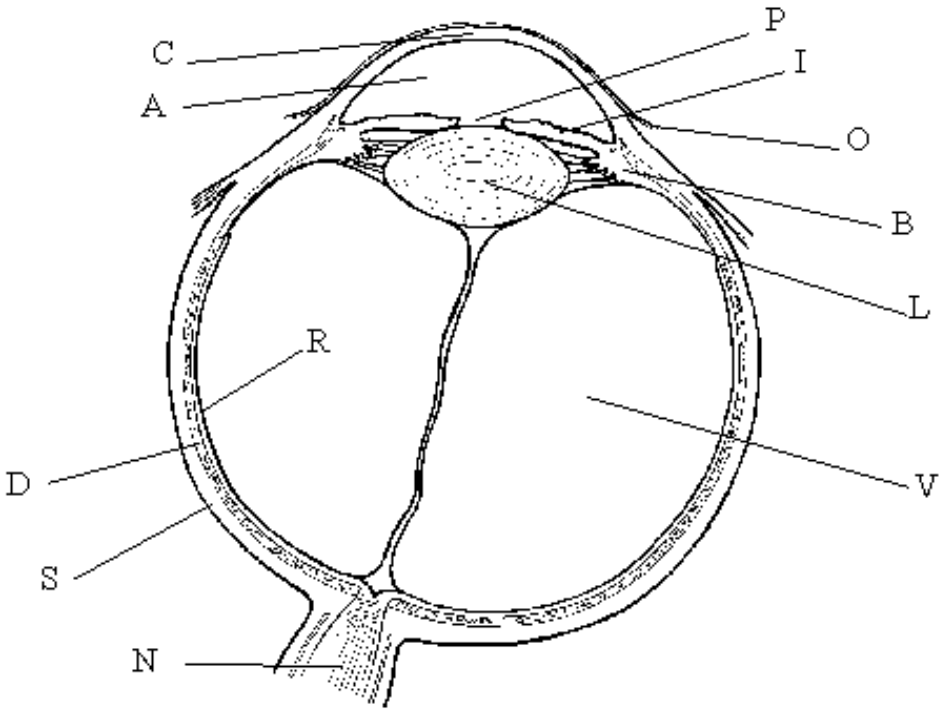

Figure 2.1 Primary ocular structures: A = anterior chamber, B = ciliary body, C = cornea, D = choroid, I = iris, L = lens, N = optic nerve, O = conjunctiva, P = pupil, R = retina, S = sclera, V = vitreous humor.

Aqueous humor supplies nourishment to the anterior segment of the eye, is constantly being filtered, and is replaced hourly. The posterior body is the larger of the two, consisting of the white colored sclera and the gel-like vitreous. The vitreous body helps maintain the general shape of the eye. Light must pass through this gel before it is focused onto the retina. Unlike the aqueous humor, the vitreous gel is not filtered and does not circulate.

The outermost protective layer of the eye is made up of the cornea and sclera, often referred to as the corneo-scleral shell. The cornea is a curved spherical structure that helps protect the lens and refract light. It is this curvature that allows it to refract light onto the inside of the eye. Contact lenses and vision correcting surgical procedures attempt to improve vision by altering the corneal curvature. The white colored sclera comprises approximately 85% of the surface area of the corneo-scleral shell. It is sometimes reported as being approximately 2.5 times as stiff as the cornea (Vito and Carnell, 1992; Kisielewicz *et al*., 1998).

After light is refracted by the cornea and passes through the aqueous humor, it is focused onto the retina by the lens. The iris, the colored part of the eye, controls the amount of light arriving at the lens. The iris accomplishes this by opening up when there is a shortage of light, and contracting when there is too much light. It is this behavior that makes the iris analogous to the aperture in a camera. The pupil is the opening in the iris through which light passes, which appears to be a black spot.

The lens is actually flexible, allowing it to finely focus the light onto the retina by changing its shape. It does this with the contraction and relaxation of the ciliary body muscles. These muscles relax to make the lens thinner, to help focus on more distant objects. Conversely, the muscles contract to form a thicker lens to help focus on nearby objects, a process called accommodation.

Once the lens has focused the light, it passes through the vitreous and is received by the retina. The retina is like the film used in a camera. It is a delicate layer that lines

the innermost surface of the posterior chamber. Images are projected onto the retina, transduced into electrical signals, and sent to the brain via the optic nerve. The signals are finally processed in the visual cortex of the cerebrum, allowing visual images to be formed.

Each eyeball is enclosed by a bony orbit formed by several skull bones (Figure 2.2). The frontal bone of the skull makes up the forehead and forms the roof of the orbit. The upper teeth are supported from the maxillary bone, or maxilla.

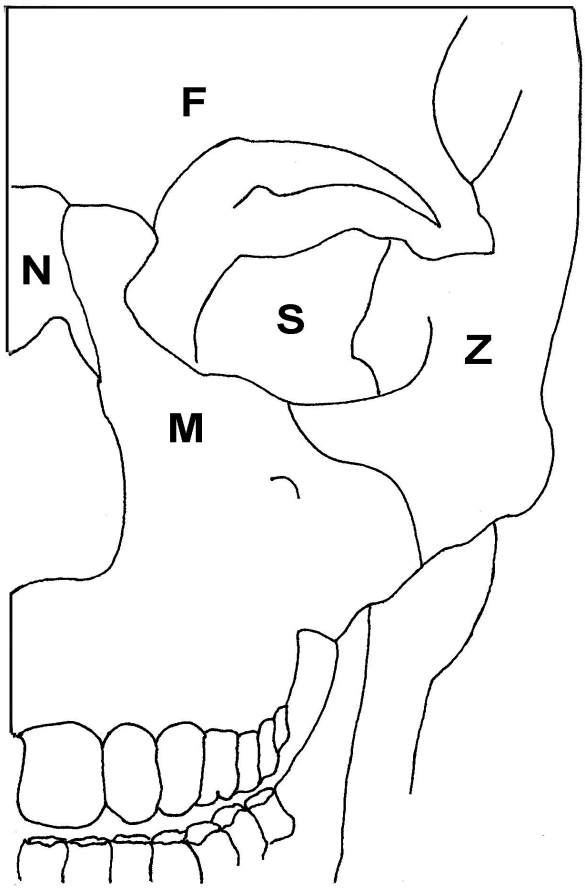

Figure 2.2 Bones Forming the Ocular Orbit: F = frontal, M = maxilla, N = nasal, S = sphenoid, Z = zygomatic.

The maxilla encloses the nasal passage and forms a portion of the orbital floor. The zygomatic bone, or cheekbone, helps form the lateral wall of the orbit. The lacrimal and ethmoid bones, both behind the nasal bone, form the medial wall. Tears drain from the surface of the eye into the nose through a duct that passes through a small opening in the lacrimal bone.

The eyeball occupies approximately the anterior half of the orbital cavity. The posterior half is filled with fatty tissue, nerves, extraocular muscles, and blood vessels that supply the eye with nutrients. There are a total of six extraocular muscles: two obliques and four rectus, which all control the movement of an eyeball (Figure 2.3).

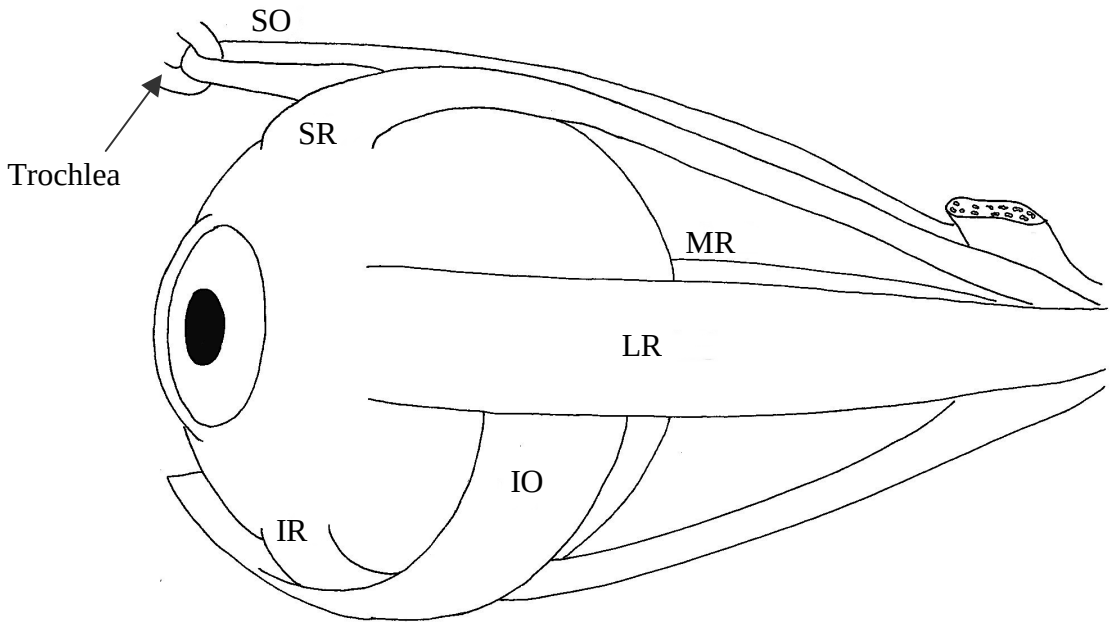

Figure 2.3 Extraocular Eye Muscles (Left Eye): IO = inferior oblique, SO = superior oblique, LR = lateral rectus, MR = medial rectus, SR = superior rectus, IR = inferior rectus.

All six of these muscles are connected to the sclera. With the exception of the inferior oblique, all six muscles originate at the posterior end of the orbit. The inferior oblique is connected to the floor of the orbit. The superior oblique passes through the trochlea, which serves as a pulley for the muscle. A seventh muscle, named the levator muscle, also originates at the posterior end but is responsible for controlling elevation of the upper eyelid rather than the globe itself.

2.2 Biomechanics of Blunt Ocular Trauma

Vinger (1994) categorizes the mechanisms of blunt ocular trauma into four major classes. Class one is the penetration of the globe by a sharp object such as glass. The second class involves ocular injuries caused by blunt objects smaller than the orbital opening, such as a paintball. Class three is identical to class two except that the blunt object is larger than the orbital opening, as with baseballs. Finally, class four defines injuries caused by indirect blows to the head, such as being punched in the back of the head with a fist. Night vision goggles are being modeled as blunt objects making contact with the eye, and therefore only categories two and three are relevant in this study. Accordingly, these two categories will be combined into a single category for the evaluation of blunt ocular trauma induced by night vision goggles.

There are three theories that describe the injury mechanism of blunt ocular trauma: coup, contrecoup, and equatorial expansion (Giovinazzo, 1987). Any single mechanism, or any combination of these three mechanisms can cause eye injuries. With coup injury, all of the kinetic energy is directly absorbed at the site of impact, which is where the localized injury occurs (Figure 2.4). Coup injuries can range from mild corneal abrasions to severe retinal detachments.

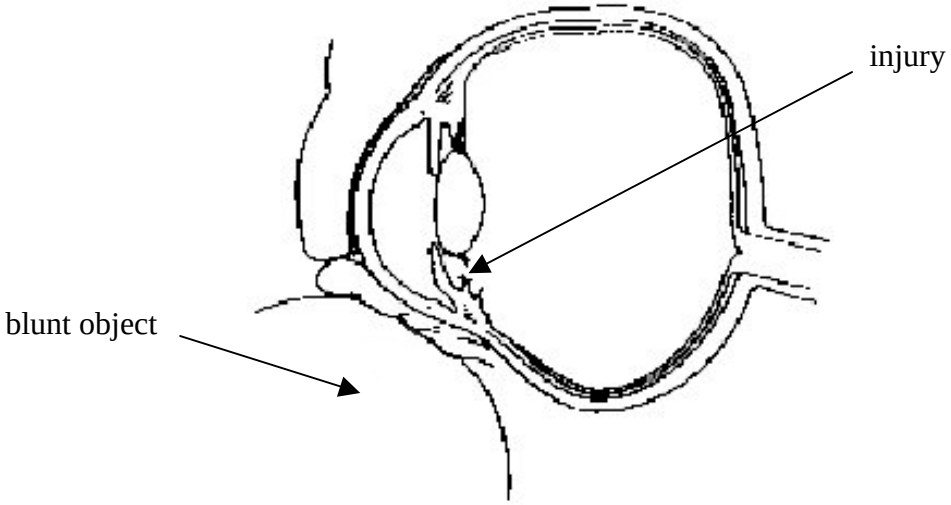

Figure 2.4 Coup injury occurring at site of impact (Giovinazzo, 1987).

The second theory, contrecoup, explains instances of tissue damage away from the site of blunt impact (Figure 2.5).

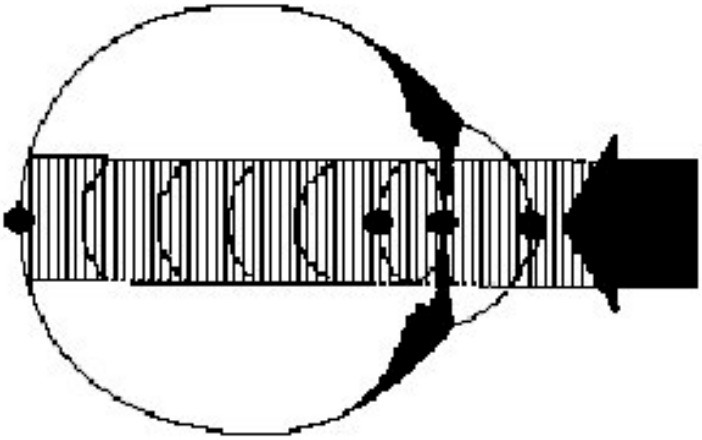

Figure 2.5 Contrecoup resulting as force propagating across the entire globe.

An impact produces a line of force that propagates along this line, traveling across the entire globe. Injuries can occur at tissue boundaries, represented by dots in the figure. These boundaries include where the optic nerve is attached to the posterior pole of the globe. Hence, the optic nerve may be damaged by contrecoup.

The third and final theory, equatorial expansion, is most widely believed to produce retinal tears (Figure 2.6). The globe compresses along the line of impact and expands perpendicular to the line of impact. As the sclera expands, tension is produced, which can cause the retina to tear away from the sclera. The choroid, a layer between the retina and sclera, is also susceptible to separation as a result of this expansion.

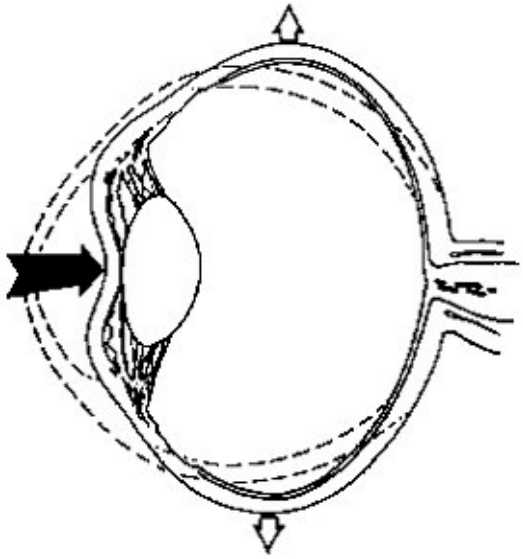

Figure 2.6 Equatorial expansion occurring perpendicular to the line of impact.

It is apparent that a blunt impact to the eye can cause a large range of ocular injuries. The most frequent objects involved in blunt ocular trauma include fists, squash balls, the ends of hockey sticks, and elbows (Chisholm, 1969). Among men, fights account for 18% of ocular injuries, while sporting activities account for 11% (Wong *et al*., 2000). The military sector of the population is also experiencing a large number of eye injuries, both in war and peacetime. Military databases report that the percentage of eye injuries sustained by soldiers in war has increased significantly in this century relative to the total number of injuries (Biehl, 1999; Doswald-Beck, 1993). One would predict that eye injuries would account for less than 1% of the total since the ocular surface area is approximately only 0.27% of the total body surface area. However, in Operation Desert Storm, the incidence of ocular injury was 13% of the total combat

injuries (Heier *et al.*, 1993). No studies have been done that report the percentage of these ocular injuries due to night vision goggles. The economic costs associated with a soldier no longer being able to serve in the military due to eye injuries can be enormous, and even greater yet for a trained pilot.

Vinger (1994) defines four main variables that govern the severity of ocular injuries from impacting objects: the maximum impacting force, time required to reach this maximum force, area of contact, and properties of the impacting object. The level of injury has also been found to be a function of the projectile kinetic energy (Duma and Crandall, 2000; Scott *et al.*, 2000). To calculate the kinetic energy of an impacting object, the velocity of the object is squared and multiplied by one half its mass. It is apparent that the velocity becomes the more critical factor in energy transfer. This explains why relatively small objects with high velocities, such as a bullet fired from a gun, can cause so much damage. It has also been found that less energy is required to produce injuries with small objects of high velocity than with large objects having a low velocity (Berger, 1978). At a given force, smaller objects induce a greater contact stress than larger objects. This is due to the smaller contact area and the fact that stress equals force divided by area.

No research has been performed to investigate injuries associated with night vision goggles impacting the ocular region. However, many studies have been done that involve other blunt objects such as BB's, metal cylinders, foam particles, paintballs, golf balls, squash balls, and baseballs (Delori *et al.*, 1969; Duma and Crandall, 2000; Galler *et al.*, 1995; Green *et al.*, 1990; Preston, 1980; Scott *et al.*, 2000; Umlas *et al.*, 1995; Vinger, 1994, Vinger *et al.*, 1997; Vinger *et al.*, 1999). In each study, the kinetic energy associated with the chosen blunt objects was calculated. Table 1 is a summary of the studies that produced open-globe, or rupture injuries, in eyes that hadn't previously undergone surgical procedures. The various objects, their diameters and masses, the species of eyes used, and kinetic energy required to rupture the globe are summarized. The theory that less energy is required of smaller objects than of larger objects to produce similar injuries is again demonstrated by the data in Table 2.1.

Table 2.1 Summary of blunt impact studies that produced globe ruptures.

5	Diameter (mm)	Mass (g)	velocity (ft/s) *(kinetic energy (J))*		
			Human Eye	Monkey Eye	Pig Eye
BB (Delori, 1969)	4.5	0.35	236 *(0.91)*		
Metal rod (Green, 1990)	12.5	303		12.2 *(2.1)*	
Paintball (Vinger, 1997)	17.5	3.55			290 *(13.9)*
Golf ball (Vinger, unpub'd)	43.0	45.4			86 *(15.6)*
Squash ball (Umlas, 1995)	41.0	24.7			150 *(25.8)*
Baseball (Vinger, 1999)	73.8	143.9	81 *(43.5)*		

Two of the blunt trauma studies impacted pig eyes without rupturing the globe (Duma and Crandall, 2000; Scott *et al*., 2000). Instead, closed globe injuries such as corneal abrasions, lens dislocations, and retinal tears were produced. From these tests, a relationship between the projectile kinetic energy and the level of injuries was investigated (Table 2.2). Scott (2000) impacted enucleated, or removed, pig eyes with metal cylinders of mass 2.6, 3.5, and 45.5 grams, at velocities between 13.1 and 125 ft/s. The 2.6 and 3.5 gram projectiles had a 6.35 mm diameter, while the 45.5 gram projectile had a 9.53 mm diameter. Lens dislocations resulted with energies above 0.75 J, and retinal injuries occurred above 1.20 J. Energy levels reached 1.91 J without any globe ruptures being produced.

Table 2.2 Summary of kinetic energies and level of injuries w/o globe rupture.

Kinetic Energy (J)	Ocular Injury
0.183 (Duma, 2000)	50% risk of corneal abrasion
0.60 to 0.75 (Scott, 2000)	injuries to the iris, ciliary body, or disruption of AC angle
0.75 to 1.20 (Scott, 2000)	injuries to the AC angle as well as a lens dislocation
1.20 to 1.91 (Scott, 2000)	lens dislocation and damage to the retina

Duma and Crandall (2000) impacted pig corneas with foam discs having a diameter of 12.5 mm at velocities ranging from 60 to 287.4 ft/s. These foam discs were representative of those used in airbag deployments. Unlike the previously mentioned study, these pig eyes were not enucleated. Rather, they remained enclosed in the bony ocular orbit and surrounding tissue, just two hours post mortem. The range of kinetic

energy was between 0.050 and 1.446 J, yet no sign of lens displacements or retinal detachments were found. Only corneal abrasions were produced, and the level of severity was measured using noninvasive fluorescein dye techniques. Finally, an injury risk function relating the amount of kinetic energy to the risk of corneal abrasion was generated. According to this function, the foam discs with an energy level of 0.183 J had a 50% chance of causing corneal abrasions.

Although none of these studies involved night vision goggles, the previous experimental work done with various blunt objects can still provide insight into the study to be presented. More specifically, the kinetic energy of the modeled night vision goggles can be compared with the kinetic energy of the projectiles that experimentally produced injuries. Finally, the injuries found experimentally at these kinetic energies can be compared to the injuries predicted by the finite element model of the human eye. This would represent an initial basis for comparison of the computer modeling efforts before experimental tests with night vision goggles are performed.

2.3 Previous Finite Element Eye Models

Many finite element (FE) models of the human eye have been presented in recent years to help better predict the change in corneal refraction after radial keratotomy and other refractive surgeries. Most of these models were of the cornea only, with a few including the sclera. Element types including thin and thick shells, membranes, and solids have been used to discretize the structures. The material properties incorporated into these models varied in complexity, with most being isotropic and a few being anisotropic. Some of the models also included nonlinear material behavior. However, most researchers have made the simplifying assumption that the material behavior is approximately linear for low deformations. This assumption may be supported by the fact that refractive surgeries are performed under physiological conditions where only a small amount of deformation is involved.

Sawusch and McDonnell (1992) sought to investigate how the stress created by intraocular pressure and a four-incision radial keratotomy procedure was distributed and how it affected corneal curvature. Assuming symmetry of the globe about the anterior-posterior geometric axis, only one quarter of the eye was modeled with finite elements. The model included the cornea, sclera, and limbus. Shell elements were chosen, but the exact number of elements was not reported. Isotropic material properties were taken from the literature. The assumed isotropic material behavior was justified by previous evidence of a random orientation of stromal (a corneal layer) collagen fibers. As previously mentioned, linear material behavior was assumed for small displacements within the physiological range. In addition, this FE model was used to calculate the gaping of the four incisions.

Vito *et al*. (1989) constructed a FE model of only the cornea to study the curvature changes during radial keratotomy surgery. They also investigated the effects of surgical errors in the length, depth, and location of one incision. Corneal tissue was assumed to have a constant thickness, undergo small deformations, and exhibit nearly incompressible, homogeneous, linear elastic, isotropic material behavior. To determine an appropriate Young's modulus, a value was chosen which produced the same radius of corneal curvature resulting from an actual procedure performed on a patient. A total of 768 three-dimensional, eight-node, brick elements were employed in the model. Even with the listed simplifying assumptions, the researchers claimed that their model gave results in qualitative agreement with experimental and clinical observations.

An additional study performed by Vito *et al*. (1992) argued that solid elements should be used when modeling the cornea. Shell elements may be the natural choice given the small thickness to radius of curvature ratio for the cornea. However, when large stress gradients through the corneal thickness are expected, such as with indenter loading of the cornea, solid elements may be better suited. Two-dimensional FE models of the cornea, with and without the limbus, were created using axisymmetric-solid quadrilateral elements. The number of such elements used in the model was not reported. Also, the varying thickness of the cornea was not considered here. The material

properties were assumed to be linear elastic and isotropic for simplicity, nearly incompressible, and gathered from the literature. It was determined that the limbus had a large effect on the results. However, it was also stated that the mechanical properties of the limbus were not well known.

Pinsky and Datye (1991a) argued that the shear and bending rigidity of the cornea are several orders of magnitude smaller than the in-plane, or membrane rigidity. This led them to model one quarter of only the cornea with 48 nine-node, membrane shell elements for the purpose of simulating the effects of radial keratotomy. The varying thickness of the cornea was included in their FE model. Again assuming only small deformations of the tissue under physiological conditions, all material behavior was assumed to be in the linear elastic region. It was also assumed that the structural behavior of the cornea was governed by the properties of the collagen fibers within the stroma. Accordingly, material properties of collagen fibers were taken from the literature for use in their model. The results predicted by their model were then compared with those expected from actual procedures. The researchers reported an excellent correspondence between the two sets of results. As an extension of this model, Pinsky and Datye (1991b) later investigated astigmatic and hexagonal keratotomy, in addition to radial keratotomy.

Bryant and McDonnell (1996) also constructed a FE model of the human cornea undergoing a four-incision radial keratotomy procedure. As a comparison, four different material models were considered: linear elastic isotropy, nonlinear elastic isotropy, linear transverse isotropy, and hyperelasticity. Each of these models consisted of 150 four-node, axisymmetric, two-dimensional elements. The material properties for each of the four models were decided upon by matching the predicted intraocular pressure versus apical displacement curves to those recorded during membrane inflation tests performed on intact human corneas. After the material properties for the four different models were chosen, a surgical FE cornea model was constructed to simulate the incisions. This model assumed the cornea to be homogeneous and consisted of 960 eight-node, three-dimensional brick elements of varying thickness. It was concluded that this linear

transverse isotropic model was incapable of representing the anisotropic behavior demonstrated by the cornea. In addition, after comparing the materially nonlinear to the linear models, it was stated that the nonlinearity was very important and should be included in any such models.

Kobayashi *et al*. (1971) built an FE model of the corneo-scleral shell to analyze its structural response to changes in intraocular pressure or to indentation or applanation tonometry. The globe was assumed to be symmetric about an anterior-posterior axis. Neither corneal nor scleral thinning was taken into consideration. Linear, isotropic material properties were used, with values taken from the literature. The corneo-scleral shell was modeled with a total of 528 axisymmetric quadrilateral elements. This same group of researchers (Woo *et al*., 1972a) then determined nonlinear material properties of the cornea and sclera by performing membrane inflation tests and measuring the displacements at the anterior and posterior poles. Then, the previously mentioned model, using trilinear stress-strain relationships, was adjusted until the predicted and experimental results were in agreement. Next, the trilinear relations were converted into exponential equations by the least squares method. Finally, these new nonlinear material properties were incorporated into the improved FE model (Woo *et al*., 1972b). In addition, the previously ignored corneal and scleral thickness variations were included in this revised model.

Another three-dimensional model of the human eye for the purpose of investigating radial keratotomy was completed by Wray *et al*. (1994). The cornea and sclera were assumed to be nearly incompressible, nonlinear, and isotropic. Exponential equations describing the nonlinear stress-strain relationship for the cornea and sclera were taken from the membrane inflation tests performed by Woo *et al*. (1972). However, the coefficients for these equations were determined from *in vivo* data. The cornea, sclera, and limbus were then modeled using a combination of twenty-node brick, and fifteen-node tetrahedral elements, 822 in total. Finally, the refractive power changes predicted by the model were compared to two independent medical studies, and found to be in good agreement with each other.

To calculate the influence of intraocular pressure on the eye resonance frequencies, Coquart *et al*. (1992) developed a two-dimensional model of the human eye submitted to vibrations. Both the cornea and sclera were modeled, first as thick shells and then as thin shells. Material behavior was first assumed to be linear and then changed to nonlinear. The vitreous gel and aqueous humor were modeled as a single incompressible fluid, having properties similar to water. All isotropic material properties were based on the experiments performed by Woo *et al*. (1972). The cornea was modeled with 8 four-node, quadrilateral elements, the sclera with 40 such elements, and the fluid with 132 eight-node, quadrilaterals plus 20 six-node triangular elements.

Hoeltzel *et al*. (1992) sought to determine whether or not the cornea could be considered to behave as a membrane. They constructed a geometrically and materially nonlinear FE model of the human cornea in accordance with the data from Woo *et al*. (1972). However, it was not reported how many membrane elements were used in the model. Membrane inflation tests were then performed on intact human corneas within the range of physiological intraocular pressure. Next, the apical deflections predicted by the FE model were compared to those found experimentally. The two sets of data were in better agreement at the physiological pressure than above or below this pressure. It was finally concluded that the cornea could be considered to behave very nearly as a membrane, with little ability to resist bending stresses.

As a first attempt to investigate the anisotropic behavior of the cornea, membrane inflation tests to examine the distribution of strain in the human cornea were performed by Shin *et al*. (1997). Unlike previous membrane inflation tests, these were not limited to measuring only deformations at the apex. Rather, measurements were recorded at several locations and from different directions. A FE model of the cornea was also completed to better understand and simulate the experimental results. This axisymmetric model of the cornea consisted of linear elastic, nearly incompressible, orthotropic thick shell elements, but the number of elements was not revealed. The geometry included varying corneal thickness. The intent of the orthotropic material behavior was to simulate a transition in

the dominant stiffness from meridional at the apex to circumferential at the limbus. They claim this transition may be due to the changing fiber orientation in the cornea observed in the literature. The results predicted by the FE model were similar to those recorded experimentally. This suggested that the preferential fiber orientation of the cornea was inconsistent with previous isotropic assumptions.

To simulate refractive surgery, Hanna *et al*. (1989a) created a FE model of the cornea and sclera with three-dimensional brick elements. They also wanted to study the effects of changing the number, length, and depth of incisions, and intraocular pressure. Assuming symmetry of the globe, brick elements were used in a quarter section of the eye, with the varying thickness of both the cornea and sclera taken into account. However, the number of brick elements used was not reported. The cornea and sclera were assumed to be elastic, nonlinear, essentially incompressible, and isotropic, with properties from the literature. Then, as an improvement to this model, Hanna *et al*. (1989b) incorporated anisotropic material behavior. Here, 618 three-dimensional brick elements were used to model half the globe. This model was used to study the effects of incisions both parallel and perpendicular to the limbus. Special emphasis was placed on the limbus due to its unique geometry and increased stiffness. It was then concluded that the limbus is a very important factor and deserves much attention in such FE models.

The section that follows describes the most relevant work related to the research presented in this study. Uchio *et al.* (1999) constructed a three-dimensional model of the human eye. This eye was then used to investigate ocular impacts from grinder debris (Kisielewicz *et al*., 1995) and airbag injuries after radial keratotomy procedures had been performed (Kisielewicz *et al*., 1996; Kisielewicz *et al*., 1998). Using Altair Hypermesh and ESI PAMCRASH software programs, the eye was modeled with a total of 6632 elements. The cornea, sclera, and iris consisted of 3680 membrane elements, while the aqueous humor and vitreous gel consisted of 2952 solid elements. Geometries for each component, including scleral thinning and the nonlinear cornea, were taken from the literature. The lens was modeled as a rigid body with its mass accounted for. Nonlinear, isotropic material properties of the sclera and cornea were gathered from uniaxial tensile

strip tests. Unlike the previous research with low deformations near physiologic conditions, these strip tests were performed up to rupture. To simulate the kinematics of airbag impacts, a dummy model with a rigid biomechanical headform model was incorporated. This headform better represented the contact with the airbag than the standard dummy ellipsoid geometries.

However, there is much room for improvement in the boundary conditions chosen for this model. The FE eye was rigidly attached to the headform model. Surrounding components such as the bony orbit, fatty tissue, and extraocular eye muscles were totally neglected. Experiments which involved inflating human cadaver eyes up to rupture illustrated the importance of the extraocular muscles (Burnstein *et al*., 1995). These cadaver eyes were found to rupture most frequently at the muscle insertion sites. The fatty tissue would also offer significant damping between the eye and the headform under loading. Therefore, structures not included in previous models such as the muscles, orbit, and fatty tissue are included in the current study.

Chapter 3
Materials and Methods

3.1 Introduction

A finite element model of the human eye was constructed using I-DEAS (SDRC, Milford, OH) and Hypermesh (Altair, Troy, MI) software programs. Ocular structures include the cornea, sclera, vitreous, aqueous humor, ciliary body, and lens. Surrounding structures not included in previous models such as the fatty tissue, six extraocular muscles, and bony orbit were also included in the FE model (Kisielewicz, 1998). Material and geometric properties were gathered from the literature wherever possible and approximated whenever not available.

Next, the FE eye was imported into Madymo (TNO, The Netherlands), a program often used to simulate automobile crashes. Madymo has many advantages, including the ability to dynamically model both rigid bodies (crash test dummy) and deformable finite elements. Madymo has available a variety of different sized dummy models, FE airbags, and a human headform model. Finally, Madymo was used to conduct a parametric study, investigating ocular injuries from night vision goggles. This parametric study determined the position of the occupant that yields the greatest stress to the eye. In addition, the effect of the muscles, fatty tissue, goggle mass, goggle breaking away from the helmet mount, and eye protection were also investigated. A rigid headform model, SPH-4B aviator's helmet, and mounted ANVIS-6 night vision goggles (ITT Industries Night Vision, Roanoke, VA) were all modeled in this study.

3.2 Formulation of the Finite Element Eye Model

Three main characteristics must be defined for every finite element model prior to applying boundary conditions and loads: geometry, material properties, and the type of element. The methods used to choose and define each of these three characteristics are

provided in the current section. Boundary conditions and applied loads will be discussed in the parametric study section.

3.2.1 Geometry

The nonuniform geometry of the cornea and sclera were gathered from the literature (Woo *et al*., 1972) and used to create the finite element model. Both the cornea and sclera are nearly spherical, with a radius of 7.8 mm and 12 mm, respectively (Figure 3.1). The cornea varies in thickness, from 0.52 mm at the apex to 0.66 mm at the limbus. The sclera also varies in thickness, from 1 mm at the posterior pole, decreasing to 0.55 mm at the equator, then increasing to 0.8 mm at the limbus. The importance of the abrupt change in geometry at the limbus, and equatorial thinning of the sclera must be noted. As the intraocular pressure within the globe increases, as with a blunt impact, these two regions act as stress concentrations. Experiments with human cadaver eyes involving increasing intraocular pressure up to rupture support this claim (Dyster-Aas, 1962). It was discovered that the most typical rupture started at the limbus, then curved backwards towards the posterior pole.

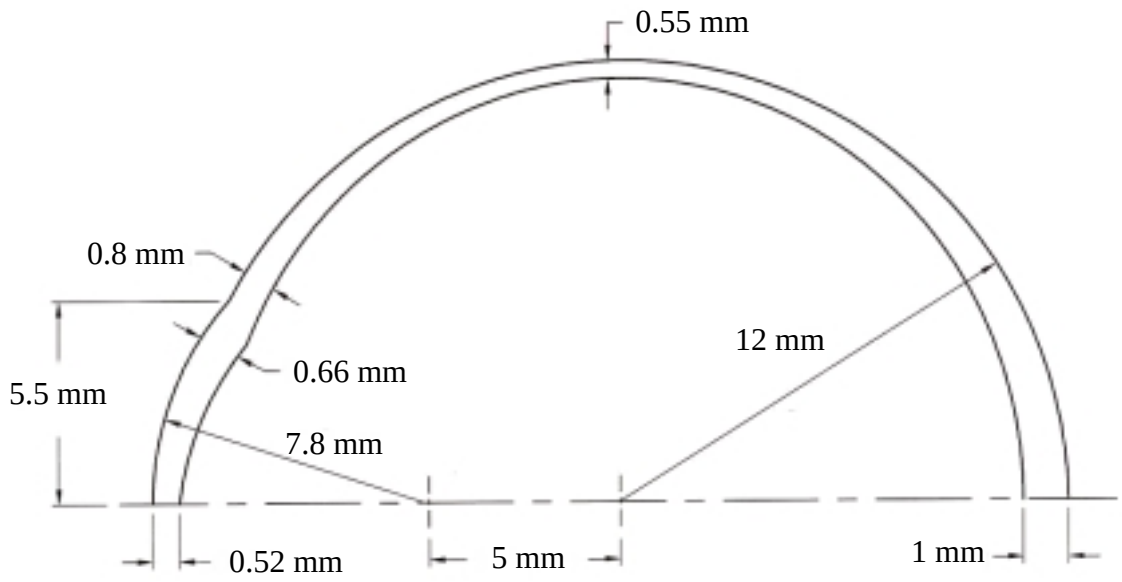

Figure 3.1 The non-uniform geometry of the cornea and sclera.

Inside the protective shell formed by the cornea and sclera, lies the lens (Figure 3.2). The lens has a 9 mm diameter and maximum thickness of 3.6 mm (Duke-Elders *et al*., 1961). The posterior radius of 5.4 mm is also steeper than the anterior radius of 9 mm. The lens was placed so that its anterior surface rested flush with the posterior boundary of the anterior chamber. The ciliary body and zonules attach to the sclera just behind the limbus, and are responsible for holding the lens in place (Takahashi, 1994). The ciliary body and zonules were grouped together as a single structure, referred to as the ciliary body throughout the remainder of this thesis. The exact dimensions of the ciliary body and zonules are unknown. Therefore, the ciliary body was modeled with an assumed thickness of 0.2 mm.

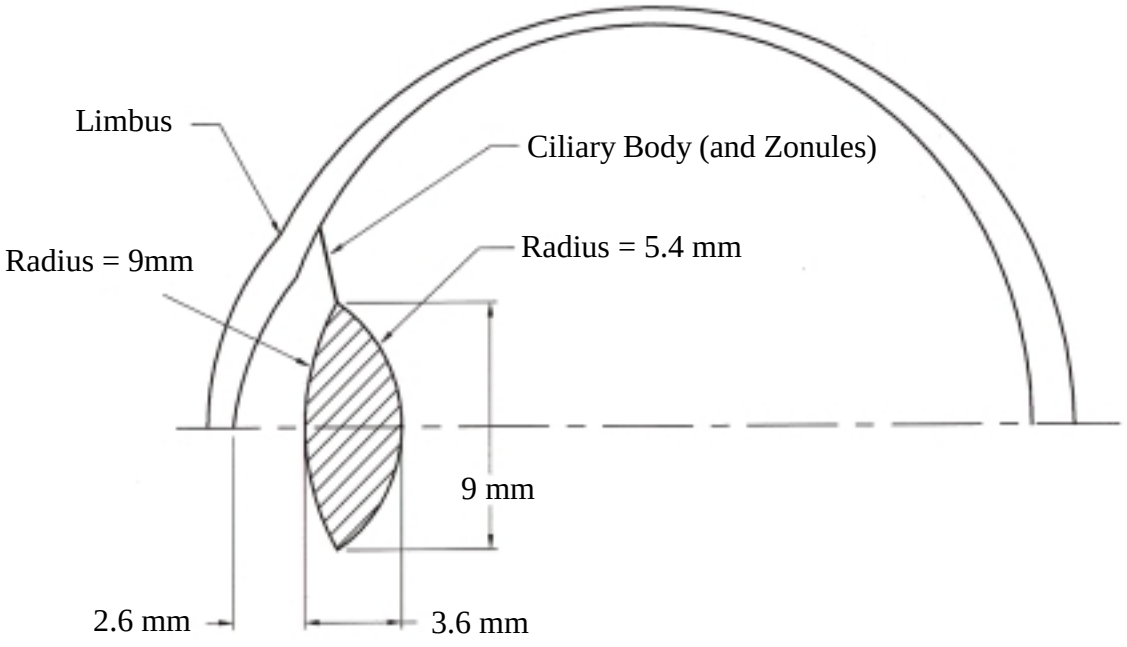

Figure 3.2 Dimensions and location of the lens.

The bony orbit surrounding the globe can be approximated as a pyramid, with the base serving as an opening for the eye and the apex being directed towards the brain (Sauerland, 1994). The medial or nasal walls of each orbit are almost parallel and are approximately 25 mm apart (Figure 3.3). The lateral walls of the two orbits are angled to such an extent that they are almost perpendicular with one another. The height of the pyramid is approximately 50 mm. Both orbital openings were approximated as squares. The opening for the eye was a square with 32 mm sides, while the opening for the optic nerve had 10 mm sides. These opening dimensions were chosen to leave enough space for the fatty tissue to occupy, while also ensuring that the lateral walls did not extend beyond the Madymo headform "temple to temple" dimension.

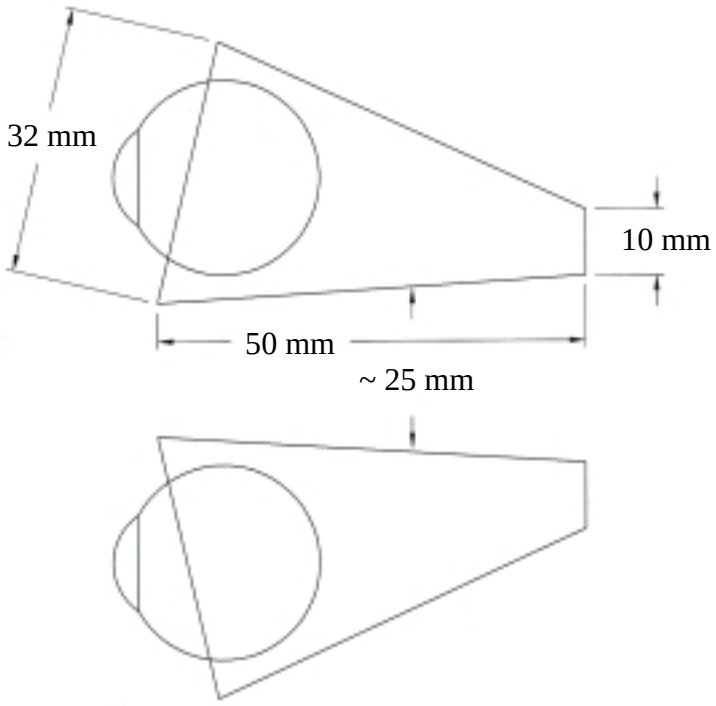

Figure 3.3 Top view of bony orbit with established dimensions.

The dimensions and attachment locations of the six extraocular muscles, which control the eye's movement, were chosen to best match pictures found in human anatomy books (Takahashi, 1994). As an initial estimate, all six muscles were defined as 0.2 mm thick. The finite element mesh of the sclera also dictated the scleral attachment locations. This is because the nodes of the muscles have to coincide with the nodes of the sclera at the points of attachment. In addition, the superior oblique muscle was "looped" through the trochlea fastened between the medial wall and roof of the orbit (Figure 3.4). The inferior oblique muscle was attached between the orbital floor and the sclera. The remaining five muscles were connected between the sclera and the posterior pole of the pyramidal orbit.

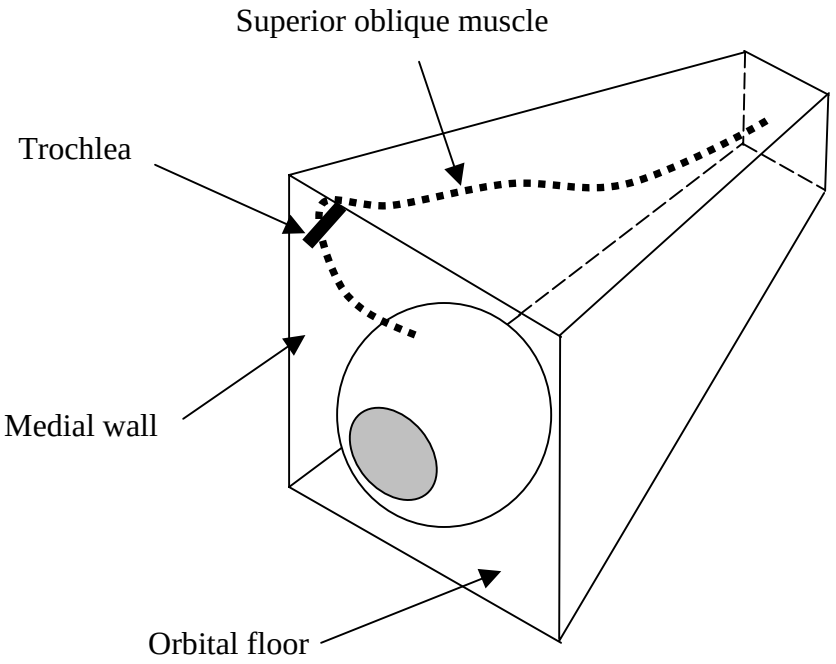

Figure 3.4 Trochlea acts as a pulley for superior oblique muscle (left orbit).

ANVIS-6 aviator night vision goggles (NVGs) and SPH-4B flyer's helmet (ITT Industries Night Vision, Roanoke, VA) were obtained to gather measurements (Figure 3.5). Basic NVG dimensions including the mass were recorded. By applying symmetry, only half of the NVG needed to be modeled (Figure 3.6). The NVG was approximated as a 117 mm long cylinder with a 34 mm diameter. The goggles attach to an aviator helmet and are only allowed to rotate about the lateral-medial axis. This gives the person wearing the helmet/NVG system the ability to flip the goggles up when necessary. The hinge that the goggles rotate about was measured to be 38 mm from the superior surface of the goggles. The goggles had a mass of 546 grams, but only half of this was modeled due to symmetry.

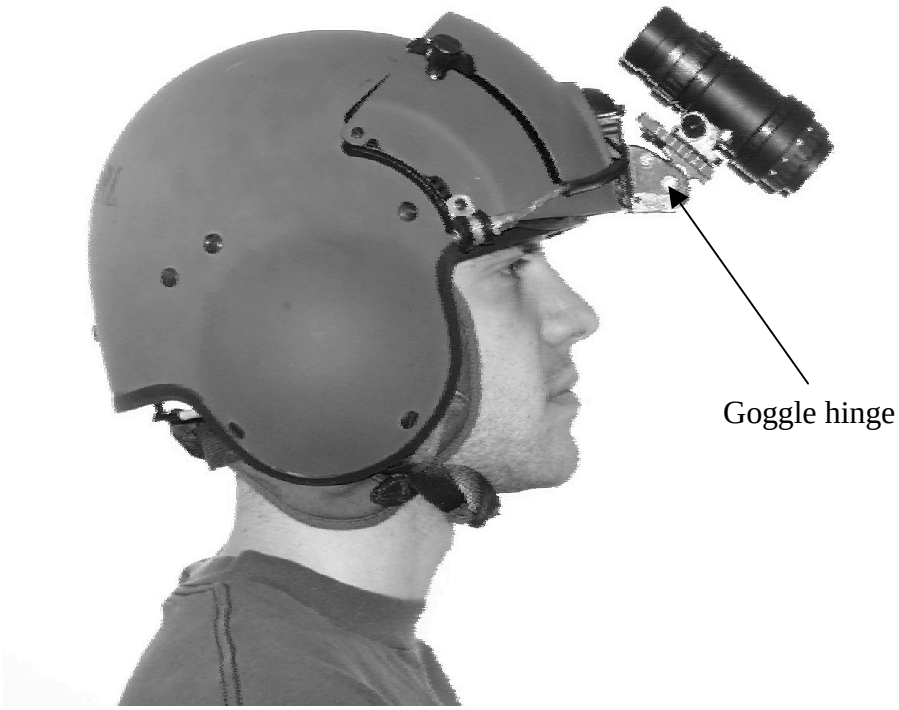

Figure 3.5 Aviator night vision goggles mounted to helmet.

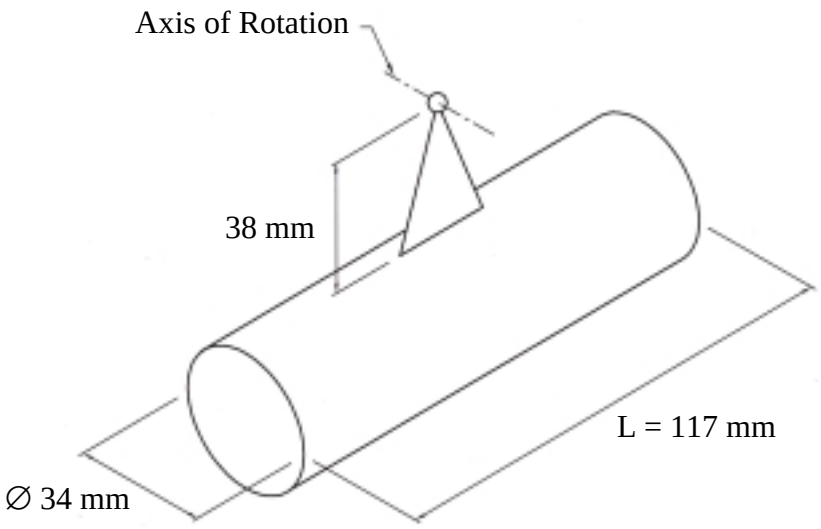

Figure 3.6 Aviator night vision goggle dimensions and axis of rotation.

There are several different sizes of helmets available to the aviator. A best attempt was made to create a helmet fitted around the Madymo rigid headform model for the 50th percentile male (Figure 3.7). This was done by sketching the geometry in I-DEAS and serves only the purpose of graphical representation. A rigid connection between the head and helmet was assumed.

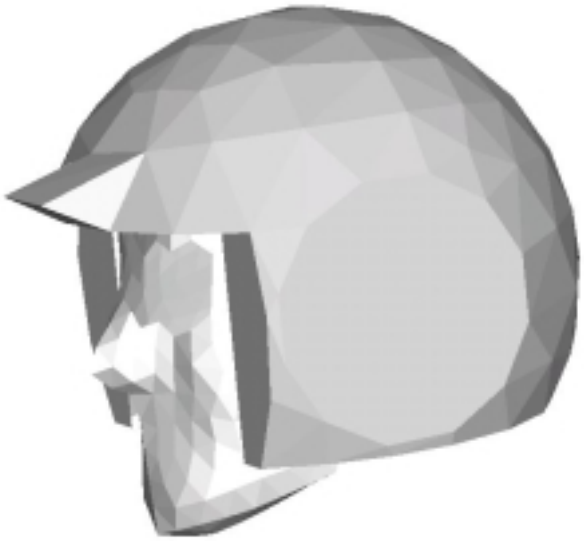

Figure 3.7 Illustration of sample aviator helmet.

3.2.2 Material Properties

Previous tests have performed to determine the material properties of the human sclera and cornea (Andreassen *et al*., 1980; Battaglioli *et al*., 1984; Bryant *et al*., 1994; Hanna *et al*., 1989; Hoeltzel *et al*., 1992; Nash *et al*., 1982; Shin *et al*., 1997; Uchio *et al*., 1999; Woo *et al*., 1972; Yamada, 1970). The methods used have been either uniaxial strip extensiometry or membrane inflation. The results showed that the human sclera and cornea exhibit non-linear material behavior, are anisotropic, and rate dependant, or viscoelastic.

Woo *et al*. (1972) used membrane inflation to determine an exponential relationship between effective stress and effective strain [1].

$$\sigma_{ef} = \alpha\left(e^{\beta\varepsilon_{ef}} - 1\right) \qquad [1]$$

Effective stress and effective strain relate to the average three-dimensional states of stress and strain [2], [3],

$$\sigma_{ef} = \frac{1}{3}\left\{(\sigma_1-\sigma_2)^2 + (\sigma_2-\sigma_3)^2 + (\sigma_3-\sigma_1)^2\right\}^{\frac{1}{2}} \qquad [2]$$

$$\varepsilon_{ef} = \frac{2}{3}\left\{(\varepsilon_1-\varepsilon_2)^2 + (\varepsilon_2-\varepsilon_3)^2 + (\varepsilon_3-\varepsilon_1)^2\right\}^{\frac{1}{2}} \qquad [3]$$

where $\sigma_1, \sigma_2, \sigma_3$, and $\varepsilon_1, \varepsilon_2, \varepsilon_3$ are the principal stress and strain components, respectively. The coefficients (α,β) for the sclera and cornea were equal to (1.8×10^4, 41.8) Pa and (5.4×10^3, 28.0) Pa, respectively. The intraocular pressure (IOP) was incrementally increased to a maximum of 40 mm Hg, a near-physiological IOP, far from that required to rupture the globe. Normal physiological IOP is between 14 and 18 mm Hg (Pinsky *et al*., 1992). Human cadaver eyes have been found to rupture at IOPs between 0.441 MPa and 0.931 MPa (Dyster-Aas, 1962). Also, these tests involved measuring changes in displacement at the anterior and posterior poles only. The cornea and sclera were experimentally determined to be isotropic at these poles. However, isotropic behavior may not hold at other locations. Shin *et al*. (1997) also used membrane inflation, but measured displacements at several locations in human corneas.

The cornea was determined to be anisotropic from these experiments. Evidence that random collagen fiber orientation at the corneal apex gives way to a circumferential orientation at the corneal limbus may be responsible (Meek *et al*., 1982, 1987).

One limitation of the previously mentioned membrane inflation tests is that they only measured tensile properties perpendicular to the tissue thickness. However, Battaglioli and Kamm (1984) conducted tests on strips of human sclera samples to determine the mechanical properties of the tissue under compression across the thickness. Compressive stress-strain curves of the samples were found to be approximately linear, with an average modulus of 3.34×10^{4} Pa. This elastic modulus for compressive strength across the thickness was found to be approximately 100 times less than the modulus for tensile strength in the tangential direction. This can be explained by the fact that layers of collagen fibers run tangentially throughout the sclera but not radially (Duke-Elders *et al*., 1961).

Unlike strip tests, membrane inflation preserves the globe geometry and collagen fiber integrity. However, many tests with strips have also been performed. Andreassen (1980), Bryant (1994), Hoeltzel (1992), and Uchio (1999) determined the stress strain curves of human corneal strips under uniaxial tension (Figure 3.8). Andreassen (1980) used a constant deformation rate of 1 cm/min up to failure. Bryant (1994) applied a rate of 0.6 cm/min to half of the samples, and 3 cm/min for the remaining half, also up to failure. The stress strain curve represents an average of all the samples. Hoeltzel (1992) applied a 0.05 cm/min deformation rate, not up to failure. Uchio (1999) tested both corneal and scleral strips up to rupture but did not report the deformation rate used.

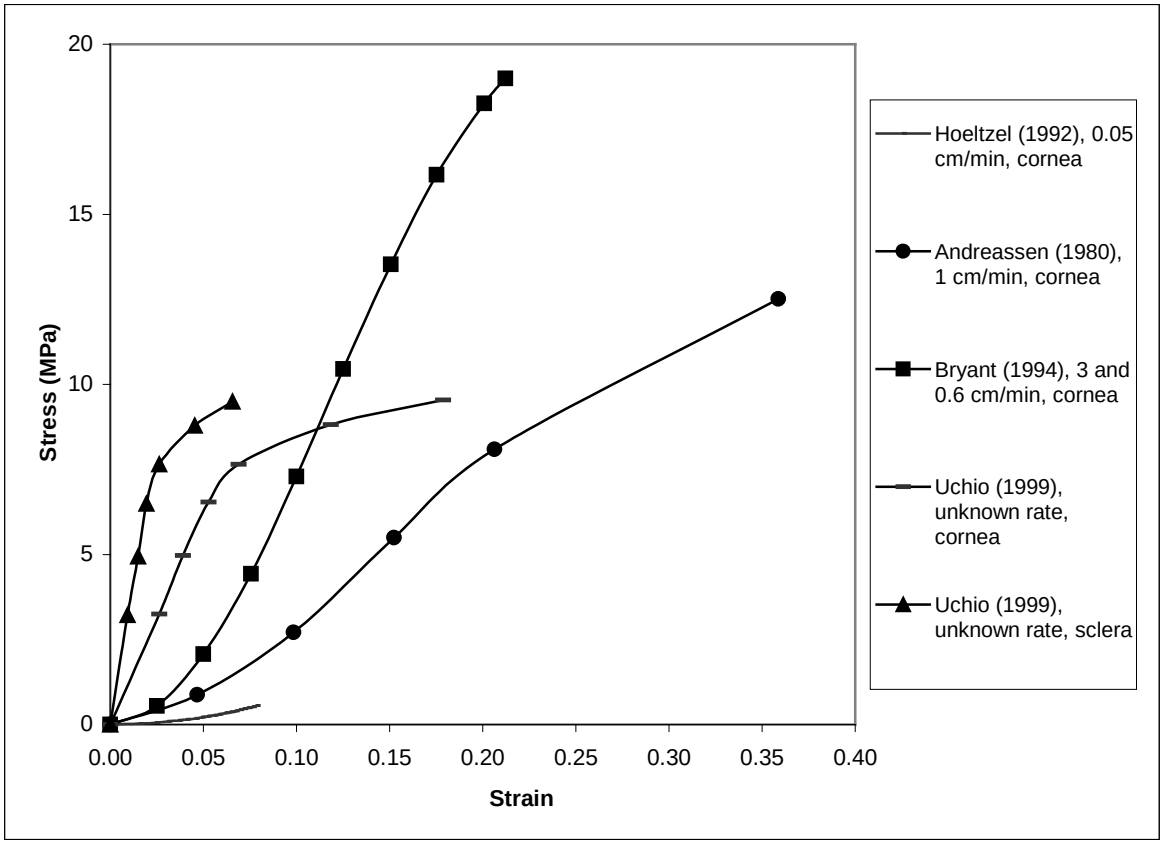

Figure 3.8 Stress-strain curves obtained with strips of human corneas and scleras.

For the scope of this project, it was necessary to input stress-strain data for the cornea and sclera up to rupture. This is because rupture, or open-globe injuries, may occur upon impact with the night vision goggles. Therefore, when evaluating which material properties to incorporate into the FE model, three options for the cornea and one for the sclera were available. The stress-strain curves established by Uchio (1999) were chosen because this was the only research done with human scleral tissue up to rupture. The corneal stress-strain data obtained by Uchio (1999) was then chosen over the others because the same group performed both set of tests, under identical test conditions. It would not be wise to use the scleral data obtained under one set of test conditions (temperature, age, postmortem time, loading rate, orientation and location of samples, etc.), and then choose corneal data collected by another research group under different conditions.

No studies were found that measured the mass density of the cornea or sclera. However, the mass densities of the major components of the cornea and sclera are known. More specifically, the mass densities of water, proteins, and collagen have been reported as 999, 1500, and 1800 kg/m^3 respectively (Kisielewicz, 1998). Accordingly, the mass density of the cornea and sclera was approximated as 1400 kg/m^3 for the model (Table 3.1). This is an average of the values reported for collagen and water. As previously discussed, the cornea and sclera were defined as nonlinear elastic isotropic materials. When nonlinear material properties are entered into Madymo, the Poisson's ratio is not entered.

Table 3.1 Summary of material properties used.

Structure	Material model	E (MPa)	Poisson's ratio	Density (kg/m^3)
Cornea	Nonlinear elastic	(Figure 3.8)	NA	1400
Sclera	Nonlinear elastic	(Figure 3.8)	NA	1400
Six muscles	Linear elastic	11.0	0.40	1600
Ciliary body	Linear elastic	11.0	0.40	1600
Fatty tissue	Linear elastic	0.047	0.49	999
Vitreous	Linear elastic	0.042	0.49	999
Aqueous	Linear elastic	0.037	0.49	999
Lens	Rigid	NA	NA	315
Orbit/Trochlea	Rigid	NA	NA	NA
Goggles	Rigid	NA	NA	Whole mass = 0.546 kg
Helmet	Rigid	NA	NA	NA

All of the remaining ocular structures were defined as either rigid or linear elastic. Linear elastic means that the stress-strain curve is linear, therefore the slope, or Young's modulus (E) is a constant value. The fatty tissue surrounding the eye was approximated as nearly incompressible "soft" human tissue with a Young's modulus of 47 kPa and a Poisson's ratio of 0.49. These values were used by Todd and Thacker (1994), and more recently by Bidar (2000) to construct finite element models of the human buttocks. The

water-like aqueous and gel-like vitreous were then given Young's moduli of 37 and 42 kPa, respectively, slightly softer than the fatty tissue. An incompressible material would have a Poisson's ratio of 0.50. Therefore, defining the ratio as 0.49 for the above structures is a reasonable approximation based on the high water content of these tissues. In addition, the density of each structure was set equal to that of water, 999 kg/m^3, an assumption justified by high water content.

No information describing the material properties of the ciliary body or extraocular muscles was available. Therefore, approximations were made as follows: Based on their high water content, but less than that of the aqueous humor, a Poisson's ratio of 0.4 was chosen for the ciliary body and extraocular muscles. The tensile strength of collagen from rat's tail tendon has been found to vary between 50 and 100 MPa, depending on the specimen age (Kisielewicz, 1998). The tensile strength of the ciliary body and extraocular muscles were then assigned a value of 11 MPa as an initial guess for this preliminary study. This initial guess is supported by the fact that the ciliary body and extraocular muscles have a large amount of collagen, but not as much as rat tail tendon, which is often considered as an excellent source of pure collagen. The mass density of each structure was also approximated as 1600 kg/m^3, which is greater than the cornea and sclera but less than pure collagen. Finally, these structures were defined as tension only materials unable to support any compressive loads. This was done to better represent only the passive strength of muscle tissue.

The lens was approximated as rigid with only its mass density accounted for. This assumption is reasonable since this preliminary study did not investigate the deformation and possible injuries to the lens. The mass density of the human lens has been found to vary between 200 and 430 kg/m^3 (Kisielewicz, 1998). Therefore, an average value of 315 kg/m^3 was selected to model the lens. The stiffness of the bony orbit, NVGs, and helmet were much greater than that of the eye tissues, and were therefore regarded as rigid objects with only their geometric properties being needed.

3.2.3 Meshing Techniques

All components of the model, both deformable and rigid, were meshed using I-DEAS software (SDRC, Milford, OH). This involved creating the geometry with the drawing capabilities of I-DEAS and then utilizing either the automesh or manual mapped meshing functions. Automeshing gives I-DEAS the responsibility of defining the density and appearance of the meshed structure. On the other hand, mapped meshing leaves this up to the user. Both have their advantages and disadvantages, with only a few being highlighted here. Automeshing can save much time when meshing nonuniform geometries, such as a car body with various curves and angles. However, although more time consuming, mapped meshing allows the user to refine the mesh in particular regions. For example, mapped meshing could be used to increase the mesh density around a hole to better illustrate the stress concentration around the circumference.

The cornea and sclera were free meshed, or automeshed in such a way that an undistorted, uniform mesh with nearly equilateral triangular elements was achieved (Figure 3.9). Elements that are undistorted usually give greatest accuracy (Cook, 1995). Therefore, the ideal triangular element would be an equilateral, a quadrilateral would be square, etc. Membrane elements were chosen based on the assumption that the cornea and sclera only support in-plane, or membrane forces. No resistance to bending exists with these elements. In this way, the corneo-scleral shell is modeled to behave much like a water balloon. Madymo has the ability to use triangular or quadrilateral shaped membrane elements. However, nonlinear material behavior is only available with the triangular elements. Therefore, the cornea was meshed with a total of 64 linear triangular (3 noded) membrane elements and 41 nodes, while the sclera required 400 linear triangular membrane elements and 193 nodes (Table 3.2).

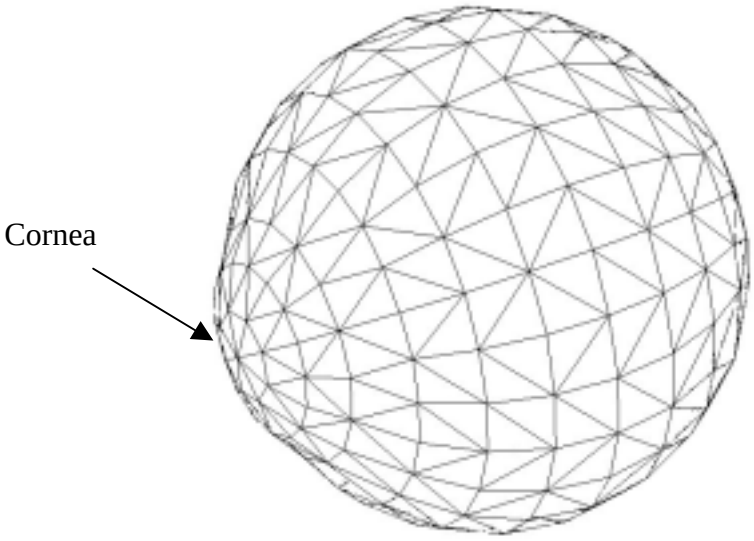

Figure 3.9 The cornea and sclera meshed with triangular membrane elements.

Table 3.2 Summary of finite elements used.

Structure	Element type	Element order	# of Elements	# of Nodes
Cornea	Membrane	Linear triangles	64	41
Sclera	Membrane	Linear triangles	400	193
Lens	Rigid	Rigid triangles	16	10
Ciliary body	Tension-only membrane	Linear triangles	32	32
Six muscles	Tension-only membrane	Linear triangles	338	251
Aqueous	Solid	Trilinear brick	72	123
Vitreous	Solid	Trilinear brick	80	125
Fatty tissue	Solid	Trilinear brick	160	294
Orbit/Trochlea	Facet	Rigid quads	94	104
Goggles	Facet	Rigid triang/quad	16/65	75
Helmet	Facet	Rigid triangles	246	139
			Total 1583	1387

All calculations for membrane elements are performed at the mid-surface. Also, each element is assigned a constant thickness about this mid-surface. Therefore, the varying thickness of the cornea and sclera needed to be discretized into sections (Figure 3.10). The sclera was divided into 10 equal sections of 15-degree increments about the center of the scleral sphere. The same approach was applied to the cornea, except that 3 equal 16-degree sections were defined about the center of the corneal sphere.

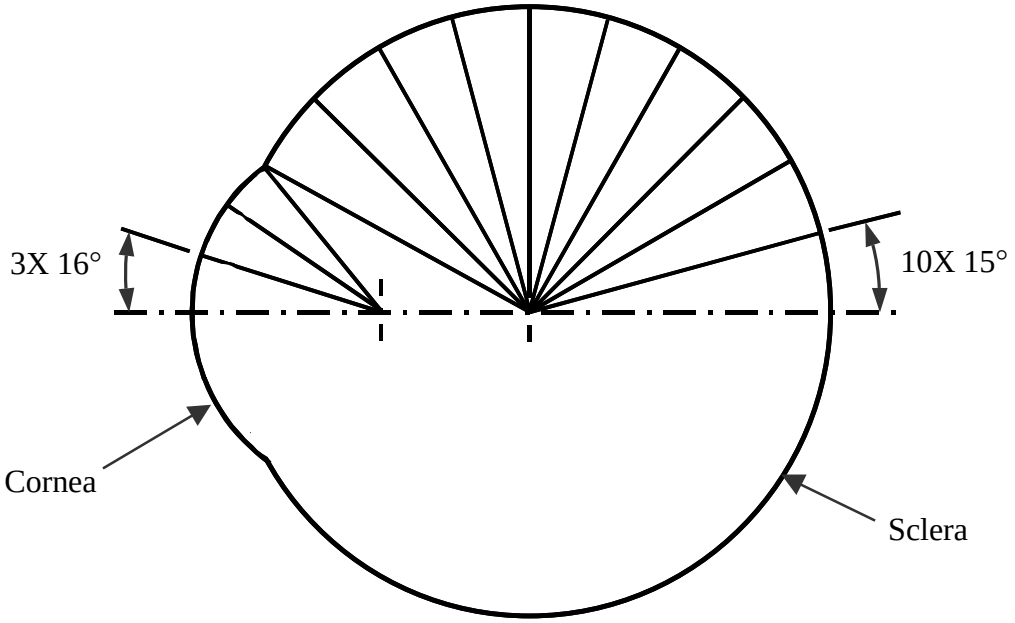

Figure 3.10 The cornea and sclera divided into equal sections.

After being divided into equal sections, a different value of thickness was then defined for each section of elements (Figure 3.11). This was done in a way to best represent the linearly varying thickness of the cornea and sclera. No interpolation exists at the boundaries between each set of constant thickness. I-DEAS does allow the user to define a method of interpolating between values of constant thickness. However, material properties defined in I-DEAS cannot be inputted into Madymo. Only the mesh properties, or node locations from I-DEAS were inputted, which is discussed further in

Chapter 3.3. This lack of membrane thickness interpolation is a limitation inherent to Madymo. Discontinuities in stress may result at the seams between sections of different thickness because of this discontinuity in thickness.

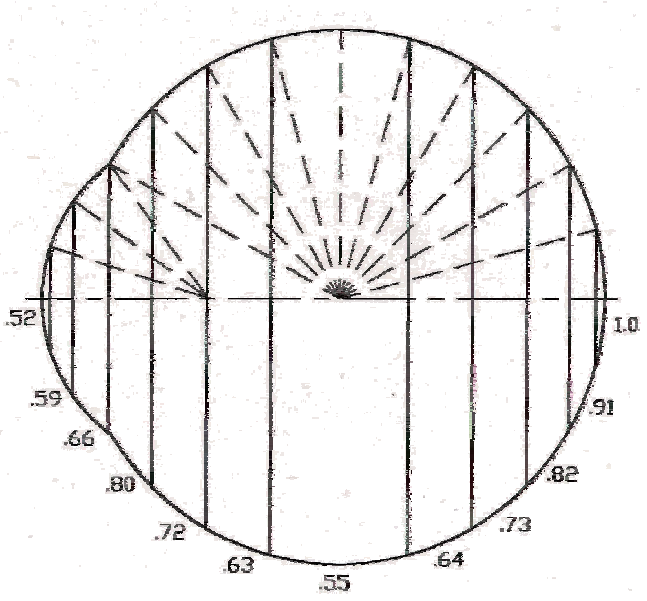

Figure 3.11 The varying thickness of the cornea and sclera (mm).

The aqueous humor was map meshed with a total of 72 trilinear (8 noded) solid brick element and 124 nodes (Figure 3.12). This manual method of meshing was very time consuming but necessary. Most finite element programs, including I-DEAS, are only able to automesh solid structures with pyramidal shaped tetrahedron elements. This is because these elements are able to represent nonuniform geometry much better than cube shaped brick elements. However, Madymo does not have a tetrahedron element in their library. This means that a structure automeshed with tetrahedral element in I-DEAS would not be able to be inputted into the Madymo syntax. Therefore, solid brick elements were used to mesh the aqueous humor. However, before this could be done, the aqueous had to be partitioned into several sections. This is because I-DEAS will often be unable to mesh solid objects that don't have many edges or flat faces. For example, with a sphere, I-DEAS would not know where to begin and end the mesh.

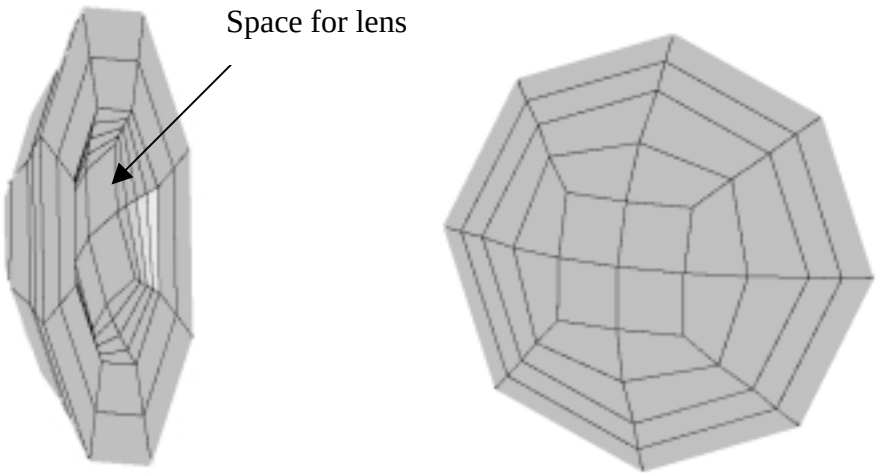

Figure 3.12 Aqueous humor map meshed with solid brick elements.

The vitreous was modeled with 80 trilinear solid brick elements and 125 nodes in the same manner as the aqueous (Figure 3.13). It should be noted that the mesh density of the vitreous and aqueous are much coarser than the cornea and sclera. This is because stresses for these fluids were not of interest in this study. Also, the indentations, or dimples in the vitreous and aqueous exist to form a pocket around the lens.

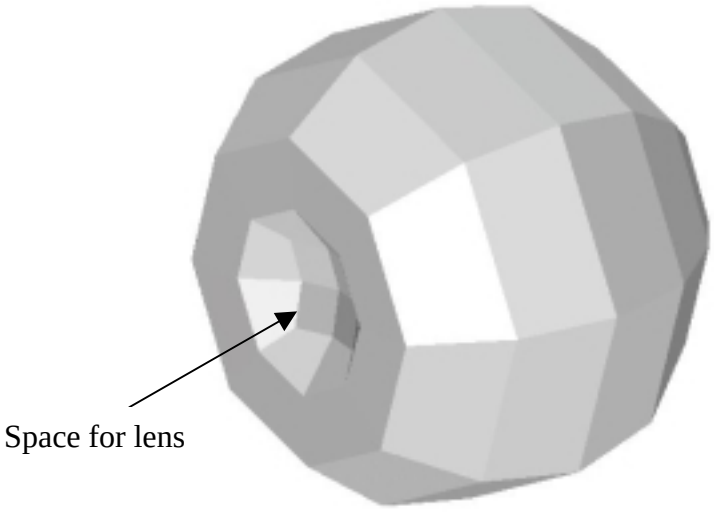

Figure 3.13 Meshed vitreous with a space formed around the lens.

The rigid lens was free meshed with 16 triangular membrane elements and 10 nodes (Figure 3.14). Membrane elements were used to mesh only the outer surface area of the lens. The material properties of these membrane elements were chosen arbitrarily because these elements were later defined as rigid elements within Madymo. After being defined as rigid elements, material properties for deformable bodies such as Young's modulus and Poisson's ratio are over-ridden since they do not exist for a rigid body. Essentially, triangular membrane elements were used only to create a mesh of the lens geometry.

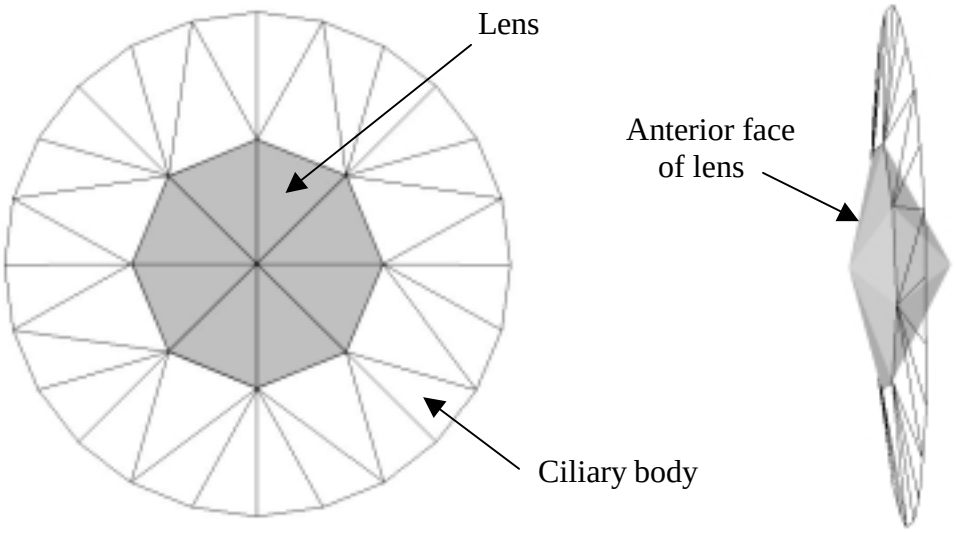

Figure 3.14 Front and side views of the meshed lens and ciliary body.

The ciliary body was free meshed element by element within the Madymo syntax. This manual process was chosen because very few elements and no additional nodes were needed to model the ciliary body. Linear, or 1st order triangular membrane elements were defined one at a time, from node to node so as to connect between the lens and sclera (Figure 3.15). The ciliary body was attached to the first available string of nodes just posterior to the limbus. This was done to best replicate the point of attachment seen in the literature on human anatomy (Takahashi, 1994). Also, triangular elements were chosen instead of quadrilateral elements to yield better stability when solving the

Madymo code. This was a recommendation from the TNO technical support group that manufacture Madymo. In total, 32 elements were needed to create the ciliary body, connecting between 8 nodes of the lens and 24 nodes of the sclera.

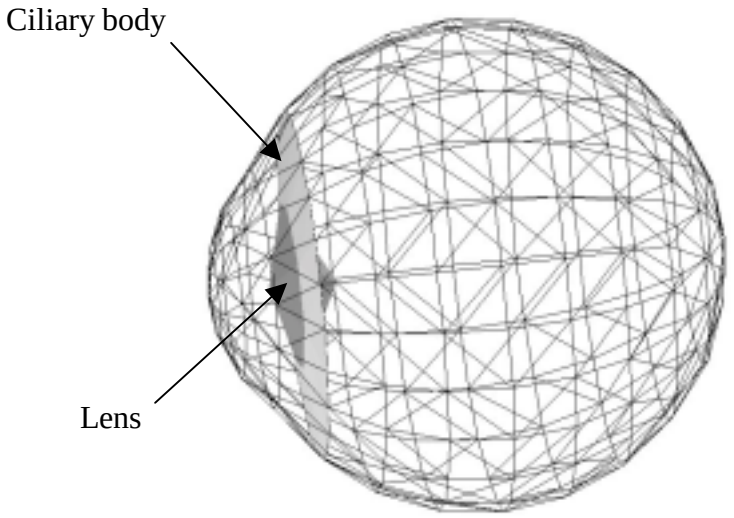

Figure 3.15 The ciliary body fastening the lens to the sclera.

All of the ocular structures previously discussed: the ciliary body, lens, aqueous humor, and vitreous, are enclosed in the shell formed by the cornea and sclera. An envelope was formed around the lens, with the aqueous humor forming the anterior face and vitreous body the posterior face.

Next, the procedures used to mesh external structures such as the muscles, fatty tissue, orbit, goggles, and helmet will be discussed. All six extraocular muscles were free meshed in I-DEAS using linear triangular membrane elements (Figure 3.16). Triangular elements were chosen over quadrilateral elements for the reasons of increased stability already discussed. Using triangular elements also leaves open the possibility of converting the muscle properties to nonlinear rather than linear, if ever needed in future studies with this FE eye model. Nonlinear quadrilateral elements cannot be defined within Madymo.

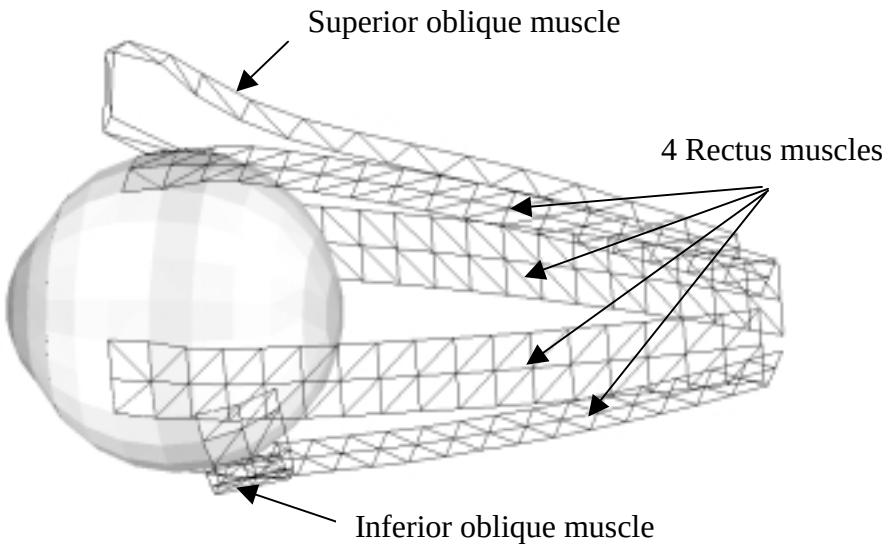

Figure 3.16 Lateral view of meshed extraocular muscles attached to sclera (left eye).

All six muscles were attached to the sclera at locations representative of those found in the literature (Takahashi, 1994). Each of the four straight muscles was meshed with 68 elements and 48 nodes. Of each set of 68 elements, four of these were used to attach each muscle to 6 nodes of the sclera. Using several nodes and elements to attach each muscle to the sclera reduces the stress concentration created at these locations. The superior oblique muscles consisted of 34 elements, 4 of which connected to the sclera, and 32 nodes. The sixth muscle, the inferior oblique, was meshed with 32 elements and 27 nodes, also attached to the sclera with four elements. In total, meshing of all six extraocular muscles required 338 elements and 251 nodes.

With the exception of the inferior oblique, all muscles were connected between the sclera and the posterior end of the orbit (Figure 3.17). Instead, the inferior oblique was connected to the floor of the orbit. Finally, the superior oblique muscle was looped through the trochlea, a hook formed in the superior-medial-anterior corner of the orbit.

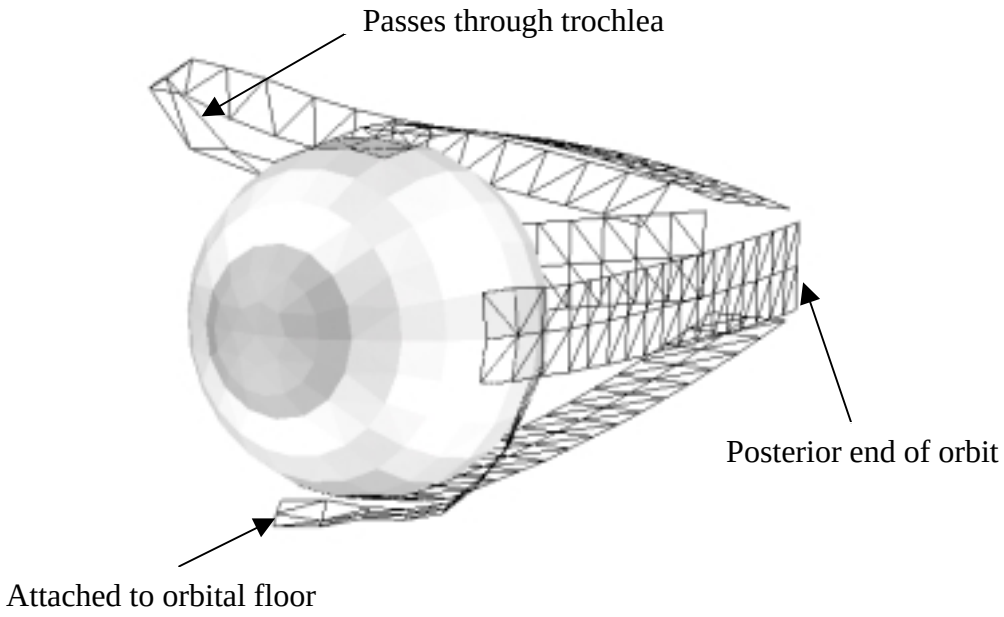

Figure 3.17 Extraocular muscles connected between the sclera and the orbit.

The fatty tissue was modeled to provide a more accurate boundary condition in the space between the globe and the orbit (Figure 3.18). This involved manually map meshing the fat with a total of 160 trilinear solid brick elements and 294 nodes. Automeshing this geometry with solid tetrahedral (4 noded) elements would have been simple. However, since only solid brick (8 noded) elements were available in Madymo, manual map meshing had to be performed. Therefore, the fat needed to be partitioned, or divided, into several smaller sections for I-DEAS to be able mesh the geometry properly.

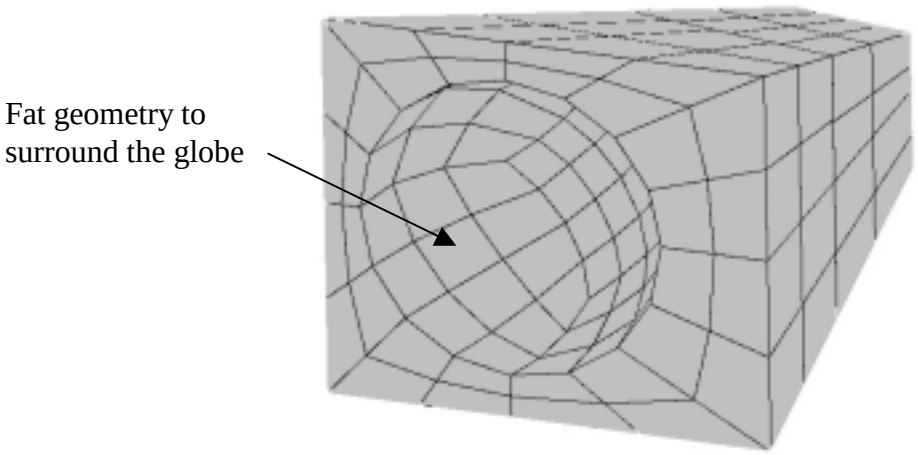

Figure 3.18 Fatty tissue meshed with solid brick elements.

The bony orbit consisted of four walls and the trochlea (Figure 3.19). Each wall was meshed with a single quadrilateral facet element. The trochlea was meshed with 90 quadrilateral facet elements. A much finer mesh was required here because of the contact between the superior oblique muscle and the trochlea. Recall that the muscle was modeled as a finite element model. In Madymo, contact between finite element models and a facet surface is recognized when an element comes into contact with the nodes (referred to as vertices within Madymo) of the facet surface. Therefore, this finely meshed trochlea was "coated" on its outer surface with 96 nodes. A total of 94 elements and 104 nodes were used to mesh the orbit and trochlea.

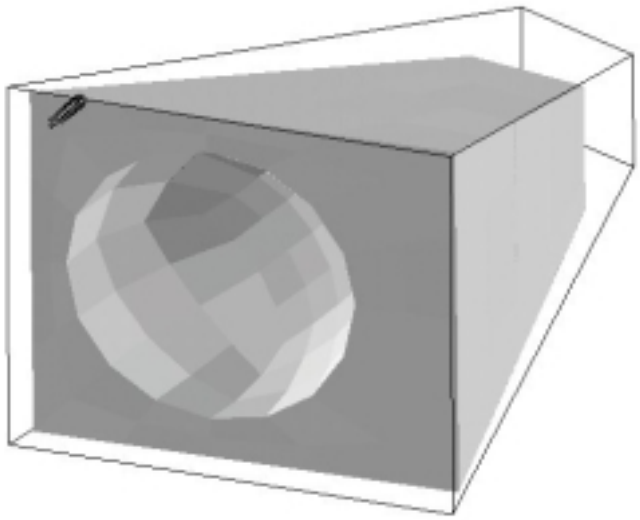

Figure 3.19 Orbit meshed with facet elements surrounding the fatty tissue.

Finally, the orbit was rigidly attached to the Maydmo facet headform model (Figure 3.20). This was done so as to create approximately 25 mm between the medial or nasal walls of the left and right orbits, if a right orbit was to be modeled.

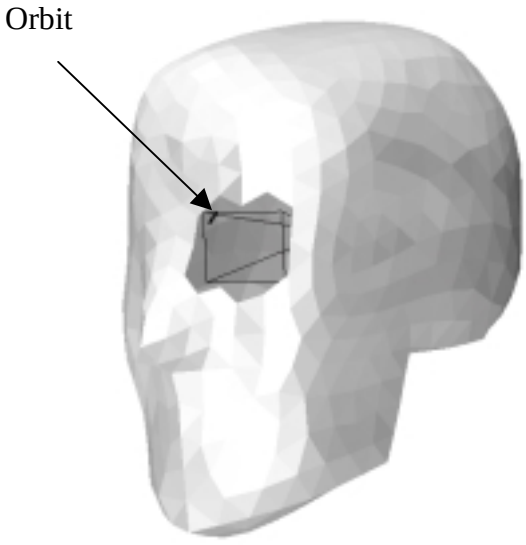

Figure 3.20 Orbit rigidly attached to the Madymo facet headform model.

However, before the orbit could be placed into the headform model, specific facet elements had to be removed. This process involved importing the headform model into Altair's Hypermesh, a meshing program, to identify specific facet element numbers. The elements to be removed were those that were to be replaced with the orbit. After removing the selected facet elements, a slightly jagged edge due to the size and shape of the facet elements was formed around the orbit (Figure 3.21). Finally, the orbit, fatty tissue, muscles, globe, and its internal structures were all set into place within the headform.

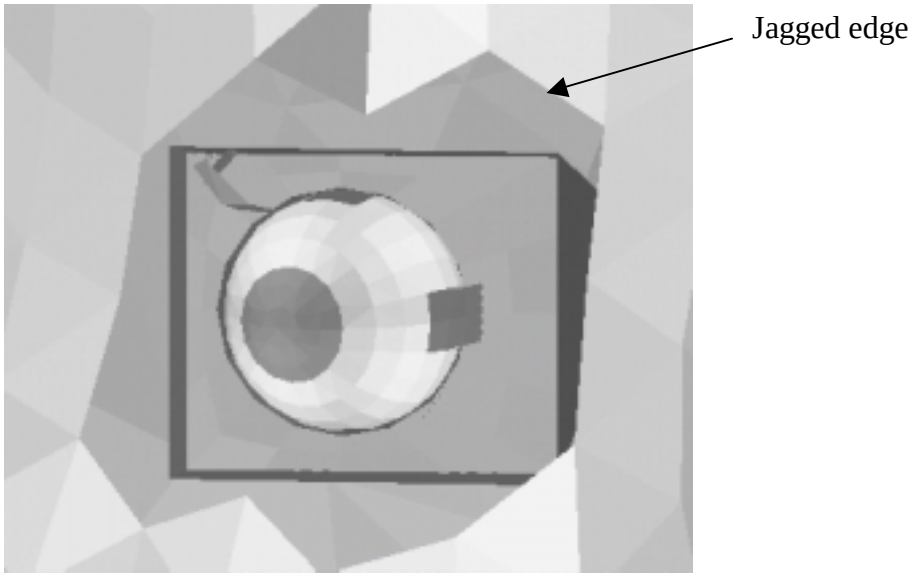

Figure 3.21 All ocular structures placed inside the headform model.

The NVGs were considered to be rigid and only its contact interaction with the ocular components was needed. Therefore, facet elements were used to represent only the geometry and surface area of the goggles (Figure 3.22). A total of 81 facet elements and 75 nodes were used. Of these 81 elements, 17 were triangular in shape and the other 64 were quadrilateral. Sixteen triangular elements were used to mesh the ends of the cylinder, 8 for each end. The seventeenth element was used to form the hinge, which attaches to the helmet. The 64 quadrilateral elements were used to mesh the circumferential surface of the goggles. With facet elements, triangular elements are no

more computationally stable than quadrilaterals. This issue, which was previously mentioned, only applies to deformable finite elements. Finally, a spherical ellipsoid was used to model the spring-loaded ball that fastens the goggles into the helmet. This ellipsoid serves no other purpose than to provide a graphical representation of this feature.

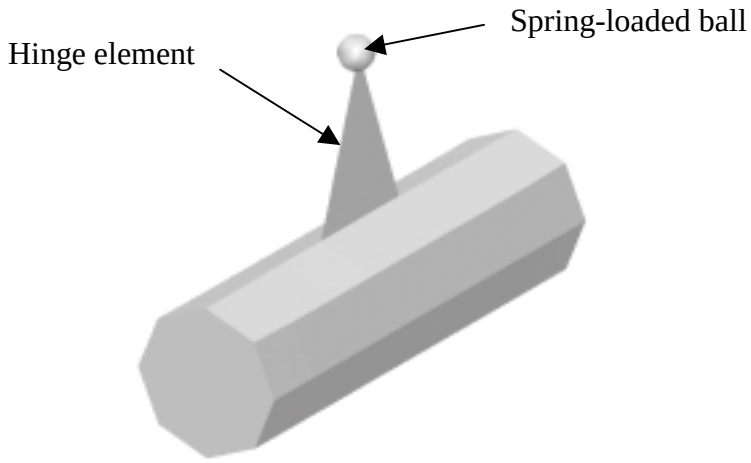

Figure 3.22 Aviator night vision goggles meshed with facet elements.

The last object to be meshed was the aviator helmet. This was done using I-DEAS automeshing capabilities (Figure 3.23). Such complex geometry would have required an extremely large amount of effort to manually map mesh. However, the approximately spherical shaped helmet had to be partitioned first, or divided into two pieces before I-DEAS would complete the meshing procedure. This partition was performed through the sagittal plane. A total of 246 triangular facet elements and 139 nodes were used to mesh the helmet.

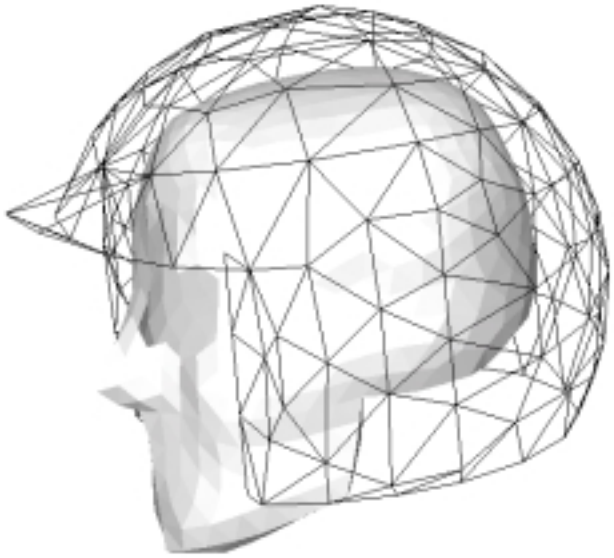

Figure 3.23 Aviator helmet automeshed with facet elements.

3.3 Inputting the Finite and Facet Element Models into Madymo

This section describes the processes used to input the finite and facet element models created using I-DEAS into the Madymo syntax file. In summary, geometry created and meshed in I-DEAS had to be converted into a Madymo format using Altair Hypermesh translation software. An example of the command prompts entered, etc. is also provided in Appendix A.

Information such as material properties, element type and thickness defined in I-DEAS cannot be inputted into the Madymo syntax file. Essentially, only the coordinates of each node comprising a mesh are transferable. In this sense, I-DEAS was used only for its drawing and meshing abilities. Also, the element types defined in I-DEAS were arbitrary. For example, when meshing the helmet with rigid facet elements, they were initially defined as triangular thin shell elements in I-DEAS. Then, these shell elements were later over-ridden and defined as triangular facet elements in the Madymo syntax.

Therefore, only the element shapes or number of nodes per element were important, as with the triangular 3 node elements in this example.

Once the mesh was created using I-DEAS, the file was exported as an I-DEAS Universal File. Hypermesh was then able to import this Universal File format. After being imported into Hypermesh, the file was exported again, this time as a Madymo Template File. This template contained the coordinates of every node, and element nodal information. Using the previous example, element one could be defined as a thin shell element formed by nodes 1, 2 and 3. Also, this shell definition could be converted to a facet definition by performing a "find and replace all" command with the keywords shell and facet respectively. Basically, Hypermesh only served the purpose of translating I-DEAS files into a Madymo format. Finally, the Madymo template file containing the proper nodal and element definitions could be cut and pasted directly into the Madymo syntax file.

3.4 Parametric Study Using Madymo

The primary objective of this study was to determine the worst-case position of the eye that induced the greatest Von Mises stress in the corneo-scleral shell upon impact with the night vision goggle. Secondary objectives included investigating the effect of the fatty tissue, extraocular muscles, goggle breaking away from the helmet mount, increased goggle mass, and wearing eye protection.

3.4.1 Dummy and Airbag Models

Madymo has a range of available dummy models, including male, female, and children models of different anthropometric dimensions. Of these different models, the adult Hybrid III is the most commonly used dummy in frontal impact applications. Therefore, a 50^{th} percentile male dummy was used in all simulations to best represent an average of the USA adult male population. Then, this dummy was positioned with the left arm at its side towards the collective, and the right arm between its legs towards the cyclic (Figure 3.24). This position visually represents that of a helicopter pilot during

flight. Next, a finite element airbag model was chosen that most resembled the actual airbag to be used inside the Army helicopters. No dynamic crash pulse was applied to the simulations in order to simplify the analysis and to compare the simulated results with experimental results performed in a laboratory.

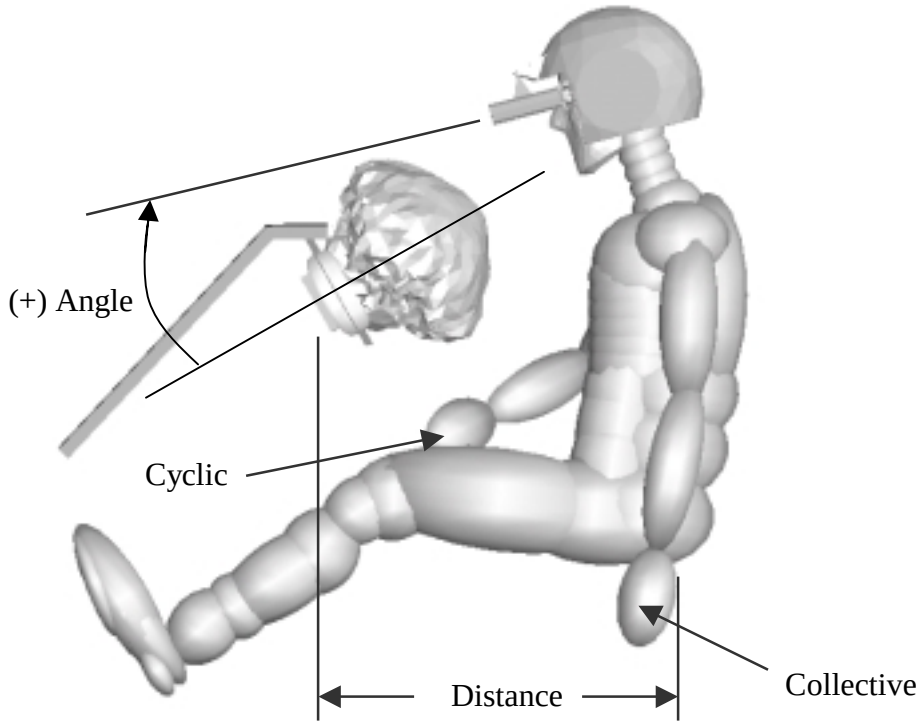

Figure 3.24 Location of the dummy and orientation of the eye, airbag deploying at time = 10 ms after trigger.

3.4.2 Worst-case Position Analysis

Three parameters were examined to establish the worst-case position. First, the distance between the eye and the goggle was varied (Figure 3.25). An arbitrary position of the dummy and orientation of the eye was chosen. This arbitrary choice is based on the assumption that the effects of changing this goggle distance would be similar at any given position and orientation. The impacting surface of the goggle was brought to within one millimeter of the apex of the cornea. The airbag was deployed and the maximum Von Mises stress sustained by the corneo-scleral shell was recorded. This same process was repeated five times, moving the goggle away from the cornea in 5 mm increments up to 25 mm.

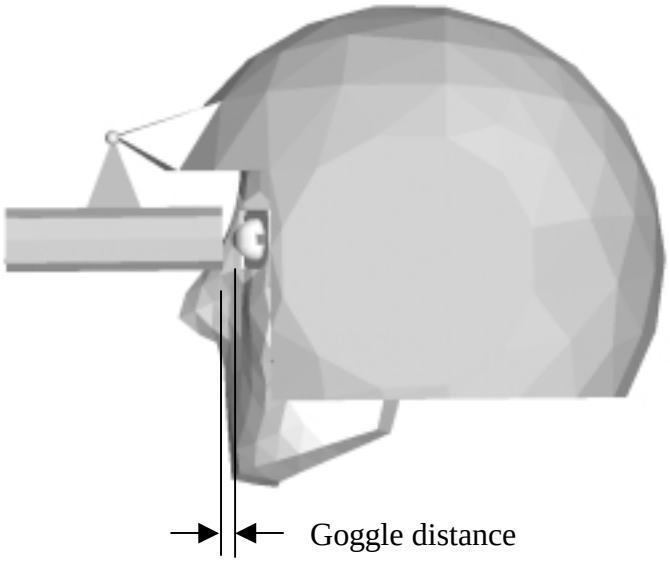

Figure 3.25 Distance varied between goggle and cornea.

Second, the horizontal distance between the occupant and the airbag module was varied (Figure 3.24). The range of horizontal distances was as follows: the dummy was brought close enough to the steering wheel so that the airbag actually pushed the goggle upwards away from the eye; then, the distance between the dummy and steering wheel was increased in increments of 50mm until the goggle was out of the airbag's reach.

Third, the angle between the line-of-sight and the normal to the airbag module was varied (Figure 3.24). The line-of-sight is also the anterior-posterior axis of the globe. For each of the above horizontal positions, the dummy's lower neck bracket was varied to create different angles between the line of sight and the airbag. The greatest angle between the line of sight and airbag that caused the airbag to push the goggle upwards and away from the eye was used as the upper limit. For example, when the dummy was looking straight ahead, or horizontally, the airbag comes into contact with the underside of goggle causing it to flip up rather than down. Once this limit was determined, the angle was decreased in increments of 6 degrees. In summary, the combination of goggle

distance, seating position, and line-of-sight angle that yielded the greatest Von Mises stress in the corneo-scleral shell was determined to be the worst-case position.

3.4.3 Effect of Fatty Tissue

After the worst-case position and orientation of the eye was determined, the fatty tissue was removed. This was done to evaluate previous studies that neglected modeling the fatty tissue (Kisielewicz, 1998). Therefore, in order to support the eye, all degrees of freedom at 9 nodes around the posterior pole of the sclera were fixed (Figure 3.26). Prior to this, the eye moved freely, only restricted by the fatty tissue and extraocular muscles. The observed behavior of the eye under impact and the maximum Von Mises stress were recorded.

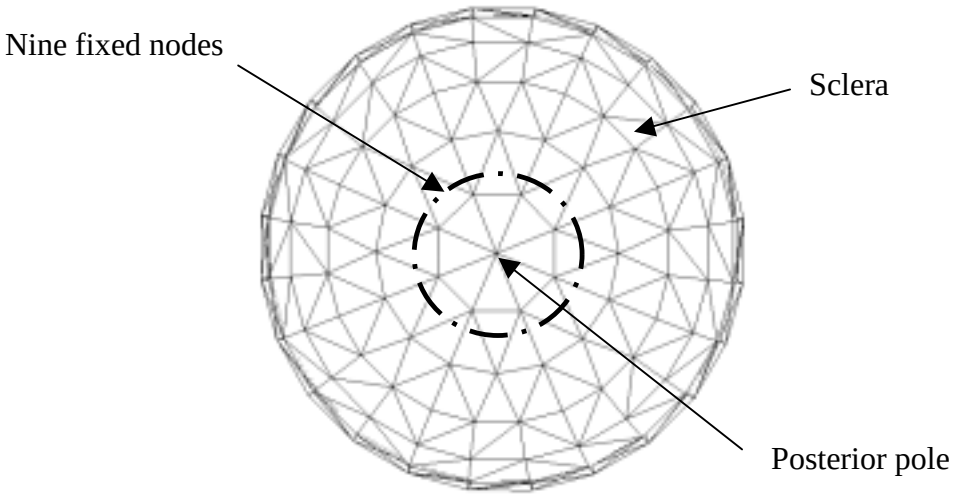

Figure 3.26 Nine nodes around the posterior pole were fixed.

3.4.4 Effect of Removing the Muscles

The boundary condition at the posterior pole was set free and the fatty tissue added back to the model. Then, all six extraocular muscles were removed to again evaluate previous studies that neglected modeling the muscles (Kisielewicz, 1998). The behavior and maximum stress under loading without the muscles were recorded.

3.4.5 Simulate Goggles Breaking Off

Pilots are recommended to fly with the goggles at distances greater than 20 mm from the eye (Figure 3.27). This distance allows the helicopter pilot to view the cockpit instrument panel by looking below rather than through the goggles.

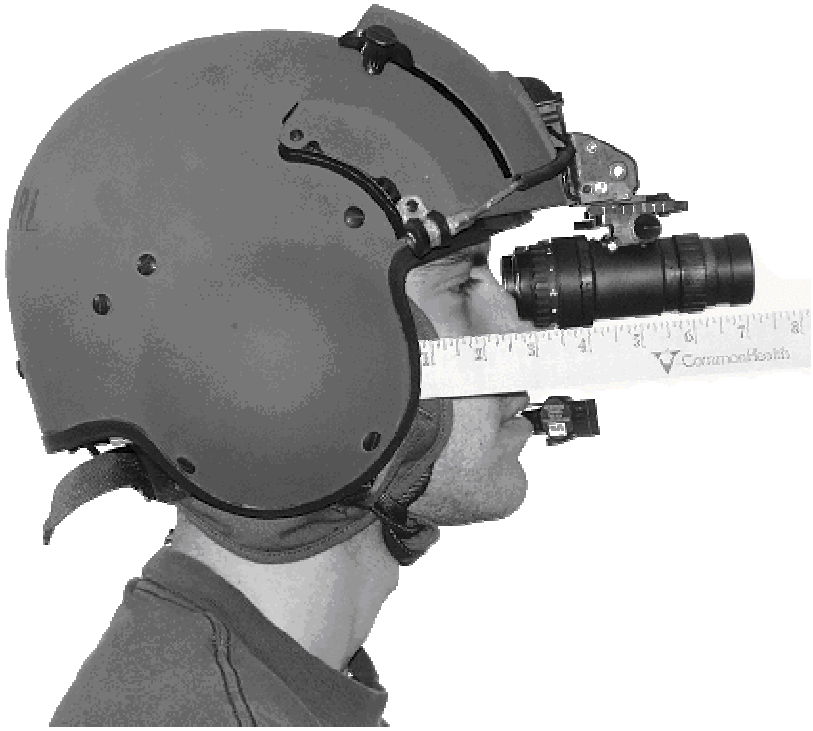

Figure 3.27 Goggle being placed at 20 mm (0.79 inches) from the apex of the cornea.

Therefore, a simulation was performed with the goggle placed at a distance of 20 mm from the eye. In order for the goggle to come into contact with the eye at this distance, the goggle would have to break away from the helmet mount. To allow this, the joint was changed to a free joint, which is analogous to no joint at all. When impacted by the airbag in the worst-case scenario, the goggle is essentially breaking off and being projected into the ocular area. The results under these conditions were recorded and compared to those found previously.

3.4.6 Increased Goggle Mass

In order to account for the load cells used in experimental tests with actual NVGs, the mass of the simulated NVGs was increased from 546 g to 620 g. Simulations in the worst-case position with the goggle breaking off from 20 mm were performed with both masses. The results were recorded and compared to investigate the effect this difference in mass would make.

3.4.7 Protective Lens Placed in Front of Eye

A sample protective lens was modeled and placed between the goggle and the eye (Figure 3.28). The lens geometry was chosen arbitrarily and meshed with rigid triangular facet elements using I-DEAS. A simulation with the lens in place was carried out under the worst-case position of the dummy. The muscles and fatty tissue were included and the 546 g NVGs were used in this simulation. The goggle was placed at 20 mm from the eye and broke away from the helmet mount as previously described.

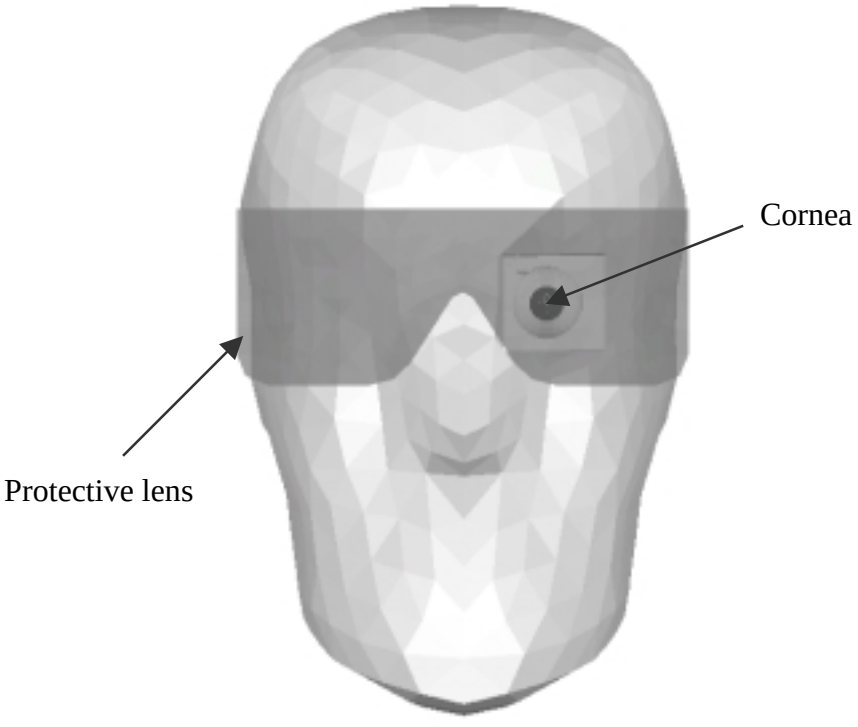

Figure 3.28 Protective lens placed in front of the finite element eye.

Chapter 4
Results and Discussion

4.1 Madymo Airbag Specifications

A simulated airbag was chosen to best represent the actual airbag used in the Army helicopters. The actual helicopter airbag volume was estimated to be 60 liters. Two finite element airbag models were available with Madymo: a driver side and a passenger side. The driver side airbag had a volume of 30 liters while the passenger bag was 160 liters. In addition, both airbag models included tethers, which makes a bag less spherical and more flat, like a donut without the hole in the middle. Also, these tethers could be removed to yield a slightly larger volume than with the restricting tethers. Accordingly, the driver side airbag model with the tethers removed was used for all simulations in this study. This airbag model had an approximate volume of 35 liters, the closest possible volume to 60 liters.

A common characteristic used to define an airbag is the leading edge velocity (Figure 4.1). This is the maximum velocity of the leading edge of the airbag during its deployment. This velocity is defined parallel to the direction of deployment.

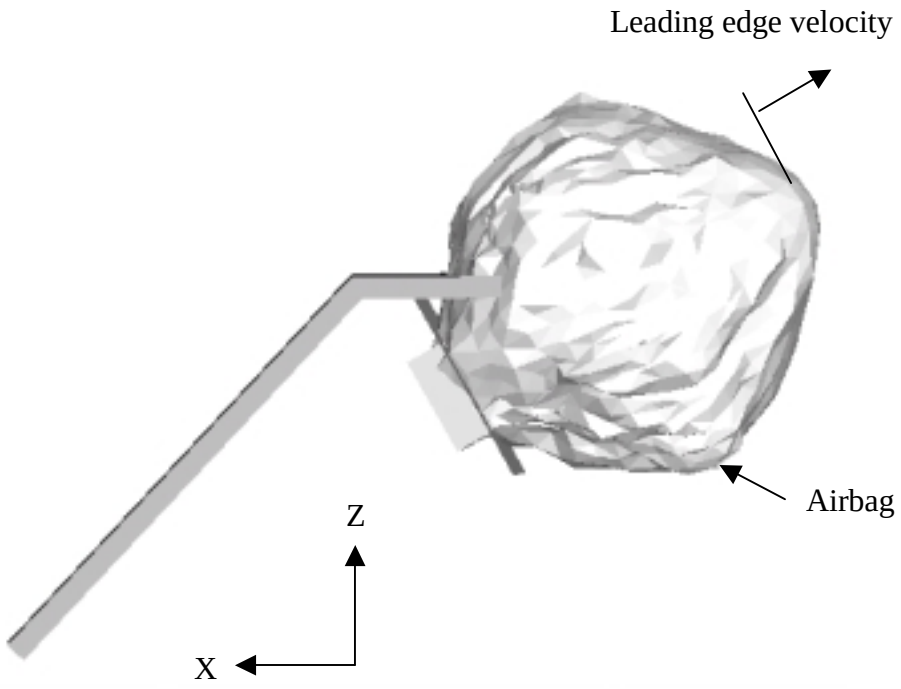

Figure 4.1 Leading edge velocity of airbag during deployment.

To determine the leading edge velocity, the velocity was recorded for a single node at the leading edge of the finite element airbag model. However, Madymo only outputs velocities in the x, y, and z coordinate directions. The direction of the airbag deployment was in the x-z plane, not aligned with either axis. Therefore, vector addition was used to determine a leading edge velocity of 81 m/s, or 181 mph. This is among the more aggressive airbags and provides a good approximation for the aggressive helicopter airbag (Powell, 1995).

4.2 Worst-case Position Analysis

First, the distance between the impacting surface of the goggle and the apex of the cornea was varied between 1 mm and 21 mm in 5 mm increments (Table 4.1). An arbitrary location of the dummy and orientation of the eye was used as discussed in Chapter 3.4.2.

Table 4.1 Goggle distance and Von Mises stress results.

Distance between goggle and eye (mm)	Max Von Mises stress (MPa)
1	8.3
6	7.9
11	7.6
16	3.7
21	0.0

On the fifth run, or 21mm away from the cornea, no contact resulted between the goggle and the cornea. This was because the goggle swings upwards towards the eye, about the revolute hinge joint at the attachment to the helmet (Figure 4.2). The goggle would continue to miss the eye at distances beyond 21 mm. Therefore, no simulations were performed beyond this distance.

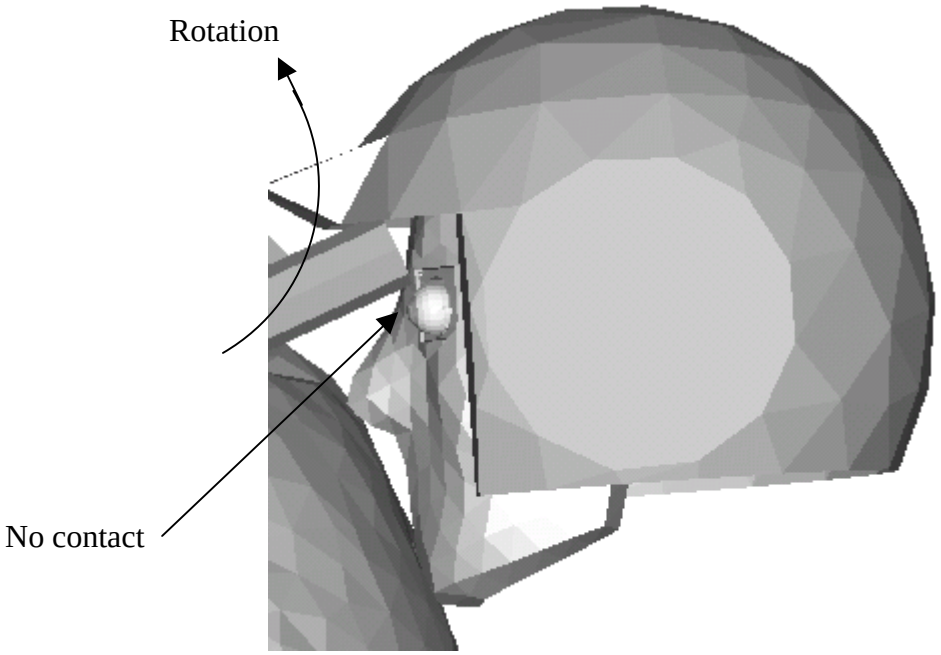

Figure 4.2 Goggle swings around revolute joint missing the eye.

For each simulation with a different goggle distance, the maximum Von Mises stress sustained by the corneo-scleral shell occurred at the point of impact with the goggle. Among all of these simulations, the minimum distance of 1 mm produced the greatest stress. Therefore, this distance was used in all remaining simulations to determine the worst-case position. The maximum stress was also found to decrease as the distance was increased (Figure 4.3). No stress resulted at the maximum distance of 21 mm because the goggle missed the eye.

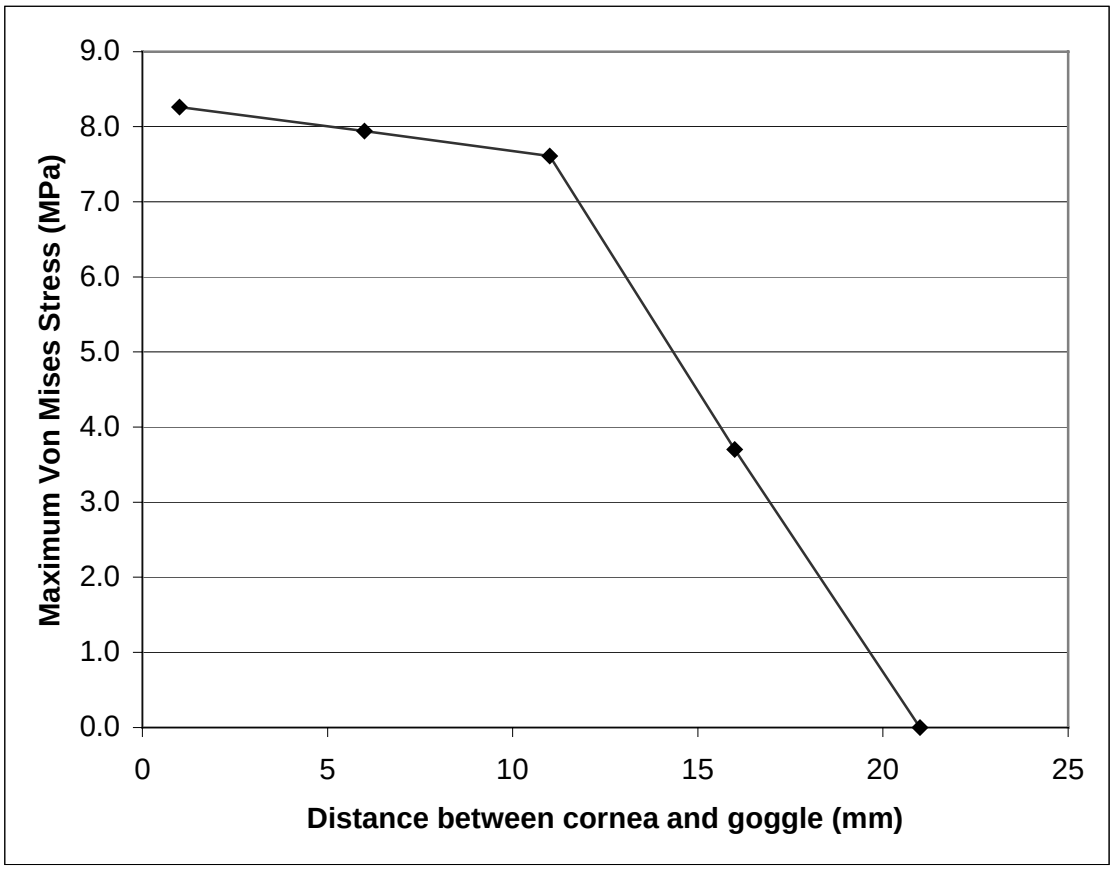

Figure 4.3 Maximum Von Mises stress in the eye versus goggle distance.

Second, the horizontal distance between the dummy and the airbag module was varied between 310 mm and 610 mm in increments of 50 mm (Table 4.2).

Table 4.2 Summary of Max Von Mises stress (MPa) results from parametric study.

Line of sight angle (deg)	Horizontal distance between dummy and the airbag module (mm)						
	310	360	410	460	510	560	610
6		Missed	Missed	Missed	Missed	Missed	
3	Missed	1.3	0.877	1.31	5.87	1.04	Missed
0					7.66		
-3	Missed	6.54	6.11	6.77	10.8	8.6	Missed
-6					8.21		
-9	Missed	7.75	8.31	7.09	9.38	6.92	Missed
-15		PC Failure	PC Failure	PC Failure	PC Failure	PC Failure	

This range of horizontal distances was chosen as follows: the dummy was brought close enough to the steering wheel so that the airbag actually pushed the goggle upwards away from the eye (Figure 4.4). Then, the distance between the dummy and steering wheel was increased in increments of 50mm until the goggle was out of the airbag's reach (Figure 4.5).

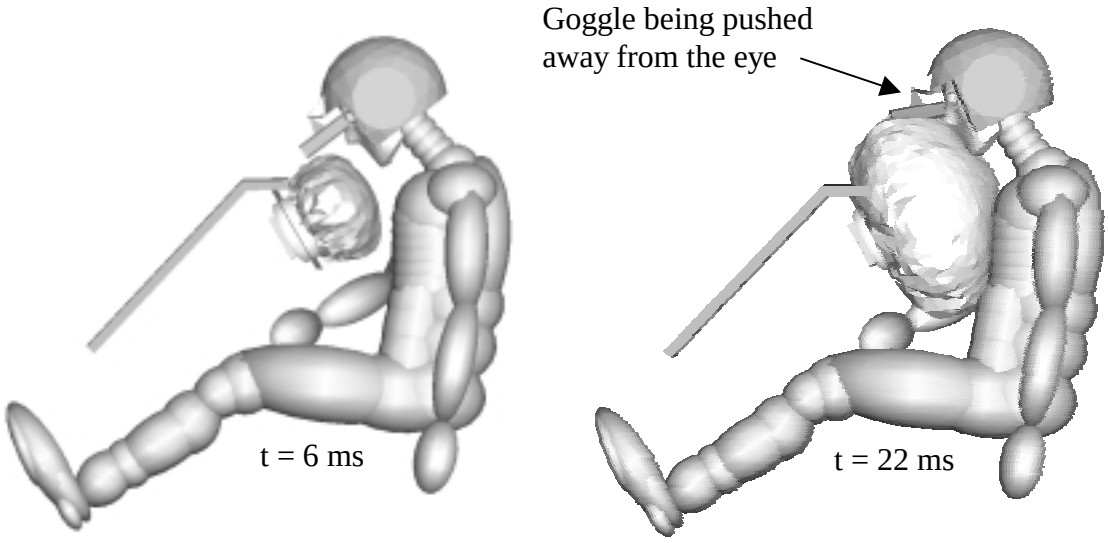

Figure 4.4 Dummy sitting too close to the airbag module, causing the airbag to push the goggle upwards (stage of deployment times listed).

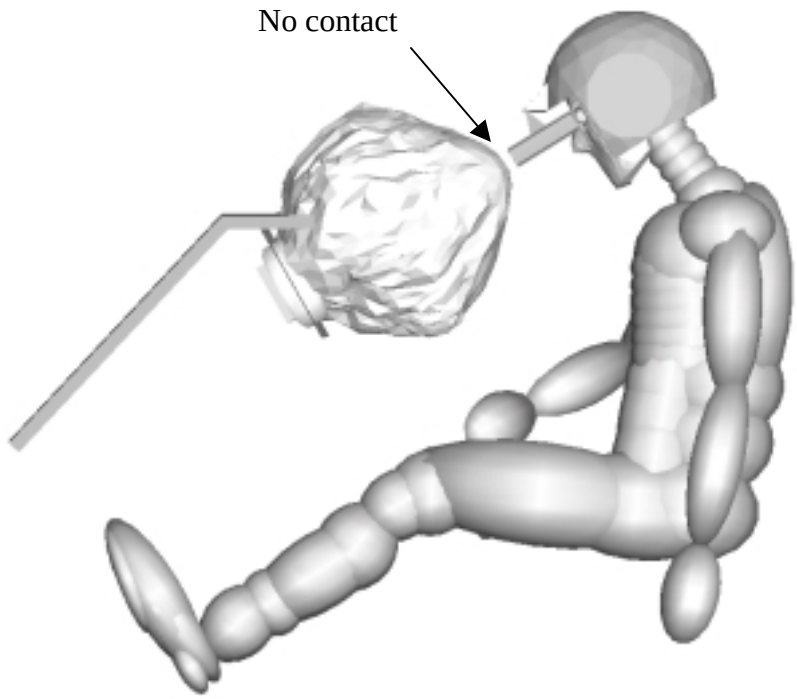

Figure 4.5 Dummy sitting out of the airbag's reach, deployed 14 ms after trigger.

Third, for each of the above positions, the dummy's lower neck bracket was varied to create different angles between the line of sight and the airbag. The greatest angle between the line of sight and airbag that caused the airbag to push the goggle upwards and away from the eye was used as the upper limit. For example, when the dummy was looking straight ahead, or horizontally, the airbag came into contact with the underside of goggle causing it to flip up rather than down. Once this limit was determined, the angle was decreased in increments of 6 degrees (Table 4.2).

With the dummy looking in the most horizontal direction, no contact occurred because the goggle was pushed upward by the airbag. When the dummy lower neck bracket was bent past a certain point, all computer simulations went unstable. More specifically, when the dummy was positioned so as to look at –15 degrees (eyes aimed towards feet), the computer crashed while solving the programs. Much effort was made to investigate and possibly solve this condition without any success. This computer

failure at an angle of –15 degrees to the airbag deployment vector took place at all dummy positions. Similar to the dummy position parameter, the line of sight parameter was also bounded at each extreme. However, one extreme contained no contact with the goggle while the other resulted in computer failures.

A worst-case distance between the dummy and the airbag became more apparent after plotting the data (Figure 4.6). At each angle simulated, this horizontal position of the dummy produced the greatest stress, always occurring at the point of impact with the goggle. This position was at neither of the extremes, but rather at the next to furthest position from the airbag. Two more intermediate points were determined at –6 and 0 degrees to check for extreme discontinuities in this worst-case distance curve (Table 4.2).

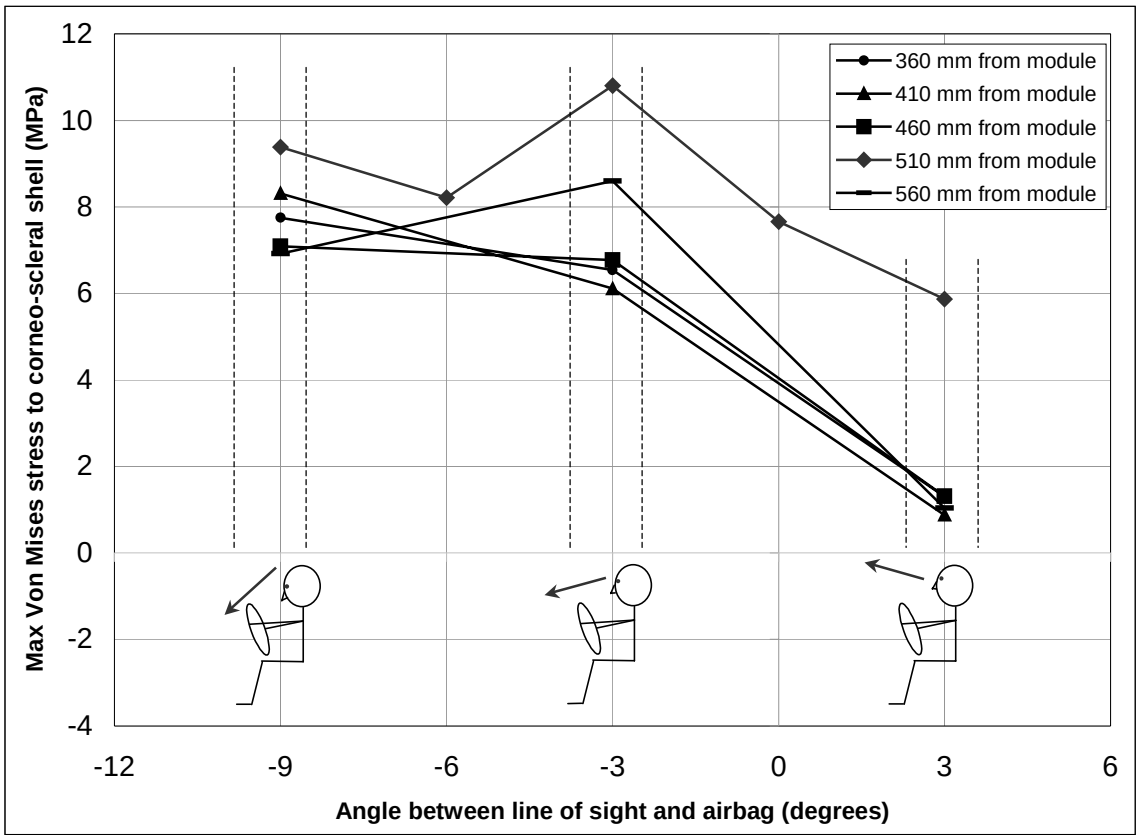

Figure 4.6 Maximum Von Mises stress as a function of sitting position and line of sight.

The maximum Von Mises stress experienced by the corneo-scleral shell was 10.8 MPa and occurred when the dummy was sitting 510 mm from the airbag module, looking at –3 degrees from the airbag. This angle was also at neither extreme, but instead in the middle of the range of angles simulated. With the dummy placed in this worst-case position and line of sight, it is looking almost directly into the center of the airbag (Figure 4.7).

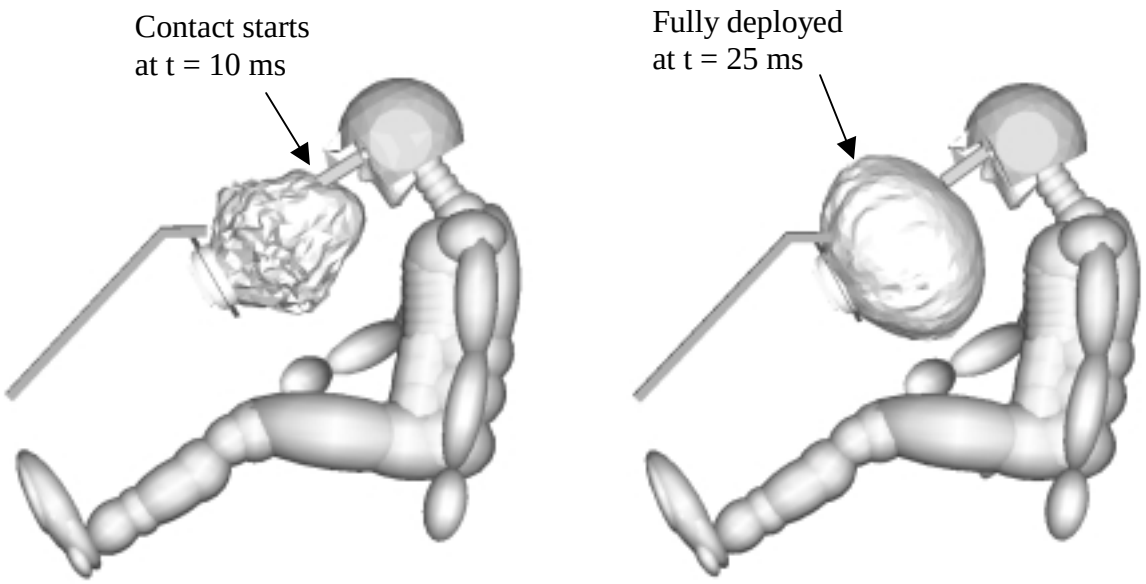

Figure 4.7 Worst-case line of sight and horizontal position of the dummy.

The airbag also begins to come into contact with the goggle at approximately half way through its deployment (Figure 4.8). The airbag requires about 25 ms to reach its fully deployed volume of 35 L. Contact with the goggle begins to occur at 10 ms after the onset of inflation. An explanation for goggle contact during this stage of deployment resulting in the maximum stress is now provided. The airbag can develop two types of forces: a punch-out and membrane force. The punch-out force is due to the fabric being projected out through the module. A membrane force results from the pressurization of the airbag by the inflator. In the initial stages of deployment, punch-out forces would be larger than membrane forces. In this stage, the goggle would be impacted with fast

moving fabric but with not much internal pressure. On the other hand, the opposite would hold if the goggle were impacted near the final stages of deployment. The velocity of the fabric would be less while the internal airbag pressure would be much larger. The result would be larger membrane than punch-out forces. Therefore, at half way through its deployment, the airbag may be transferring a combination of these two forces to the goggle.

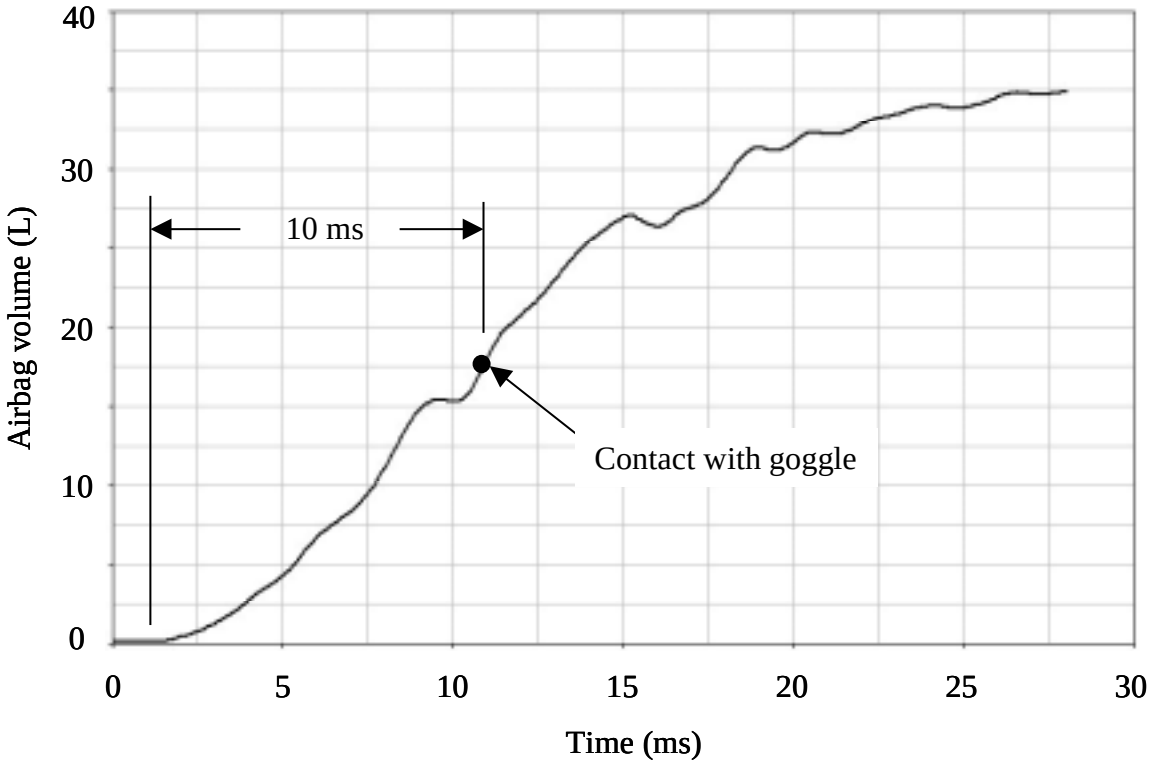

Figure 4.8 Contact between goggle and airbag for the worst-case scenario.

As seen in Figure 4.6, there is no obvious relationship between maximum Von Mises stress sustained by the eye and line of sight at a given sitting distance. At the worst-case distance of 510 mm, the stress fluctuates as the dummy head is raised. This is due to the fact that the horizontal and vertical distances between the eye and the airbag change as the dummy head is rotated. For example, consider two cases: dummy A is looking downward, while dummy B is looking forward (Figure 4.9). Although dummy A

and B are sitting the same distance from the airbag module, the eyes of dummy A end up being closer to the airbag because of the lower neck angle.

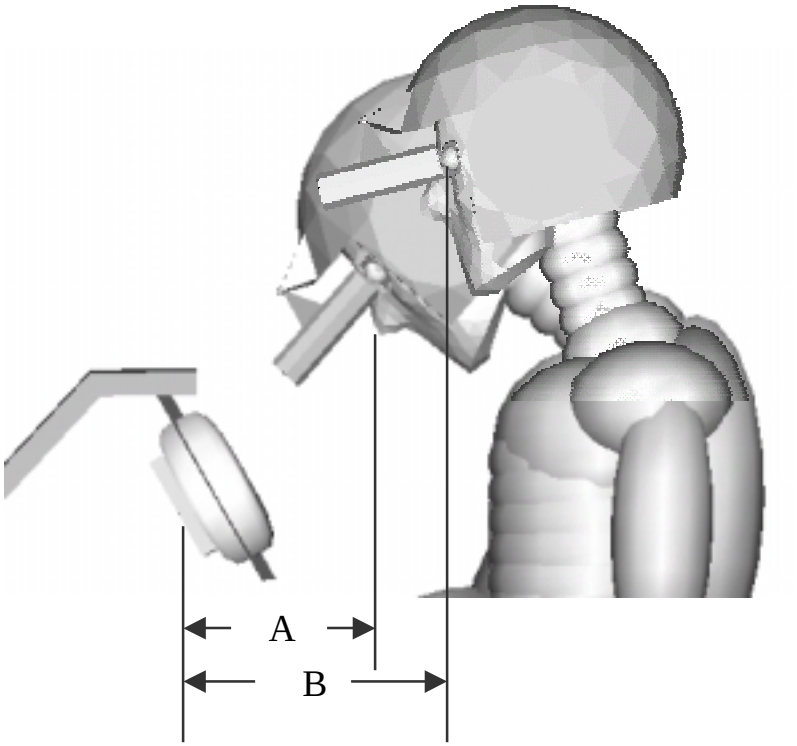

Figure 4.9 Distance between airbag and eye change as the lower neck angle varies.

The above phenomenon made it necessary to calculate the horizontal and vertical distances between the apex of the cornea and the center of the airbag module (Table 4.3). By doing so, the positions can be more accurately reproduced in future experimental tests and the results better correlated.

Table 4.3 Horizontal and vertical distance between apex of the cornea and center of the airbag module: horizontal (vertical) (mm).

Line of sight angle (deg)	Horizontal distance between dummy and the airbag module (mm)						
	310	360	410	460	510	560	610
6		Missed	Missed	Missed	Missed	Missed	
3	Missed	182 (278)	232 (278)	282 (278)	332 (278)	382 (278)	Missed
0					324 (267)		
-3	Missed	169 (260)	219 (260)	269 (260)	319 (260)	369 (260)	Missed
-6					311 (243)		
-9	Missed	156 (238)	206 (238)	256 (238)	306 (238)	356 (238)	Missed
-15		PC Failure	PC Failure	PC Failure	PC Failure	PC Failure	

4.2.1 Post Processing Analysis

As mentioned, the worst-case combination of distance between the goggle and the cornea, eye and the airbag module, and line of sight orientation, produced a maximum Von Mises stress of 10.8 MPa within the corneo-scleral shell. This maximum stress occurred just below the apex of the cornea where the goggle made contact (Figure 4.10).

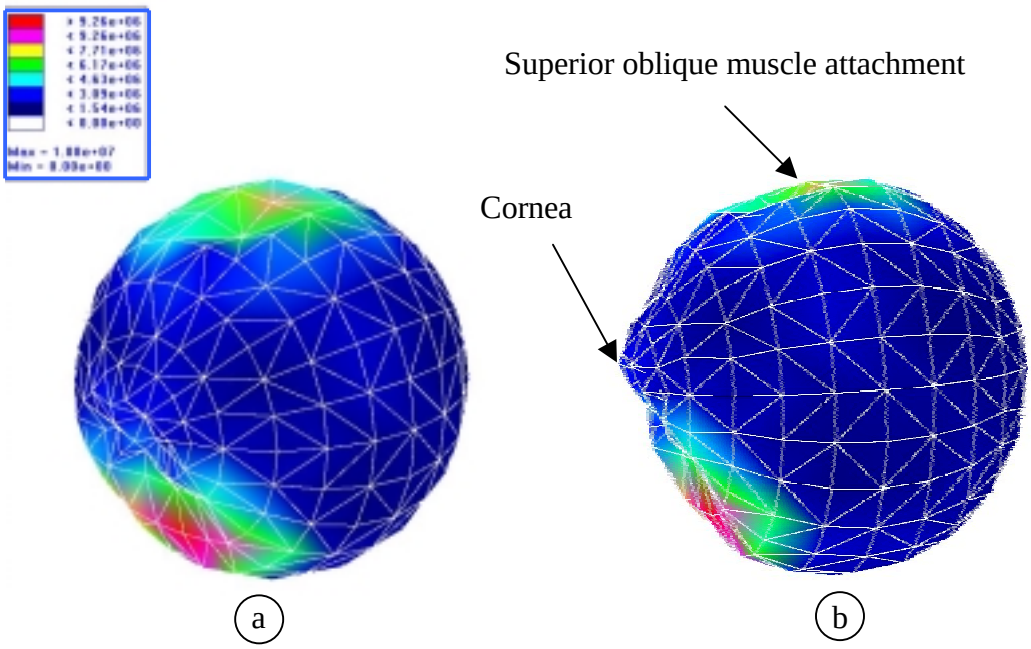

Figure 4.10 Contour plot showing stress concentrations of the deformed eye after being impacted with the NVG: a) isometric view, b) nearly lateral view

Another region of high stress developed at the superior area of the sclera. This may have been due to the tension produced by the superior oblique muscle under loading. As the goggle came into contact with the inferior region of the cornea, the globe rotated so that the cornea was pointing upwards toward the roof of the orbit (Figure 4.11). The superior oblique muscle provides resistance to this rotating motion. A second possible contributor to this region of stress at the superior region of the sclera is the pressure between the globe and orbital fatty tissue as the globe is being pressed upward by the impacting goggle.

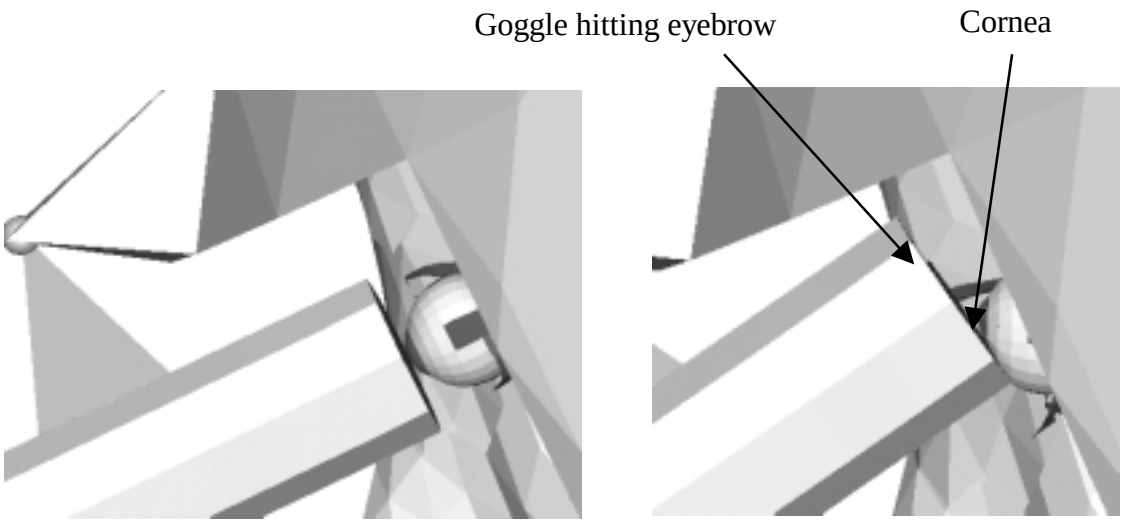

Figure 4.11 Goggle impact causing the eye to aim upward, then hitting the forehead.

4.2.2 Contact Forces to Eye and Orbit

Both the contact force between the rigid goggle and the eye, as well as the headform, were calculated for the worst-case position. The goggle-headform and goggle-eye contact interactions were defined to behave like skin contacting a rigid surface (Appendix B, page 131). This contact type was already available in Madymo, used to represent the forehead skin coming into contact with rigid, or nearly rigid surfaces. Reported in a tabular form, surface interaction properties such as coefficient of friction are included in this "skin" contact interaction.

The contact force to the eye was 14.1 N for the worst-case position. The contact force to the eyebrow region of the frontal bone was 1255 N (Figure 4.12). The large discrepancy in these two forces can be explained by the different elastic foundations. The fatty tissue provides a large amount of dampening behind the eye, allowing it to compress into the eye socket under loading. On the other hand, the eyebrow of the headform is nearly rigid, with the damping material properties of forehead skin being included. Schneider and Nahum (1972) impacted the skull bones with a 1.0 in^2 cylindrical impactor to determine the force required to cause fractures. The frontal bone was impacted in the forehead region and had a fracture force of 5780 N. An orbital bone, the zygomatic bone, required 1450 N to fracture. Therefore, the 1255 N force induced to the eyebrow region by the goggle may cause fracture. This level of force is significant enough to require attention in future laboratory experiments.

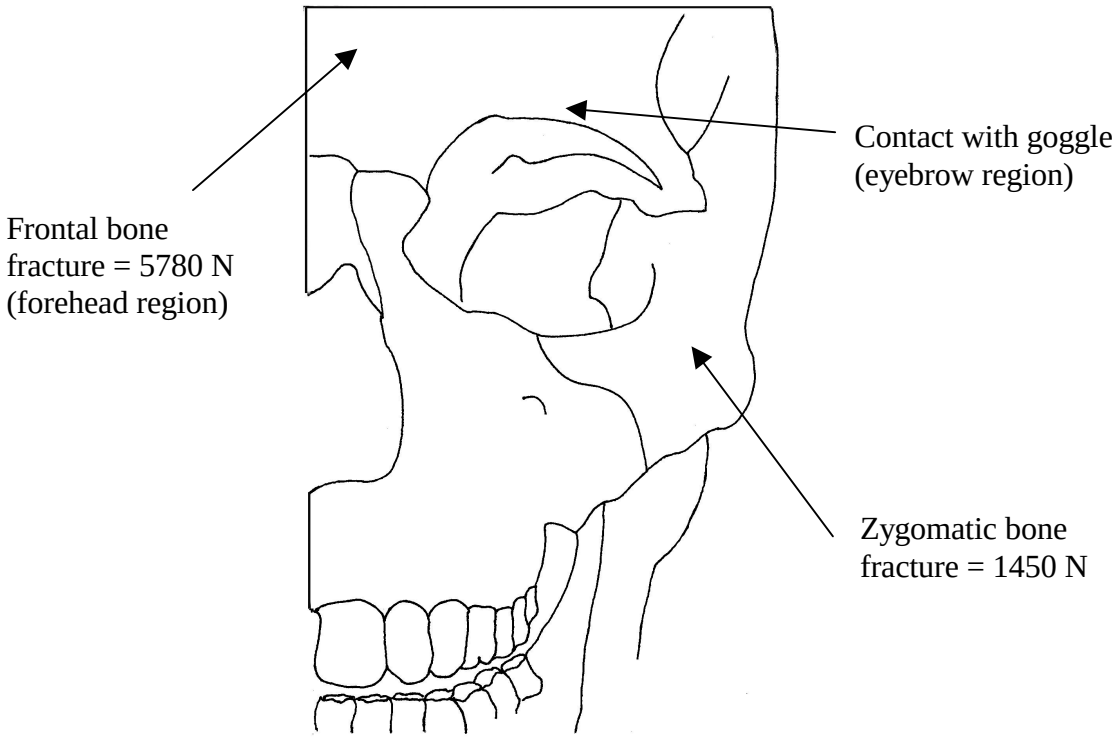

Figure 4.12 Fracture strength of orbital and facial bones.

4.3 Effect of Fatty Tissue

The boundary condition around the posterior pole of the sclera was fixed and the fatty tissue removed as mentioned in chapter 3.4.3. Nine nodes around the pole were fixed rather than one to facilitate distributing the stress concentration. As would be expected, this fixed condition greatly increased the stress experienced by the eye (Table 4.4). The level of force and deformation under these conditions cause the model to approach non-stable conditions. Therefore, more effort in increasing this stability is required before the level of increased stress can be quantified.

Table 4.4 Summary of max Von Mises stress in the eye for each simulation.

	With muscles	No muscles	With muscles, fixed pole
546 gram goggles Revolute joint Does not break off Worst-case position	10.8 MPa	7.11 MPa	Much larger
546 gram goggles Free joint Goggles break off 20 mm from eye	4.0 MPa	NP	NP
620 gram goggles Free joint Goggles break off 20 mm from eye	4.4 MPa	NP	NP
546 gram goggles Free joint Goggles break off 20 mm from eye Protective lens in place	2.2 MPa	NP	NP

* NP = Not Performed

4.4 Effect of Removing the Muscles

With the fatty tissue added back to the model, all six extraocular muscles were removed from the worst-case scenario to investigate their effect, if any, on the maximum stress and behavior sustained by the eye under impact. Without the muscles, the maximum Von Mises stress decreased to 7.11 MPa, compared with 10.8 MPa with the muscles (Table 4.4). At first, such a large change would not be expected since the four straight muscles were modeled as tension-only materials and are being loaded in compression. However, all six muscles add resistance to rotations of the eye. Without the muscles, the eye was able to rotate within the fatty tissue without resistance (Figure 4.13). The goggle caused the eye to spin, aiming the cornea upward further. The globe actually spun 90 degrees so that the line of sight was directly toward the roof of the orbit. The muscles add stiffness to these rotations under loading (Figure 4.10). Thus, stiffer boundary conditions will result in greater stress as seen in these simulations.

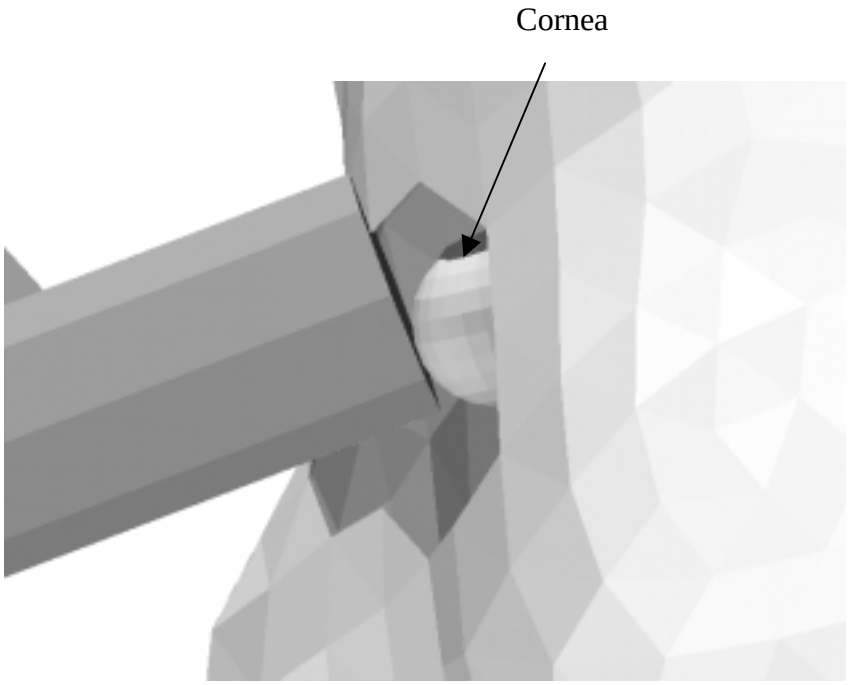

Figure 4.13 Goggle causing the eye to spin without the muscles (fat and orbit removed for illustration only).

4.5 Simulate Goggles Breaking Off

Pilots are recommended to place the NVGs no closer than 20 mm from the apex of the cornea. Therefore, a simulation was performed with the goggle placed at 20 mm from the eye. The joint was changed to a free joint to allow the goggle to break off and be projected into the ocular area. The maximum Von Mises stress was 4.0 MPa under these conditions. As would be expected from the results in chapter 4.2, this stress was less than the stress of 10.8 MPa with the goggle approximately 1mm from the eye.

4.6 Increased Goggle Mass

Using the above conditions, the entire goggle mass was increased from 546 g to 620 g to account for the added mass of load cells used under experimental conditions. The maximum Von Mises stress in the eye was 4.0 MPa with the 546 gram goggle. With the 620 gram goggle, the maximum stress was slightly higher at a peak of 4.4 MPa. Although at first this seems counterintuitive due to the increased inertia of the heavier NVG, closer examination of the airbag kinematics explains the increase in peak stress. The airbag used for these simulations is very aggressive and seems to be a good match for the actual airbag used in the experiments. For small masses such as the 546 g and the 620 g, the airbag deployment is unaffected. In other words, the airbag is so powerful that the leading edge velocity of the airbag is unchanged by the mass of the NVG. Therefore, both NVGs are traveling at the same velocity when they impact the eye. Thus, the heavier NVG has slightly more kinetic energy and results in slightly higher eye stress. The same trend was seen with the loads on the rigid orbital structures.

In summary, the difference in stress observed in the eye for the two NVGs of different masses was less than 10%. Given the aggressiveness of the airbag, and the accuracy of the simulations, it does not appear that this change in mass will have any appreciable affect on the experimental results.

4.7 Protective Lens Placed in Front of Eye

As described in Chapter 3.4.7, a rigid protective lens was placed between the eye and 546 gram goggle (Figure 4.14). The goggle was allowed to break off at 20 mm from the eye with the dummy in the worst-case scenario. After breaking away from the helmet mount, the goggle was projected in the protective lens, propelling the lens into the cornea and headform model. The protective lens made less contact with the eye, experiencing a maximum Von Mises stress of 2.2 MPa, approximately one half of the 4.0 MPa found without the protective lens. In contrast, the contact force to the eyebrow region of the headform model increased to 1760 N, greater than the 1255 N force generated in the worst-case scenario without a protective lens. This interaction seems logical as the protective lens shields the eye and transfers the energy to the orbital bones, which protect the globe from impacts with objects larger than the orbital opening.

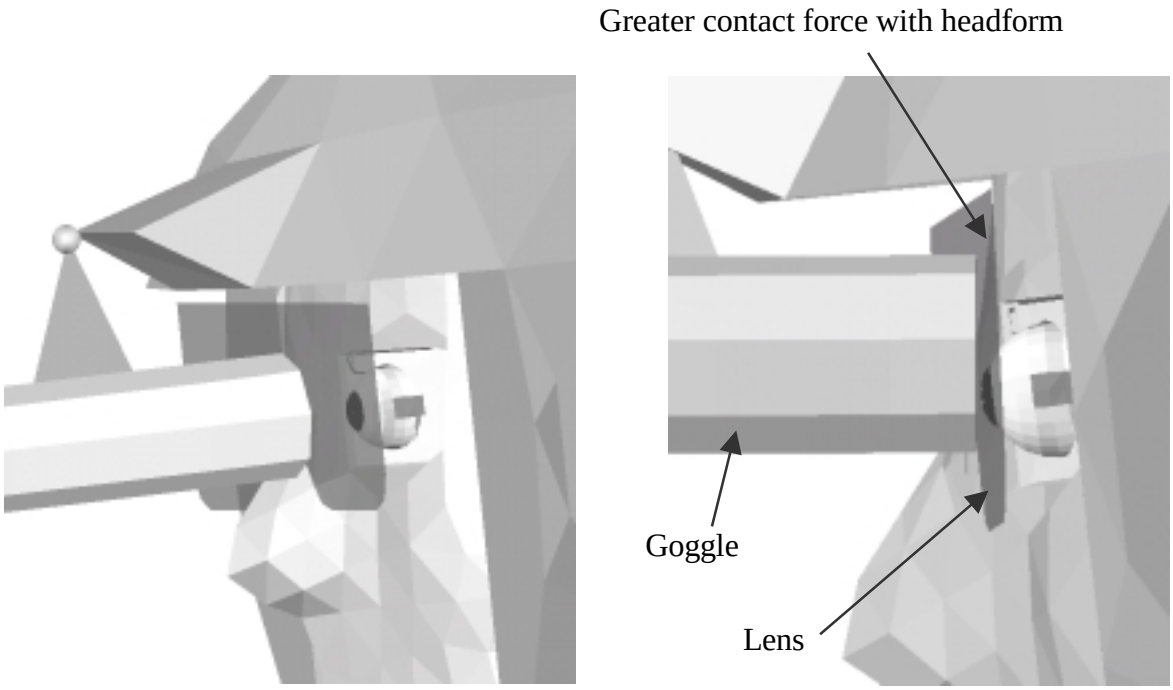

Figure 4.14 Protective lens making contact with the headform and corneal apex.

4.8 Comparison with Experimental Results Found in the Literature

Although the primary objective of this study was to determine the worst-case position of the helicopter pilot, the stresses predicted by the finite element eye model were compared with experimental results found in the literature. This was done to get a quantifiable assessment of the validity of the results predicted by the eye model. Finite element models can be very powerful tools to the engineer, but can also become dangerous if no hand calculations, or comparison with experimental results is performed to get a better feel of how realistic the predicted results are.

Ideally, experiments with human eyes being impacted with night vision goggles would need to be performed to validate the model. At the time of this report, these tests were in progress. No other such data was available in the literature. However, many tests have been performed using pig eyes because of their similarity with human eyes. Scott (2000) impacted pig eyes with cylindrical steel rods of various sizes and mass. It was determined that a relationship between the level of projectile kinetic energy and ocular injury severity existed. No globe ruptures were produced in these tests, even with kinetic energies reaching 1.9 J. Vinger (1997) impacted pig eyes with paintballs and golf balls. From these tests, it was determined that the globe ruptured at kinetic energies above 13.9 J.

The simulation with the 273 gram goggle breaking off was used to model a cylindrical rod being projected at the eye. The stress produced to the corneo-scleral shell was 4.0 MPa in this simulation, which would not cause rupture according to the material properties gathered from the literature and used in the formulation of the eye model (Figure 4.15).

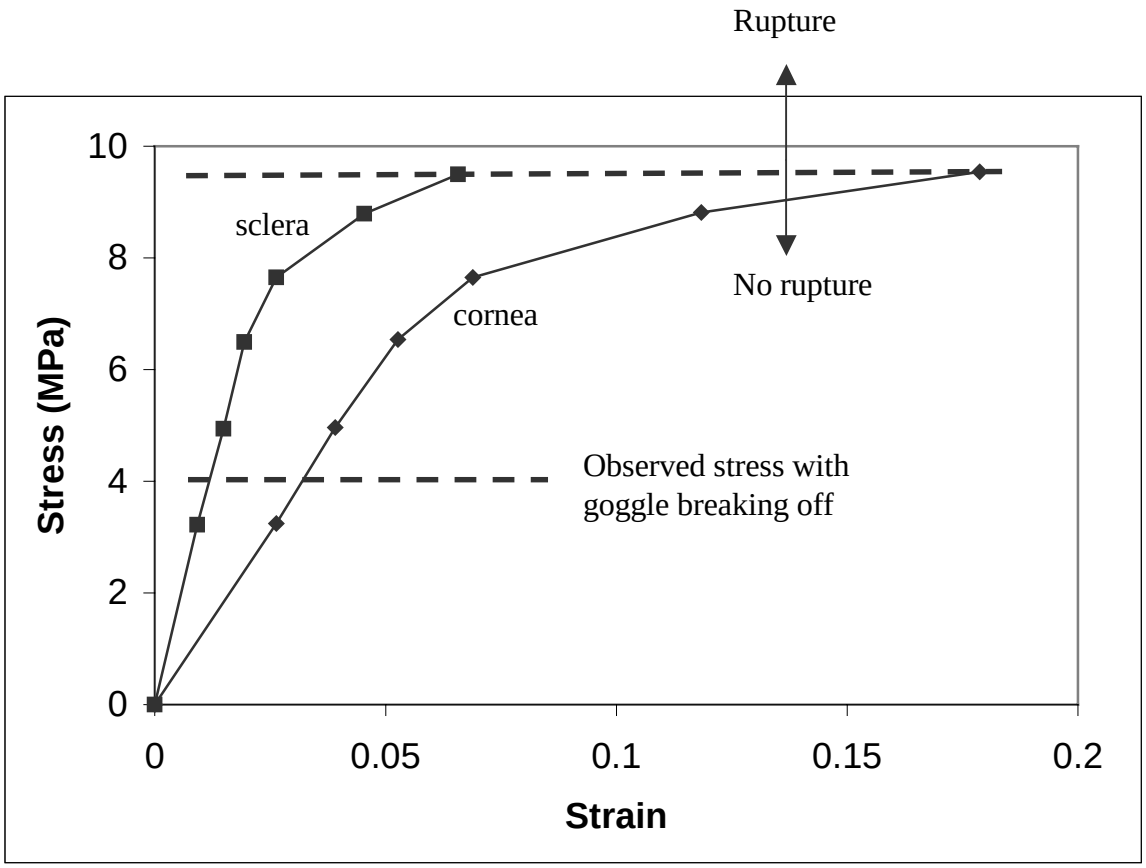

Figure 4.15 Rupture strength of the human cornea and sclera from strip tests.

Next, the velocity of this projected goggle was found to be 7.16 m/s, determined by the Madymo linear velocity output file (*.lvl). Using the 273-gram mass of the goggle, the kinetic energy ($\frac{1}{2} \times Mass \times Velocity^2$) was determined to be 7.0 J. This energy is below the 13.9 J required to cause rupture in pig eyes with various spherical objects (Figure 4.16). It is also greater than the 1.9 J that produced various internal injuries without rupture in pig eyes with cylindrical rods.

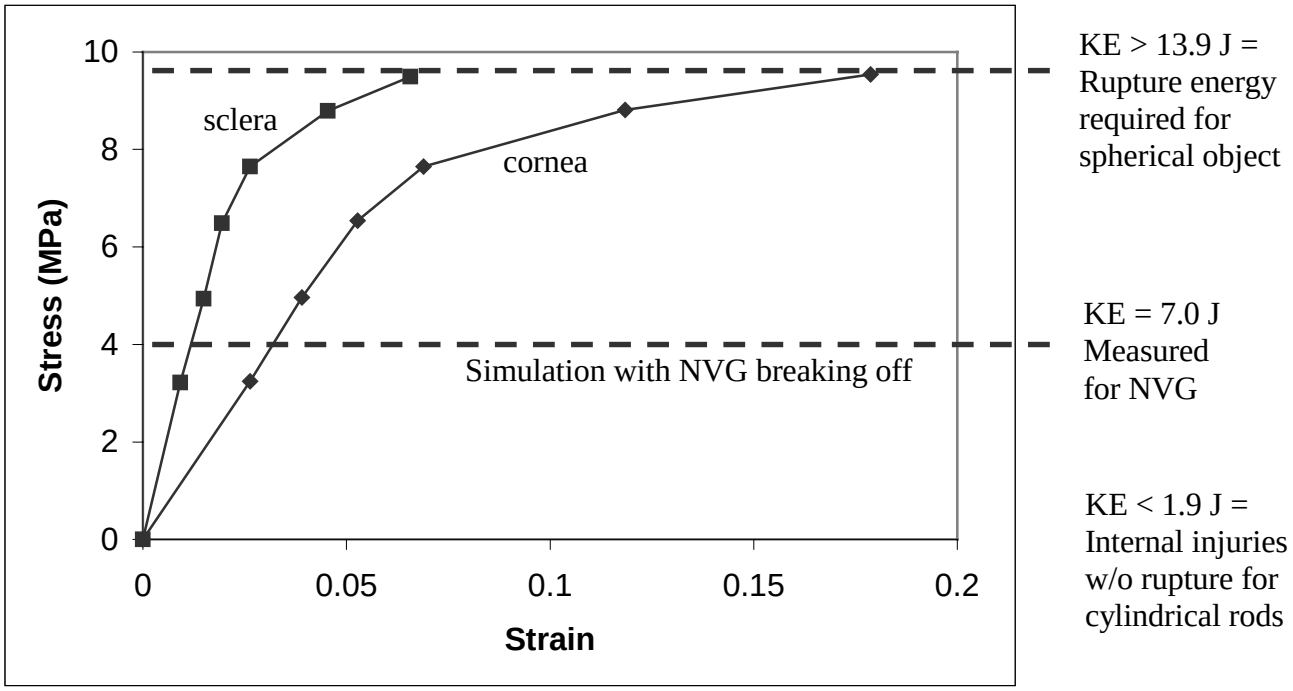

Figure 4.16 Kinetic energy of the goggle is less than rupture energy for pig eyes.

In summary, when the kinetic energy of the projected goggle was 7.0 J, the FE eye model predicted no globe rupture. With experiments involving pig eyes, no ruptures occurred with energies below 1.9 J (cylindrical rods), but did occur above 13.9 J (spherical objects). Therefore, although the experiments were with pig eyes and NVGs were not used, this comparison does provide a quantifiable assessment of the validity of the results predicted by the eye model.

Chapter 5
Conclusions and Recommendations

5.1 Conclusions

The primary objective of this research was to determine the worst-case position and orientation of a helicopter pilot wearing night vision goggles to be in during an airbag deployment. This worst-case position resulted in the greatest Von Mises stress in the finite element eye model. This position was then used to help guide experimental tests. At the time of this report, these tests were currently being conducted. From the findings of this study, the following worst-case scenario was recommended for testing (Figure 5.1):

1) Orient the pilot so as to look directly into the airbag
2) Allow the airbag to begin making contact with the NVGs in the middle of its deployment stage
3) Place the NVGs as close the eyes as realistically possible
4) Leave the extraocular muscles and fatty tissue intact

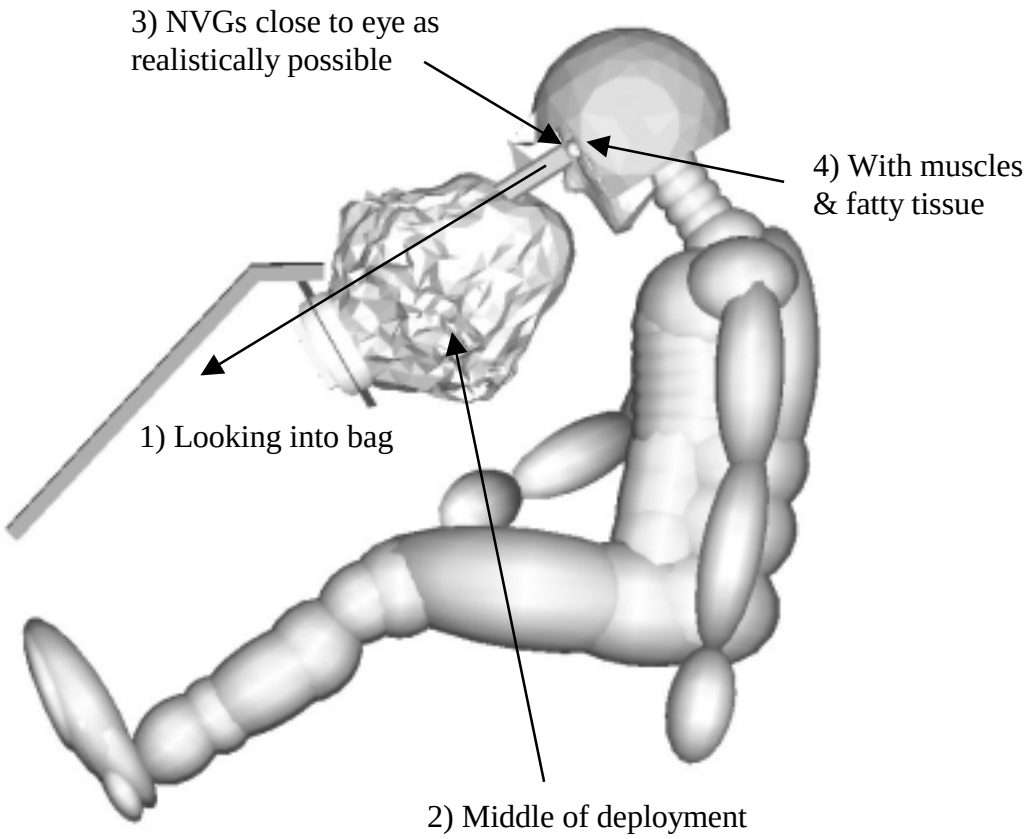

Figure 5.1 Worst-case position and orientation of pilot recommended for testing.

Rather than recommending specific distances between the globe and airbag module, the above normalized recommendations were provided. These recommendations were all made with respect to the airbag used in Madymo but can still be applied to the actual airbag used in helicopters. Specific distances relative to the airbag module would not be valid and should not be recommended until the actual airbag is modeled with Madymo, as discussed in Chapter 4.1. The Madymo technical support staff is sometimes willing to provide specific airbag models upon request. Therefore, a bag with the actual airbag volume could be used in future simulation work.

In addition to the primary objective of this study being satisfied, all secondary objectives were completed. Not included in previous studies, the fatty tissue and extraocular muscles were found to have a significant effect on the results in this study. By removing the fatty tissue and fixing the posterior pole of the globe, the stress in the eye greatly increased. The extraocular muscles provided resistance to rotations of the globe under loading. Without the muscles, the eye was free to spin within the orbit and the stress in the eye decreased. In addition, simulations with both the goggle remaining fastened and breaking away from the aviator helmet were performed. To account for the additional mass of load cells used in experiments, NVGs of 546 g and 620 g mass were projected into the ocular region. The stresses induced to the eye for the two different goggles were within 10% agreement of each other. Finally, placing a protective lens in front of the eyes was found to reduce the stress to the eye but increase the force experienced by the surrounding orbital bones.

At the time of this report, tests were being conducted under the recommended worst-case positions. So far, all the results found experimentally qualitatively agree with those predicted by this study. When the NVGs were placed at a distance of at least 20 mm from the eye, the goggles broke off, the globe did not rupture, and the orbital bones fractured. As predicted by this study, the globe would not rupture with the goggles breaking off from this distance to the eye. The contact force to the orbital bones was between 1 and 4 kN, in the range of those predicted in this study. No other quantitative data to compare with was available at the time of this report.

5.2 Additional Applications with the FE Human Eye Model

Many people requiring vision correction elect to have a surgical procedure performed. Some of these procedures involve several incisions that form into scar tissue (radial, hexagonal, and astigmatic keratotomy), while newer laser methods do not.
Most research suggests that eyes having undergone incisional refractive surgery are significantly more susceptible to injury (Alvi *et al*., 1995; Binder *et al*., 1988; Rashid and Waring, 1992; Vinger *et al*., 1996). Even the newer methods with lasers may result in an

increased risk of ocular injury from blunt trauma (Lemley *et al*., 2000; Leung *et al*., 2000; Norden *et al*., 2000). Such procedures could be investigated with the FE eye model presented. The geometry and material properties of the resulting scar tissue would need to be incorporated.

The structure of the orbit will be different for individual pilots. This difference based on ethnic origin may place some pilots at a higher risk of ocular injury due to less pronounced frontal and nasal bones. These parameters could be examined with additional simulations that included more accurate and detailed orbital bone geometries. More accurate material properties of the bony orbit could also be incorporated to investigate orbital blowout fractures. An orbital blowout fracture refers to fracture of the orbital floor or walls without fracture of the orbital rim. Airbags have been found to produce enough force to cause a blowout fracture. A 37-year old woman sustained a blowout fracture after her airbag was deployed during a 30 mph collision (Cacciatori *et al*., 1997).

Efforts to include the material properties of PVC or other materials into the design of the protective lens could be incorporated in future work, but would likely have a minimal affect on the results found here. On the other hand, a modification that could be examined that would have more practical implications is the design and geometry of the protective lens. The lens design could be maximized to distribute the impact force over the largest area or the strongest bones in the orbit.

5.3 Recommendations for Future Simulation Improvements

Several assumptions were made in the formulation of the finite element eye model. All of these assumptions, such as geometry of the muscles, or material properties of the vitreous and aqueous were made because no data was available. This data should be incorporated into the model when made available. All anisotropic and viscoelastic behavior was also neglected. Ocular tissues have been found to exhibit both of these behaviors. Therefore, it is recommended that such behavior be included in future

improvements to the FE eye model. Further validation of the model should be conducted when the results of the experimental work currently in progress are made available.

No mesh convergence was performed in this study but should be done in the future. The process of completing a mesh in I-DEAS and translating it into Madymo via Hypermesh is a very time consuming process. As the mesh is refined, the elements become smaller, and thus require a smaller time step for Madymo to solve the models. The time step used to solve the Madymo model with the dummy and airbag, but no ocular structures, was 0.2×10^{-4} seconds and required approximately 1 minute to solve. On the other hand, with the FE eye included, a time of step of 1.1×10^{-6} seconds was used, requiring approximately 18 minutes to solve. TNO advises that time steps below 1.0×10^{-6} seconds are not normally used. TNO also stated that many Madymo users believe that smaller time steps lead to errors. However, no justification for this belief is available. Time steps below 1.0×10^{-6} seconds were attempted in this study, but all of these models failed. This may be justification for the use of a different software package.

In addition, the models presented crashed when a time step of 1.0×10^{-6} seconds was used. TNO reported that this phenomenon might just be a bug within Madymo. Also unexplainable, is that one time step below1.0×10^{-6} seconds did solve. With a time step of 6.05×10^{-7} seconds, the modeled solved rather than crashing or locking up. However, incorrect airbag behavior was exhibited with this time step, and it was therefore avoided (Figure 5.2). Warning message that the airbag volume is negative were also frequently observed with time steps below 1.1×10^{-6} seconds.

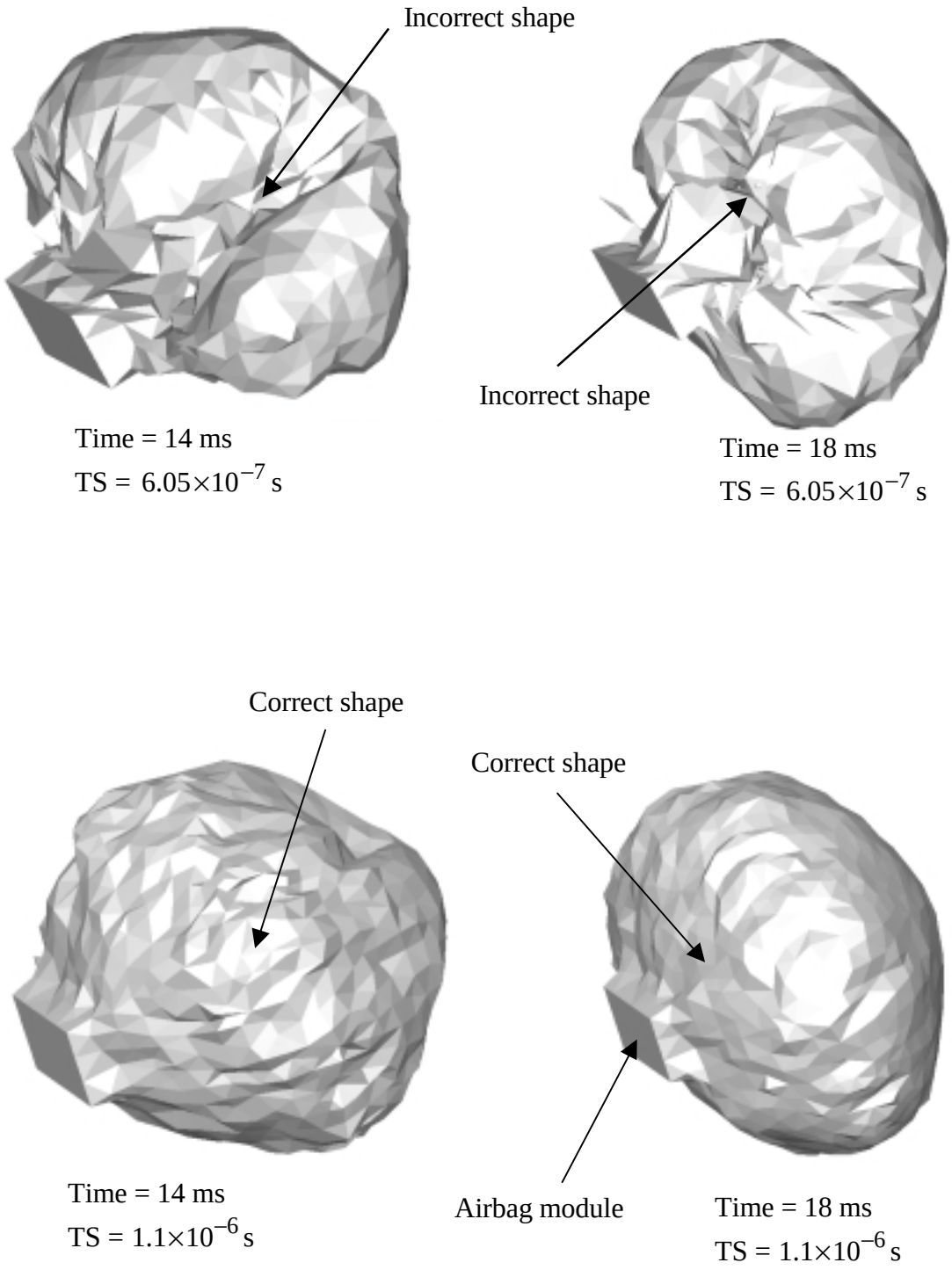

Figure 5.2 Incorrect behavior exhibited by the airbag with decreasing time step (airbag deployment times and time steps (TS) used are shown).

References

Alvi NP, Donohue EK, Curnyn K, Sugar J. Rupture of radial keratotomy sites after presumed blunt trauma. *Ophthalmic Surg Lasers* 1995;26:574-5.

Andreassen TT, Simonsen AH, Oxlund H. Biomechanical properties of keratoconus and normal corneas. *Exp Eye Res* 1980;31:435-441.

Battaglioli JL, Kamm RD. Measurements of the compressive properties of scleral tissue. *Invest Ophthalmol Vis Sci* 1984;25:59-65.

Berger RE. A model for evaluating the ocular contusion injury potential of propelled objects. J of Bioengineering 1978;2:345-358.

Bidar M, Ragan R, Kernozek T, Matheson JW. Finite element calculation of seat-interface pressures for various wheelchair cushion thicknesses. 24th Annual Proceedings Presented to the American Society of Biomechanics, Chicago, IL, July 2000, pp 215-216.

Biehl JW, Valdez J, Hemady RK, Steidl SM, Bourke DL. Penetrating eye injury in war. *Military Medicine* 1999 Nov;164(11):780-784.

Binder PS, Waring GO, Arrowsmith PN, Wang C. Histopathology of traumatic corneal rupture after radial keratotomy. *Arch Ophthalmol* 1988;106:1584-1590.

Bryant MR, Szerenyi K, Schmotzer H, McDonnell PJ. Corneal tensile strength in fully healed radial keratotomy wounds. *Invest Ophthalmol Vis Sci* 1994;35(7):3022-3031.

Bryant MR, McDonnell PJ. Constitutive laws for biomechanical modeling of refractive surgery. *J Biomech Eng* 1996 Nov;118:473-481.

Burnstein Y, Klapper D, Hersh PS. Experimental globe rupture after excimer laser photorefractive keratectomy. *Arch Ophthalmol* 1995 Aug;113:1056-1059.

Cacciatori M, Bell RWD, Habib NE. Blow-out fracture of the orbit associated with inflation of an airbag: a case report. *Br J of Oral and Maxillofacial Surgery* 1997;35:241-242.

Chisholm L. Ocular injury due to blunt trauma. *Applied Therapeutics* 1969 Nov;11(11):597-8.

Cook RD. Finite element modeling for stress analysis. John Wiley & Sons Inc., Toronto, Canada, 1995.

Coquart L, Depeursinge C, Curnier A, Ohayon R. A fluid-structure interaction problem in biomechanics: prestressed vibrations of the eye by the finite element method. *J Biomechanics* 1992;25(10):1105-1118.

Delori F, Pomerantzeff O, Cox MS. Deformation of the globe under high speed impact: its relation to contusion injuries. *Invest Ophthalmol* 1969;8:290-301.

Doswald-Beck EL. Blinding weapons. Geneva, International Committee of the Red Cross, 1993.

Duke-Elders S, Wybar KC. The anatomy of the visual system, system of ophthalmology, volume 2. The C.V. Mosby Company, St. Louis, 1961.

Duma SM, Crandall JR. Eye injuries from airbags with seamless module covers. *J of Trauma* 2000 April;48(4):786-9.

Dyster-Aas K, Krakau CET. The elasticity of the eyeball and measurement of its mechanical impedance. *Acta Opthalmologica* 1962;40:117-119.

Galler El, Umlas JW, Vinger PF, Wu HK. Ocular integrity after quantitated trauma following photorefractive keratectomy and automated lamellar keratectomy. Presented at Association for Research in Vision and Ophthalmology, May 16, 1995, Ft. Lauderdale, FL. Abstracts in: Investigative Ophthalmology and Visual Science 1995; v36 no 4, p S580, Association for Research in Vision and Ophthalmology, Inc. at JB Lippincott CO, Hagerstown, MD.

Giovinazzo VJ. The ocular sequelai of blunt trauma. *Adv Ophthalmic Plast Reconstr Surg* 1987;6:107.

Green RP, Peters DR, Shore JW, Fanton JW, Davis H. Force necessary to fracture the orbital floor. *Ophthalmol Plastic and Recinstructive Surg* 1990;6:211-217.

Hanna KD, Jouve FE, Waring GO, Ciarlet PG. Computer simulation of arcuate and radial incisions involving the corneoscleral limbus. *Eye* 1989;3:227-239.

Hanna KD, Jouve FE, Waring GO. Preliminary computer simulation of the effects of radial keratotomy. *Arch Ophthalmol* 1989 June;107:911-918.

Heier JS, Enzenauer RW, Wintermeyer SF, *et al*. Ocular injuries and diseases at a combat support hospital in support of Operations Desert Shield and Desert Storm. *Arch Ophthalmol* 1993;111:795-8.

Hoetzel DA, Altman P, Buzard KA, Choe K. Strip extensiometry for comparison of the mechanical response of bovine, rabbit, and human corneas. *J Biomech Eng* 1992 May;114:202-215.

Kisielewicz LT, Kodama N, Chhor A, Ohno S, Uchio E. Preliminary investigation of grinders debris impacting a human eye using numerical simulation. PAM Users Conference in Asia PUCA '95, Shin-Yokohama, Japan, November 1995.

Kisielewicz LT, Niizeki H, Endo M, Ohno S, Uchio E, Kuramoto Y. Simulation of debris and airbag impacts on a human eye healed after radial keratotomy. PAM Users Conference in Asia PUCA '96, Shin-Yokohama, Japan, November 1996.

Kisielewicz LT, Kodama N, Ohno S, Uchio E. Numerical prediction of airbag caused injuries on eyeballs after radial keratotomy. SAE International Congress and Exposition, Detroit, MI, Feb 23-26, 1998.

Kobayashi AS, Woo SL, Lawrence C, Schlegel WA. Analysis of the corneo-scleral shell by the method of direct stiffness. *J Biomechanics* 1971;4:323-330.

Lemley HL, Chodosh J, Wolf TC, Bogie CP, Hawkins TC. Partial dislocation of laser in situ keratomileusis flap by air bag injury. *J Refract Surg* 2000;16:373-4.

Leung AT, Rao SK, Lam DS. Traumatic partial unfolding of laser in situ keratomileusis flap with severe epithelial ingrowth. *J Cataract Refract Surg* 2000;26:135-139.

Meek KM, Elliot GF, Hughes RA, Nave C. The axial electron density in collagen fibrils from human corneal stroma. *Current Eye Res* 1982;2:471-7.

Meek KM, Blamires T, Elliot GF, Gyi TJ, Nave C. The organization of collagen fibrils in the human corneal stroma: a synchrotron x-ray diffraction study. *Current Eye Res* 1987;6:841-6.

Nash IS, Greene PR, Foster CS. Comparison of mechanical properties of keratoconus and normal corneas. *Exp Eye Res* 1982;35:413-423.

Norden RA, Perry HD, Donnenfeld ED, Montoya C. Air bag-induced corneal flap folds after laser in situ keratomileusis [In Process Citation]. *Am J Ophthalmol* 2000;130:234-5.

Pinsky PM, Datye DV. A microstructurally-based finite element model of the incised human cornea. *J Biomechanics* 1991;24(10):907-922.

Pinsky PM, Datye DV. Numerical modeling of radial, astigmatic, and hexagonal keratotomy. *Refractive and Corneal Surgery* 1992 Mar/Apr;8:164-172.

Powell MR, Lund AK. Leading edge deployment speed of production airbags. SAE

Paper 950870, International Congress and Exposition, Detroit, MI, 1995.
Preston JD. Review of standard consumer safety specification for non-powder guns (ANSI/ASTM F589-78) and non-powder gun projectiles and propellants (ANSI/ASTM F590-78). Mechanical and Textile Division, Engineering Sciences, CPSC, Washington, Feb 8, 1980.

Rashid ER, Waring GO. Complications of refractive keratotomy. In: Waring GO, ed. *Refractive Keratotomy for myopia and astigmatism*. St. Lewis, MO: Mosby;1992:863-936.

Sauerland EK. Grant's dissector. Williams & Wilkins, Baltimore, MD, 1994.

Sawusch MR, McDonnell PJ. Computer modeling of wound gape following radial keratotomy. *Refractive and Corneal Surgery* 1992 Mar/Apr;8:143-145.

Scott WR, Lloyd WC, Benedict JV, Meredith R. Ocular injuries due to projectile impacts. 44th Annual Proceedings Presented to the Association for the Advancement of Automotive Medicine, Chicago, Ill, Oct 2000, pp 205-217.

Shin TJ, Vito RP, Johnson LW, McCarey BE. The distribution of strain in the human cornea. *J Biomechanics* 1997;30(5):497-503.

Takahashi T. Atlas of the human body. Kodansha Ltd., Japan, 1994.

Todd BA, Thacker JG. Three-dimensional computer model of the human buttocks, *in vivo*. *J Rehabil Res Dev* 1994;31(2):111-119.

Uchio E, Ohno S, Kudoh J, Aoki K, Kisielewicz LT. Simulation model of an eyeball based on finite element analysis on a supercomputer. *Br J Ophthalmol* 1999;83:1106-11.

Umlas JW, Galler El, Vinger PF, Wu HK. Ocular integrity after quantitated trauma in radial keratotomy eyes. Presented at Association for Research in Vision and Ophthalmology, May 16, 1995, Ft. Lauderdale, FL. Abstracts in: Investigative Ophthalmology and Visual Science 1995; v36 no 4, p S583, Association for Research in Vision and Ophthalmology, Inc. at JB Lippincott CO, Hagerstown, MD.

Vinger PF. The eye and sports medicine. In Duane's Clinical Ophthalmology. Philadelphia, Pennsylvania, JB Lippincott Company, 1994, pp 1-94.

Vinger PF, Mieler WF, Oestreicher JH, Easterbrook M. Ruptured globes following radial and hexagonal keratotomy surgery. *Arch Ophthalmol* 1996;114:129-134.

Vinger PF, Sparks JJ, Mussack KR, Dondero J, Jeffers JB. A program to prevent eye injuries in paintball. *Sports Vision* 1997;3:33-40.

Vinger PF, Duma SM, Crandall J. Baseball hardness as a risk factor in eye injuries. *Arch Ophthalmol* 1999;117:354-358.

Vito RP, Shin TJ, McCarey BE. A mechanical model of the cornea: the effects of physiological and surgical factors on radial keratotomy surgery. *Refractive and Corneal Surgery* 1989 Mar/Apr;5:82-88.
Vito RP, Carnell PH. Finite element based mechanical models of the cornea for pressure and indenter loading. *Refractive and Corneal Surgery* 1992 Mar/Apr;8:146-151.

Wong TY, Smith GS, Lincoln AE, Tielsch JM. Ocular Trauma in the united states army: hospitalization records from 1985 through 1994. *Am J of Ophthalmology* 2000 May;129(5):645-650.

Woo SL, Kobayashi AS, Lawrence C, Schlegel WA. Mathematical model of the corneo-scleral shell as applied to intraocular pressure-volume relations and applanation tonometry. *Annals of Biomedical Engineering* 1972;1:87-98.

Woo SL, Kobayashi AS, Schlegel WA, Lawrence C. Nonlinear material properties of intact cornea and sclera. *Exp Eye Res* 1972;14:29-39.

Wray WO, Best ED, Cheng LY. A mechanical model for radial keratotomy: toward a predictive capability. *J Biomech Eng* 1994 Feb;116:56-61.

Yamada H. Strength of biological materials. The Williams & Wilkins Company, Baltimore, 1970.

APPENDIX A

Command Prompts for Translation into Madymo

The following procedure was used to import finite element models meshed with I-DEAS into the Madymo syntax *.dat file:

1) Begin with geometry meshed with I-DEAS
2) Select File – Export – I-DEAS Simulation Universal File – click OK
3) Save filename as MESH.unv
4) Use Hypermesh to import MESH.unv
5) Select File – Import - Translator = Ideas.exe – Filename = MESH.unv – Import
6) May need to zoom in or out in order to view imported model
7) Create a Madymo template of the nodal coordinates using Hypermesh
8) Select Export – Template = Madymo/Madymo53.tpl – Filename = MESH
9) Open MESH with a text editor such as wordpad or textpad
10) Cut and paste the nodal coordinates and element definitions directly into the Madymo synax *.dat file

APPENDIX B

Truncated Madymo Code

```
MADYMO Aviator Night Vision Goggle/Airbag Application
Frontal Impact,FE Bag,Eye,Muscles,Fat,Headform,Orbit,Helmet,NVG
March 2001, Virginia Tech Impact Biomechanics Laboratory
!*****************************************************************
GENERAL INPUT
  T0     0.0000   ! start time
  TE     0.0280   ! airbag to goggle contact starts ~ 0.008 sec
  INT    EULER    ! better than RUKU4 method for FE's
  TS     1.1E-6   ! time step (sampling), validate w/.rep file
  RAMP   0.0000  0.1000
  RACO   0.0100  0.1000
END GENERAL INPUT
!*****************************************************************
! SYSTEM 1 Vehicle
! SYSTEM 2 50th% Hybrid III dummy, facet headform/orbit, NVG/helmet
!*****************************************************************
SYSTEM 1
  Vehicle
  CONFIGURATION
    3   2   1
    15  2   1
    4   1
    5   1
    6   1
    11  10  9  8  7  1
    12  10  9  8  7  1
    16  13  1
    14  1
    19  18  17 1
    21  20  17 1
  END
  GEOMETRY
!  1:5
    0.000  0.000  0.000  0.000  0.000  0.000  VEHICLE
   -1.400  0.000  0.035  0.000  0.000  0.000  FLOOR
    1.000  0.000  0.000  0.000  0.000  0.000  TOE BOARD
   -1.450  0.700  0.250  0.000  0.000  0.000  RETRACTOR
   -1.550  0.650  1.000  0.000  0.000  0.000  HEIGHT ADJUSTER
!  6:10
   -1.450  0.700  0.100  0.000  0.000  0.000  ANCHOR POINT
 ! -0.225         0.200      initially,   moves wheel and bag
   -0.225  0.200  0.200  0.000  0.000  0.000  RACK
   -0.300  0.125  0.225  0.000  0.000  0.000  COLUMN
    0.400  0.000  0.000  0.000  0.000  0.000  AXIAL
    0.050  0.000  0.000  0.000  0.000  0.000  HUB
!  11:15
    0.050  0.000  0.000  0.000  0.000  0.075  BOTTOM RIM
    0.050  0.000  0.000  0.000  0.000  0.116  TOP RIM
    0.000  0.000  0.000  0.000  0.000  0.000  LEFT BOLSTER
    0.000  0.000  0.000  0.000  0.000  0.000  RIGHT BOLSTER
    0.900  0.225  0.000  0.200  0.000  0.000  ACCELERATOR
!  16:20
   -0.250  0.450  0.330 -0.200  0.000  0.000  BRAKE
   -1.250  0.350  0.080  0.000  0.000  0.000  FRAME
    0.100  0.000  0.050  0.000  0.000  0.000  SEAT
   -0.225  0.000  0.150 -0.075  0.000  0.200  BACK
   -0.075 -0.275  0.100  0.000  0.000  0.000  PRETENTIONER
```

```
!  21:
    0.000  0.000  0.000  0.000  0.000  0.000  BUCKLE
  END
  INERTIA
!  1:5
    0.1  0.01  0.01  0.01
    0.1  0.01  0.01  0.01
    0.1  0.01  0.01  0.01
    0.1  0.01  0.01  0.01
    0.1  0.01  0.01  0.01
!  6:10
    0.1  0.01  0.01  0.01
   10.0  1.00  1.00  1.00
    5.0  0.10  0.10  0.10
    1.0  0.10  0.10  0.10
    1.0  0.10  0.10  0.10
!  11:15
    0.5  0.10  0.10  0.10
    0.5  0.10  0.10  0.10
    1.0  0.01  0.01  0.01
    1.0  0.01  0.01  0.01
    1.0  0.01  0.01  0.01
!  16:20
    0.5  0.01  0.01  0.01
    5.0  0.05  0.05  0.05
    5.0  0.05  0.05  0.05
    2.0  0.05  0.05  0.05
    0.1  0.01  0.01  0.01
!  21:
    0.1  0.01  0.01  0.01
  END
  JOINTS
!  1:5
    1  BRACKET
    2  REVOLUTE
    3  REVOLUTE
    5  TRANSLATIONAL
    4  TRANSLATIONAL
!  6:10
    6  BRACKET
    7  TRANSLATIONAL
    8  SPHERICAL
    9  TRANSLATIONAL
    10 UNIVERSAL
!  11:15
    11 REVOLUTE
    12 REVOLUTE
    13 TRANSLATIONAL
    14 TRANSLATIONAL
    15 REVOLUTE
!  16:20
    16 REVOLUTE
    17 TRANSLATIONAL
    18 REVOLUTE
    19 REVOLUTE
    20 REVOLUTE
!  21:
```

```
    21 TRANSLATIONAL
  END
  ORIENTATIONS
!   `ksi' left, `eta' rear, `zeta' up
    2  1  1   3   1.5708
    2  2  1   3   1.5708
!   `ksi' right, `eta' front/up, `zeta' up/rear
    3  2  1   3  -1.5708   1   0.87266
    3  3  1   3  -1.5708
!   `ksi' up/inward/rear, `eta' left, `zeta' rear
    5  1  4  -0.1000 -0.2500  0.9000  0.  1.  0.
    5  5  4  -0.1000 -0.2500  0.9000  0.  1.  0.
!   `ksi' up/rear, `eta' left, `zeta' rear
    4  1  4  -0.1000  0.0000  0.9000  0.  1.  0.
    4  4  4  -0.1000  0.0000  0.9000  0.  1.  0.
!   `ksi' rear, `eta' right, `zeta' up
    7  1  1   2   3.14159
    7  7  1   2   3.14159
!   `ksi' rear/up/(slightly left) (parallel to column),
!   `eta' right, `zeta' up/front (both perpendicular to column)
    8  7  4  -0.3692  0.0200  0.2096   0.000 -1.000  0.000
    8  8  1   2  0.0000
!   `ksi' rear/up (parallel to column)
!   `eta' right, `zeta' up/front (both perpendicular to column)
    9  8  1   2   0.0000
    9  9  1   2   0.0000
!   `ksi' left, `eta' up/front (both perpendicular to column)
!   `zeta' front/down (parallel to column)
    10 9  1   3  -1.57080  1  1.57080
    10 10 1   3  -1.57080  1  1.57080
!   `eta' front/down (parallel to column)
!   `ksi' right, `zeta' up/front (both perpendicular to column)
    11 10 1   3   1.57080
    11 11 1   3   1.57080
!   `eta' rear/up (parallel to column)
!   `ksi' left, `zeta' up/front (both perpendicular to column)
    12 10 1   3  -1.57080
    12 12 1   3  -1.57080
!   `ksi' rear, `eta' right, `zeta' up
    13 1  1   3   3.14159
    13 13 1   3   3.14159
!   `ksi' rear, `eta' right, `zeta' up
    14 1  1   3   3.14159
    14 14 1   3   3.14159
!   `ksi' left, `eta' rear, `zeta' up
    15 2  1   3   1.57080   1  -0.87266
    15 15 1   3   1.57080
!   `ksi' right, `eta' front, `zeta' up
    16 13 1   3  -1.57080   1   0.87266
    16 16 1   3  -1.57080
!   `ksi' front/up (parallel to seat track)
!   `eta' left, `zeta' up/rear (both perpendicular to seat track)
    17 1  4   0.250  0.000  0.020   0.000  1.000  0.000
    17 17 4   0.250  0.000  0.020   0.000  1.000  0.000
!   `ksi' left, `eta' rear, `zeta' up
    18 17 1   3  1.57180
    18 18 1   3  1.57180
```

```
!   `ksi' left, `eta' rear, `zeta' up
    19 18 1   3  1.57180
    19 19 1   3  1.57180
!   `ksi' left, `eta' rear, `zeta' up
    20 17 1   3  1.57180
    20 20 1   3  1.57180
  END
  STIFFNESS
    10 1  0  5730.   0.0   10.0   0.0  +
       2  0  8595.   0.0   10.0   0.0
    11 3  0  2865.   0.0   10.0   0.0
    12 3  0  2865.   0.0   10.0   0.0
    9  4  0  0.0E0   0.0   10.0   0.0
    15 5  0  0.5E6   0.0    0.0  50.0
    16 5  0  0.5E6   0.0    0.0  50.0
    18 6  0  1.0E6   0.0  100.0 100.0
    19 7  0  0.1E6   0.0   50.0  50.0
    20 0  0  0.0E0   0.0    1.0   0.0
    21 8  0  0.0E0   0.0   10.0   0.0
    4  9  0  1.0E6   0.0   10.0   0.0
  END
  FUNCTIONS
!  1: steering wheel up/down bending
    4
   -0.34907  -1500  -0.17453  -1000   0.17453   1000   0.34907   1500
!  2: steering wheel lateral bending
    4
   -0.34907  -2250  -0.17453  -1500   0.17453   1500   0.34907   2250
!  3: rim deflection (halfed)
    4
   -0.34907   -750  -0.17453   -500   0.17453    500   0.34907    750
!  4: colum axial translation
    2
   -1.000  -5.0E+6   1.000   5.0E+6
!  5: pedal rotation
    2
   -1.57080   -100   1.57080    100
!  6: seat rotation
    4
   -1.57080  -2500  -0.74533  -2500   0.74533   2500   1.57080   2500
!  7: back bending
    4
   -1.57080  -1000  -0.74533  -1000   0.74533   1000   1.57080   1000
!  8: pretensioner characteristics (50mm displacement)
    3
    0.090    -5000   0.110     5000   1.000     5000
!  9: load limiter characteristics (4kN load)
    4
   -0.006    -6000   0.004     4000   0.100     4000   0.110    14000
  END
  PLANES
!  1:5
    18 0.225  0.250  0.210  -0.200  0.250  0.080  -0.200 -0.250  0.080
3  4  HY3C   seat cushion
    19 0.017  0.250 -0.050  -0.175  0.250  0.450  -0.175 -0.250  0.450
3  4  HY3C   seat back
```

```
    3  0.400  0.600  0.000   0.000  0.600  0.000   0.000  0.000  0.000
0  0  0.0E0  toe board
    2  1.000  0.600  0.000   0.000  0.600  0.000   0.000  0.000  0.000
0  0  0.0E0  floor
    13 -0.700  0.330  0.425  -0.780  0.330  0.600  -0.780  0.660  0.600
1  0  0.5E6  left bolster
!  6:10
    14 -0.700  0.000  0.425  -0.780  0.000  0.600  -0.780  0.330  0.600
1  0  0.5E6  right bolster
    13 -0.550  0.330  0.350  -0.700  0.330  0.425  -0.650  0.660  0.425
2  0  0.5E6  left underside
    14 -0.550  0.000  0.350  -0.700  0.000  0.425  -0.650  0.330  0.425
2  0  0.5E6  right underside
    10 0.010  0.071 -0.061   0.010  0.071  0.041   0.010 -0.071  0.041
0  0  0.0E0  module opposite
    10 0.051  0.071 -0.060   0.009  0.071 -0.060   0.009 -0.071 -0.060
0  0  0.0E0  module bottom
!  11:15
    10 0.051  0.070 -0.061   0.051  0.070  0.041   0.009  0.070  0.041
0  0  0.0E0  module left
    10 0.009 -0.070  0.041   0.051 -0.070  0.041   0.051 -0.070 -0.061
0  0  0.0E0  module right
    10 0.009  0.071  0.040   0.051  0.071  0.040   0.051 -0.071  0.040
0  0  0.0E0  module top
    12 0.000  0.160  0.000   0.000  0.160  0.110   0.000 -0.160  0.110
0  0  0.0E0  module facing 1
    12 0.000  0.110  0.110   0.000  0.110  0.160   0.000 -0.110  0.160
0  0  0.0E0  module facing 2
!  16:18
    11 0.000  0.160 -0.110   0.000  0.160  0.000   0.000 -0.160  0.000
0  0  0.0E0  module facing 3
    11 0.000  0.110 -0.160   0.000  0.110 -0.110   0.000 -0.110 -0.110
0  0  0.0E0  module facing 4
    1  -1.050  0.600  1.075   -.600  0.700  0.700   -.425  -.006  0.721
0  0  0.0E0  windscreen
  END
  FUNCTIONS
!  1: knee bolster loading
    6
    0.000        0   0.010   1.0E+3   0.030   2.0E+3   0.040   2.5E+3
0.050   4.0E+3
    0.060   4.0E+3
!  2: under bolster loading
    4
    0.000        0   0.010   1.0E+3   0.030   2.0E+3   0.040   2.0E+3
!  3: seat cushion loading
    5
    0.000        0   0.050   0.2E+3   0.070   1.5E+3   0.090   4.0E+3
0.100   5.0E+3
!  4: seat cushion unloading
    5
    0.000        0   0.050   0.1E+3   0.070   0.3E+3   0.090   1.0E+3
0.100   5.0E+3
  END
  ELLIPSOIDS
!  1:5
    21 0.030 0.010 0.020 -0.0300 0.0000 0.0000  4  0  0  0.0    Buckle
```

```
    18 0.025 0.250 0.025  0.1500 0.0000 0.1250  2  1  0  1.E6   Seat
Structure
    11 0.020 0.065 0.020  0.0000 0.0000 -.1750  2  0  0  0.0    Rim
South
    11 0.020 0.065 0.020  0.0000 -.0672 -.1621  2  0  0  0.0    Rim SSW
    11 0.020 0.065 0.020  0.0000 -.1234 -.1234  2  0  0  0.0    Rim SW
!  6:10
    11 0.020 0.065 0.020  0.0000 -.1621 -.0672  2  0  0  0.0    Rim WSW
    10 0.020 0.065 0.020  0.0500 -.1750 0.0000  2  0  0  0.0    Rim
West
    12 0.020 0.065 0.020  0.0000 -.1621 0.0672  2  0  0  0.0    Rim WNW
    12 0.020 0.065 0.020  0.0000 -.1234 0.1234  2  0  0  0.0    Rim NW
    12 0.020 0.065 0.020  0.0000 -.0672 0.1621  2  0  0  0.0    Rim NNW
!  11:15
    12 0.020 0.065 0.020  0.0000 0.0000 0.1750  2  0  0  0.0    Rim
North
    12 0.020 0.065 0.020  0.0000 0.0672 0.1621  2  0  0  0.0    Rim NNE
    12 0.020 0.065 0.020  0.0000 0.1234 0.1234  2  0  0  0.0    Rim NE
    12 0.020 0.065 0.020  0.0000 0.1621 0.0672  2  0  0  0.0    Rim ENE
    10 0.020 0.065 0.020  0.0500 0.1750 0.0000  2  0  0  0.0    Rim
East
!  16:20
    11 0.020 0.065 0.020  0.0000 0.1621 -.0672  2  0  0  0.0    Rim ESE
    11 0.020 0.065 0.020  0.0000 0.1234 -.1234  2  0  0  0.0    Rim SE
    11 0.020 0.065 0.020  0.0000 0.0672 -.1621  2  0  0  0.0    Rim SSE
    10 0.030 0.100 0.075  0.0500 0.0000 -.0100  4  0  0  0.0    Hub
    8  0.225 0.025 0.025  0.2250 0.0000 0.0000  2  0  0  0.0
Steering Column
!  21:24
    8  0.025 0.060 0.025  0.3000 0.0600 0.0000  4  0  0  0.0
Ignition Lock
    16 0.050 0.100 0.015  -.2000 0.0000 0.0000  4  0  0  0.0    Brake
    15 0.125 0.050 0.015  0.1250 0.0000 0.0000  4  0  0  0.0
Accelerator
    1  0.300 0.025 0.025  -.8750 0.6500 0.9000  2  0  0  0.0    A
Pillar
  END
  FUNCTIONS
!  1: Seat Structure loading
    2
    0.000        0   0.100   5.0E+3
  END
  ORIENTATIONS
!  Rim ellipsoids
    3  0   1   1  -0.000
    4  0   1   1  -0.393
    5  0   1   1  -0.785
    6  0   1   1  -1.178
    7  0   1   1  -1.571
    8  0   1   1  -1.963
    9  0   1   1  -2.356
    10 0   1   1  -2.749
    11 0   1   1  -3.142
    12 0   1   1  -3.534
    13 0   1   1  -3.927
    14 0   1   1  -4.320
    15 0   1   1  -4.712
```

```
    16 0   1   1  -5.105
    17 0   1   1  -5.498
    18 0   1   1  -5.890
!  Ignition Lock ellipsoid
    21 0   1   3  -0.5236
!  A Pillar
    24 0   4  -1.1000 -0.2500  0.9000  0.  1.  0.
  END ELLIPSOIDS
! **********************
FACET SURFACE 1
panel
COORDINATES
       1  0.260825266700      0.000000000000      0.052841508510
       … !(ABBREVIATED)
       5  0.160825266720      0.700000000000      0.031211542090
END COORDINATES
FACETS
       1  QUAD       1         2         4         3
       … !(ABBREVIATED)
      10  QUAD       7        15        13         5
END FACETS
GEOMETRIES
  THICKNESS    0.001
  SET          1:5,7:11,13,15
  END GEOMETRIES
SECTIONS
  BODY         10
  SET          1:5,7:11,13,15
 INITIAL CONDITIONS
    0  .19  0.40  -0.02
  ORIENTATIONS
    0  0  1  1  0.0  2  0.50  3  3.18159
 END ORIENTATIONS
END SECTIONS
END FACET SURFACE 1
!**********************************************************************
*
  INITIAL CONDITIONS

  JOINT DOF
    1  LOCK
    5  LOCK
    4  FREE   0.0000
    6  LOCK
    8  FREE   1.0000   0.0000   0.0000   0.0000 +
       0.0000   0.0000   0.0000
    9  FREE   0.0000
    10 FREE   0.0000   0.0000
    11 FREE   0.0000
    12 FREE   0.0000
    15 FREE   0.0000
    16 FREE   0.0000
    17 LOCK   0.0000
    18 FREE   0.0000
    19 FREE   0.0000
    20 FREE  -1.0472
    21 LOCK   0.1500
```

```
  END
  SWITCH
    21 BREAK LOGIC  2
    21 LOCK LOGIC   3
  END
END SYSTEM 1
!************************************************************************
*
!
! MADYMO 3D 50th percentile Hybrid III (sitting) male dummy model
! with 45 deg soft stop ankle,
! with 5-joint neck model
!
! Filename                     $RCSfile: a3frtapp.dat,v $
! Database version             $Revision: 1.2 $
! Developed for MADYMO version 5.4
!                              $Date: 1999/04/01 07:50:02 $
! Release status               $State: Exp $
!
!************************************************************************
*
!
! Revision 5.5 of d3hyb350.dat :
! Modifications to d3hyb350.dat revision 5.3 comprise:
! a.\  sliding knee implemented
! b.\  foot and ankle based on FTSS 45 deg soft stop ankle and foot
! c.\  shoes implemented as separate bodies
! d.\  additional ellipsoids defined for tibias
! e.\  improved lumbar spine model based on extensive dynamic component
tests
! f.\  improved hip model based on modified femurs
! g.\  mass redistributed around lower lumbar and upper lumbar load
cells
! h.\  facet shoe model added
!
! Revision 5.5.1.1 of d3hyb350.dat :
! a.\  neck model slightly improved for rearward loading
! b.\  minor improvement in foot/shoe connection
!
! Revision 5.5.1.2 of d3hyb350.dat :
! a.\  neck model with 5 joints instead of the standard 2 joints
!      bodies/joints 10-34 are renumbered to 13-37
!      ellipsoid numbering is unchanged, additional neck ellipsoids are
appended
! b.\  facet head model added
!
! Revision 5.6 of d3hyb350.dat :
! a.\  Injury criteria added for MADYMO 5.4
!
!************************************************************************
*
!
! Data origin        :
! Extensive measurement programme,
! see the database manual
!
! Validation         :
```

```
! The database was validated in forward and/or vertical loading,
! see the database manual
!
! Remarks            :
! recommended timestep is 1E-4 s or lower
! facet shoes and head are commented out: see INCLUDE d3hyb350.facets
!
!*******************************************************************
*
!
SYSTEM 2
50% Hybrid III
  CONFIGURATION
    2  1
    35 6  5  4  3  1
    38 14 13 12 11 10 9  8  7  5  4  3  1
    21 19 17 15 5  4  3  1
    22 20 18 16 5  4  3  1
    36 33 31 29 27 25 23 1
    37 34 32 30 28 26 24 1
  END
  GEOMETRY
!   1:5
    0.0000 0.0000 0.0000  -.0178 0.0000 0.0328  Lower Torso
    0.0500 0.0000 0.0846  0.0000 0.0000 0.0000  Abdomen
    -.0805 0.0000 0.0773  -.0034 0.0000 0.0339  Lower Lumbar
    -.0030 0.0000 0.0723  0.0108 0.0000 0.0788  Upper Lumbar
    0.0028 0.0000 0.1327  -.0034 0.0000 0.0618  Upper Torso
!   6:10
    0.1517 0.0000 0.0762  0.0000 0.0000 0.0000  Ribs
    0.0161 0.0000 0.2376  0.0000 0.0000 0.0000  Lower Neck Bracket
    -.0508 0.0000 -.0254  0.0508 0.0    0.0442  Lowr Neck Sens+Disk1
    0.0508 0.0    0.0442  -.0023  .0     .0141  Disk2
    0.0    0.0    0.0282  -.0023  .0     .0141  Disk3
!   11:15
    0.0    0.0    0.0282  -.0023  .0     .0141  Disk4
    0.0    0.0    0.0282  -.0023  .0     .0202  Disk5
    0.0000 0.0000 0.0404  0.0000 0.0000 0.0000  Nodding Plate
    0.0000 0.0000 0.0178  0.0203 0.0000 0.0292  Head
    0.0125 0.0156 0.1848  -.0247 0.1012 -.0001  Clavicle Left
!   16:20
    0.0125 -.0156 0.1848  -.0247 -.1012 -.0001  Clavicle Right
    -.0257 0.1724 -.0003  0.0009 -.0025 -.1323  Upper Arm Left
    -.0257 -.1724 -.0003  0.0009 0.0025 -.1323  Upper Arm Right
    0.0000 0.0000 -.2646  -.0013 -.0017 -.0885  Lower Arm Left
    0.0000 0.0000 -.2646  -.0013 0.0017 -.0885  Lower Arm Right
!   21:25
    0.0000 0.0000 -.2512  0.0035 0.0017 -.0547  Hand Left
    0.0000 0.0000 -.2512  0.0035 -.0017 -.0547  Hand Right
    0.0000 0.0850 0.0000  0.1611 0.0047 -.0036  Femur Left
    0.0000 -.0850 0.0000  0.1611 -.0047 -.0036  Femur Right
    0.2965 0.0000 0.0000  0.0523 0.0047 -.0036  Knee Left
!   26:30
    0.2965 0.0000 0.0000  0.0523 -.0047 -.0036  Knee Right
    0.1046 0.0000 0.0000  -.0029 0.0000 -.0201  Upper Tibia Left
    0.1046 0.0000 0.0000  -.0029 0.0000 -.0201  Upper Tibia Right
    0.0424 0.0000 -.0963  0.0000 -.0003 -.1100  Middle Tibia Left
```

```
    0.0424 0.0000 -.0963  0.0000 -.0003 -.1100  Middle Tibia Right
!   31:35
    0.0000 0.0000 -.2375  0.0112 0.0003 -.0347  Lower Tibia Left
    0.0000 0.0000 -.2375  0.0112 -.0003 -.0347  Lower Tibia Right
    0.0175 0.0000 -.0760  0.0518 0.0000 -.0302  Foot Left
    0.0175 0.0000 -.0760  0.0518 0.0000 -.0302  Foot Right
    0.0000 0.0000 0.0000  0.0000 0.0000 0.0000  Sternum
!   36:38
    0.0000 0.0000 -.0800  0.0518 0.0000 0.0000  Shoe Left
    0.0000 0.0000 -.0800  0.0518 0.0000 0.0000  Shoe Right
  ! world coords, moves goggles and ball hinge, cg=.05525m below hinge
  !   x      y       z      cg...    30 mm of adjustment in x direction
    0.164  0.027   .103   0.000  0.000 -.05525  Goggles
  END
  INERTIA
!   1:5
    16.6107  0.1300  0.0887  0.1297         0    0.0087         0
     0.64    0.01    0.01    0.01
     1.3493  0.0025  0.0023  0.0010
     3.2249  0.0042  0.0046  0.0035
     9.5251  0.1305  0.0971  0.0728         0    -.0088         0
!   6:10
     1.20    0.01    0.01    0.01
     0.01    0.001   0.001   0.001
     0.10    0.001   0.001   0.001
     0.19    0.001   0.001   0.001
     0.19    0.001   0.001   0.001
!   11:15
     0.19    0.001   0.001   0.001
     0.36    0.001   0.001   0.001
     0.01    0.001   0.001   0.001
     4.40    0.0204  0.0211  0.0143
     2.03    0.01    0.01    0.01
!   16:20
     2.03    0.01    0.01    0.01
     2.06    0.0122  0.0125  0.01
     2.06    0.0122  0.0125  0.01
     1.71    0.0133  0.0153  0.01
     1.71    0.0133  0.0153  0.01
!   21:25
     0.60    0.01    0.01    0.01
     0.60    0.01    0.01    0.01
     5.69    0.0117  0.0480  0.0477
     5.69    0.0117  0.0480  0.0477
     1.71    0.01    0.0144  0.0143
!   26:30
     1.71    0.01    0.0144  0.0143
     1.31    0.01    0.009   0.01
     1.31    0.01    0.009   0.01
     2.12    0.03    0.0271  0.01
     2.12    0.03    0.0271  0.01
!   31:34
     0.71    0.01    0.006   0.01
     0.71    0.01    0.006   0.01
     1.48    0.002   0.0064  0.0064
     1.48    0.002   0.0064  0.0064
     0.30    0.01    0.01    0.01
```

```
!   36:38
     0.643   0.002   0.007   0.007
     0.643   0.002   0.007   0.007
!  mass (kg)   Ixx      Iyy    Izz (kg*m^2) of the goggles
     0.273   0.00127  0.00004   0.00127
  END
  ORIENTATIONS
!   Head principal inertia frame
    14  0  3  0.62472 0.00000 0.78084 0.00000 1.00000 0.00000 -.78084
0.00000 0.62472
  END
  JOINTS
!   dummy
    1   FREE
!   abdomen
    2   TRANSLATIONAL
!   lower lumbar spine bracket
    3   BRACKET
!   flexible lumbar spine with characteristics defined under
!   PROTECTED joint resistance models
    4   FREE
!   upper lumbar spine bracket
    5   BRACKET
!   ribs
    6   FREE
!   neck angle adjustment bracket (must be locked under JOINT DOF)
    7   REVOLUTE
!   lower neck load sensor
    8   BRACKET
!   neck pivots
    9   SPHERICAL
    10  SPHERICAL
    11  SPHERICAL
    12  SPHERICAL
!   nodding joint
    13  REVO
!   upper neck load sensor
    14  BRACKET
!   clavicles
    15  UNIVERSAL
    16  UNIVERSAL
!   shoulders
    17  UNIVERSAL
    18  UNIVERSAL
!   elbows
    19  UNIVERSAL
    20  UNIVERSAL
!   wrists
    21  UNIVERSAL
    22  UNIVERSAL
!   hips
    23  SPHERICAL
    24  SPHERICAL
!   femur load cells
    25  BRACKET
    26  BRACKET
!   knees (rotation+sliding)
```

```
    27  CRT
    28  CRT
!   upper tibia load cells
    29  BRACKET
    30  BRACKET
!   lower tibia load cells
    31  BRACKET
    32  BRACKET
!   ankles
    33  SPHERICAL
    34  SPHERICAL
!   sternum compression
    35  TRANSLATIONAL
!   shoes
*   36  TRANSLATIONAL
*   37  TRANSLATIONAL
    36  FREE
    37  FREE
! hinge between goggles and pilot's helmet
    38  REVOLUTE
  END
  ORIENTATIONS
!   for dummy positioning these orientations should NOT be modified
!   this should be done under INITIAL CONDITIONS using ORIENTATIONS
and/or JOINT DOF
!   dummy local: x front, y left, z up
    1   0   1   2  0.00000
    1   1   1   2  0.00000
!   abdomen joint
    2   1   1   2  2.87980
    2   2   1   2  2.87980
!   lower lumbar load sensor 22 deg. rearward
!   lower lumbar local 22+2 deg. forward
    3   1   1   2  -.38397   1  3.14159
    3   3   1   2  -.41888   1  3.14159
!   lumbar spine joint
    4   3   1   2 -1.57080
    4   4   1   2 -1.57080
!   upper torso local 22+2 deg. forward wrt spine
!   joint 9 deg rearward wrt upper torso
    5   4   1   2  0.26178   1  3.14159
    5   5   1   2  -.15710   1  3.14159
!   ribs joint
    6   5   1   2 -0.27053
    6   6   1   2  0.00000
!   spine box top plate y-rotated -10.38 deg wrt lower plate
!   if the neck bracket is in zero position, the neck mounting plate
!   is y-rotated 13.75 deg wrt spine box upper plate
!   adjust bracket only under JOINT DOF !!!!
    7   5   1   2  0.05882   3  1.57080
    7   7   1   3  1.57080
!   lower neck load cell in line with lower neck mounting plate
    8   7   1   2  0.00000   1  3.14159
    8   8   1   2  0.00000   1  3.14159
!   neck upper (nodding) joint: in line with neck
!   nodding plate local: x front, y left, z up
    13  12  1   3  1.57080
```

```
    13  13  1   3  1.57080
!   upper neck load cell 4.75 deg. rearward wrt nodding plate, y right,
z down
    14  13  1   1  3.14159   2  0.08290
    14  14  1   1  3.14159
!   left/right clavicle joints
    15  5   1   2 -0.17453   1  1.41372
    15  15  1   1  1.57080
    16  5   1   2 -0.17453   1  1.72788
    16  16  1   1  1.57080
!   left/right shoulder joints
    17  15  1   2  2.93215   3  1.57080
    17  17  1   3 -1.57080   2  3.14159
    18  16  1   2  2.93215   3  1.57080
    18  18  1   3 -1.57080   2  3.14159
!   left/right elbow joints
    19  17  1   2 -1.57080
    19  19  1   2 -1.57080
    20  18  1   2 -1.57080
    20  20  1   2 -1.57080
!   left/right wrist joints
    21  19  1   2 -1.57080   1 -1.57080
    21  21  1   2 -1.57080   1 -1.57080
    22  20  1   2 -1.57080   1 -1.57080
    22  22  1   2 -1.57080   1 -1.57080
!   left/right hip joint
!   modified for protected hip resistance model
    23  1   1   3  0.00000
    23  23  1   3  -.02862   2 -0.12217
    24  1   1   3  0.00000
    24  24  1   3  0.02862   2 -0.12217
!   left/right femur load cells
    25  23  1   2 -1.69297   1  3.11297
    25  25  1   2 -1.69297   1  3.11297
    26  24  1   2 -1.69297   1 -3.11297
    26  26  1   2 -1.69297   1 -3.11297
!   left/right knee joints
    27  25  1   2  2.87999
    27  27  1   2  2.86234
    28  26  1   2  2.87999
    28  28  1   2  2.86234
!   upper tibia load cells
    29  27  1   1  3.14159
    29  29  1   1  3.14159
    30  28  1   1  3.14159
    30  30  1   1  3.14159
!   lower tibia load cells
    31  29  1   1  3.14159
    31  31  1   1  3.14159
    32  30  1   1  3.14159
    32  32  1   1  3.14159
!   ankle joints
    33  31  1   2 -0.145280  1 -1.570796  3 -1.570796
    33  33  1                1 -1.570796  3 -1.570796
    34  32  1   2 -0.145280  1 -1.570796  3 -1.570796
    34  34  1                1 -1.570796  3 -1.570796
!   sternum oriented as rib body
```

```
    35  6   1   2  0.00000
    35  35  1   2  0.00000
!   shoe-foot joint
    36  33  1   2 -1.57080
    36  36  1   2 -1.57080
    37  34  1   2 -1.57080
    37  37  1   2 -1.57080
!   goggles
    38  14  1   3 -1.57080
  END
  STIFFNESS
!   abdomen decompression-compression
    2   1  0    0.0    0.000   250.0   0.0
!   clavicles elevation-depression, anterior-posterior rotation
    15  2  0    0.0    0.000     2.5   0.0  +
        3  0    0.0    0.000     2.5   0.0
    16 13  0    0.0    0.000     2.5   0.0  +
        3  0    0.0    0.000     2.5   0.0
!   shoulders flexion-extension, abduction-adduction
    17  4  0    0.0    0.000     0.0  20.1  +
        5  0    0.0    0.000     0.0  20.1
    18  4  0    0.0    0.000     0.0  20.1  +
        6  0    0.0    0.000     0.0  20.1
!   elbows lateral-medial rotation, flexion-extension
    19  0  0    0.0    0.000     0.0   0.1  +
        7  0    0.0    0.000     1.0   4.0
    20  0  0    0.0    0.000     0.0   0.1  +
        7  0    0.0    0.000     1.0   4.0
!   wrists lateral-medial rotation, flexion-extension
    21  0  0    0.0    0.000     0.0   0.1  +
        8  0    0.0    0.000     0.0   0.4
    22  0  0    0.0    0.000     0.0   0.1  +
        9  0    0.0    0.000     0.0   0.4
!   knees flexion-extension, compression
    27  10 0    0.0    0.000     0.0  21.3   +
        11 0    0.0    0.000     0.0 500.0
    28  10 0    0.0    0.000     0.0  21.3   +
        11 0    0.0    0.000     0.0 500.0
!   sternum compression
    35  12 0    0.0    0.000   800.0   0.0
  END
  FUNCTIONS
!   1: abdomen compression loading (dynamic test TNO 93-E1506/E1508)
    8
    -.020 -2080.0  0.000     0.0  0.020  2080.0  0.030  3850.0  0.040
6240.0
    0.050 10000.0  0.060 14940.0  0.070 22140.0
!   2: clavicles depression->elevation loading (static test TNO-FAT
751860026)
    5
   -0.087  -346.5  -.044   -86.6  0.000     0.0  0.044   86.6  0.087
346.5
!   3: clavicles anterior->posterior rotation loading (static test TNO-
FAT 751860026)
    5
   -0.109  -311.3  -.055   -77.8  0.000     0.0  0.055   77.8  0.109
311.3
```

```
!   4: shoulders flexion->extension loading (static test TNO-FAT
751860026)
    9
   -4.294  -555.0 -4.218   -70.8 -4.107   -34.8 -3.995   -15.0 -3.863
-6.6
   -3.474     0.0  0.488     0.0  0.612    54.0  0.761   325.2
!   5: left shoulder adduction->abduction loading (static test TNO-FAT
751860026)
    8
   -0.186  -314.4  0.000     0.0  2.672     0.0  3.040    19.2  3.186
58.2
    3.269   105.0  3.342   190.8  3.516   538.8
!   6: right shoulder abduction->adduction loading (static test TNO-FAT
751860026)
    8
   -3.516  -538.8 -3.342  -190.8 -3.269  -105.0 -3.186   -58.2 -3.040
-19.2
   -2.672     0.0  0.000     0.0  0.186   314.4
!   7: elbows flexion->extension loading (static test TNO-FAT
751860026)
    9
   -3.032  -529.7 -2.032   -29.7 -1.980   -18.1 -1.834    -6.4 -1.650
0.0
    0.000     0.0  0.139    19.7  0.260    62.3  0.313   153.6
!   8: left wrist flexion->extension loading (static test TNO-FAT
751860026)
    5
   -2.379  -500.0 -1.379     0.0  0.000     0.0  1.379     0.0  2.379
500.0
!   9: right wrist extension->flexion loading (static test TNO-FAT
751860026)
    5
   -2.379  -500.0 -1.379     0.0  0.000     0.0  1.379     0.0  2.379
500.0
!   10: knees extension->flexion loading (static test TNO-FAT
751860026)
    12
   -1.716  -128.4 -1.605   -12.0 -1.553    -6.0 -0.521     0.0  0.000
0.0
    0.570     0.0  0.688     5.4  0.900    18.6  0.997    40.8  1.077
90.0
    1.160   198.0  1.320   529.8
!   11: knee sliding, loading
    4
    -1     -6.0E6
     0.0    0.0
     0.021  3.0E3
     1      6.0E6
!   12: sternum compression
    3
    -1.0  -1.0E5  0.0  0.0  1.0  1.0E5
!   13: clavicle right depression->elevation loading (same as left for
50th)
    5
   -0.087  -346.5  -.044   -86.6  0.000     0.0  0.044   86.6  0.087
346.5
  END FUNCTIONS
```

```
  COULOMB FRICTION
!  Friction can be adjusted in the real dummy;
!  below usual values are given, but tuning of the model friction
!  may be needed for certain experiments (adjust only the first two
parameters)
!
!  hips
!  Calibration requirements indicate 56.1 Nm
!  The database uses 12.8 Nm, which is a more usual value
    23   12.8   12.8    0.0044  0.0044
    24   12.8   12.8    0.0044  0.0044
!  ankles
    33    4.0    2.0    0.0048  0.0024
    34    4.0    2.0    0.0048  0.0024
  END COULOMB FRICTION
!*********************************************************************
*
! Protected Joint resistance models
! These models operate at the joints given after VAR;
! # VAR X Y puts model X of the include file at joint Y of the database
! also see the USERS MANUAL for information on VARIABLE EXPANSION
!*********************************************************************
*
! Lumbar spine
# var  1  "  4"
  INCLUDE h350lumb.v04
! Hip joints
# var  1  " 23"
# var  2  " 24"
  INCLUDE h350hips.v01
! 5-joint neck
# var  1  "9 "
# var  2  "10"
# var  3  "11"
# var  4  "12"
# var  5  "13"
  INCLUDE h350n5pv.v02
! ankle joints
# var  1  " 33"
# var  2  " 34"
  INCLUDE h350anks.v01
!*********************************************************************
*
  CARDAN RESTRAINTS
!   ribs x,y,z rotation
    6   1  0    0.0    0.000  +
        2  0    0.0    0.000  +
        3  0    0.0    0.000  +
                          29.1    10.92   21.8   0.0   0.0   0.0
!   shoes
    36  4  7   -2E3    0.000  +
        5  7   -2E3    0.000  +
        6  7   -2E3    0.000  +
                           2.0     1.0     2.0   0.0   0.0   0.0
    37  4  7   -2E3    0.000  +
        5  7   -2E3    0.000  +
        6  7   -2E3    0.000  +
```

```
                          2.0     1.0     2.0   0.0   0.0   0.0
  END
  ORIENTATIONS
!   ribs joint 15.5 deg. backward from up,
    6   5   1   2 -0.27053
    6   6   1   2  0.00000
  END
  FUNCTIONS
!   1:  ribs, x rotation
    3
    -1.0  -2908.8  0.0  0.0  1.0  2908.8
!   2: ribs, y rotation
    3
    -1.0  -1090.8  0.0  0.0  1.0  1090.8
!   3: ribs, z-rotation
    3
    -1.0  -2184.0  0.0  0.0  1.0  2184.0
!   4: shoes, x-rotation
    5
    -1.0   -200.0
    -0.2    -25.0
     0.0      0.0
     0.2     25.0
     1.0    200.0
!   5: shoes, y-rotation
    5
    -1.0   -300.0
    -0.2    -25.0
     0.0      0.0
     0.2     25.0
     1.0    300.0
!   6: shoes, z-rotation
    5
    -1.0   -300.0
    -0.2    -25.0
     0.0      0.0
     0.2     25.0
     1.0    300.0
!   7: shoes, x/y/z-rotation unloading
    5
    -1.0    -50.0
    -0.2     -8.0
     0.0      0.0
     0.2      8.0
     1.0     50.0
  END
!*********************************************************************
*
  PLANES
   36 -.0300 -.0300 0.0000  0.1300 -.0300 0.0000  0.1300 0.0300 0.0000
+
         0  0  0  L-shoe-inr-sole
   37 -.0300 -.0300 0.0000  0.1300 -.0300 0.0000  0.1300 0.0300 0.0000
+
         0  0  0  R-shoe-inr-sole
  END PLANES
```

```
!*********************************************************************
*
  ELLIPSOIDS
!   1:5
    1   0.118  0.183  0.090  -.0120 0.0000 -.0150  2  8  0  0.0
Lower Torso
    2   0.070  0.155  0.110  0.0000 0.0000 -.0300  2  0  0  0.0
Lower Abdomen
    2   0.070  0.140  0.170  0.0000 0.0000 0.0300  2  0  0  0.0
Middle Abdomen
    2   0.070  0.140  0.110  0.0000 0.0000 0.0900  2  0  0  0.0
Upper Abdomen
    3   0.105  0.150  0.090  0.0510 0.0000 0.0223  2  8  0  0.0
Lower Lumbar
!   6:10
    4   0.105  0.150  0.090  0.0500 0.0000 0.0425  2  8  0  0.0
Upper Lumbar
    5   0.070  0.158  0.180  -.0059 0.0000 0.0620  2  2  3  2.0E6
Upper Torso Back
    5   0.060  0.075  0.050  0.0090 0.0000 0.2270  2  0  0  0.0
Collar
    6   0.100  0.110  0.090  -.0710 0.0440 0.0900  2  5  0  4.0E5  Left
Up Torso
    6   0.100  0.110  0.090  -.0710 -.0440 0.0900  2  5  0  4.0E5
Right Up Torso
!   11:15
    6   0.0812 0.0712 0.050  -.0470 0.0558 0.0711  2  6  0  0.0    Left
Rib nr 1
    6   0.0939 0.0839 0.050  -.0594 0.0558 0.0427  2  6  0  0.0    Left
Rib nr 2
    6   0.0990 0.0890 0.050  -.0642 0.0545 0.0142  2  6  0  0.0    Left
Rib nr 3
    6   0.1003 0.0903 0.050  -.0651 0.0545 -.0142  2  6  0  0.0    Left
Rib nr 4
    6   0.0969 0.0869 0.050  -.0614 0.0553 -.0427  2  6  0  0.0    Left
Rib nr 5
!   16:20
    6   0.0914 0.0814 0.060  -.0556 0.0558 -.0711  2  6  0  0.0    Left
Rib nr 6
    6   0.0812 0.0712 0.050  -.0470 -.0558 0.0711  2  6  0  0.0
Right Rib nr 1
    6   0.0939 0.0839 0.050  -.0594 -.0558 0.0427  2  6  0  0.0
Right Rib nr 2
    6   0.0990 0.0890 0.050  -.0642 -.0545 0.0142  2  6  0  0.0
Right Rib nr 3
    6   0.1003 0.0903 0.050  -.0651 -.0545 -.0142  2  6  0  0.0
Right Rib nr 4
!   21:25
    6   0.0969 0.0869 0.050  -.0614 -.0553 -.0427  2  6  0  0.0
Right Rib nr 5
    6   0.0914 0.0814 0.060  -.0556 -.0558 -.0711  2  6  0  0.0
Right Rib nr 6
    8   0.0430 0.043  0.030  0.0508 0.0    0.0301  2  0  0  0.0
Neck-Disk1
    13  0.0400 0.025  0.005  0.0000 0.0000 0.0000  8  0  0  0.0
Nodding Plate
!   replaced ellipsoidal head with facet headform model
```

```
    14  0.0001 0.001  0.001  0.0136 0.0000 0.0326  2  0  0  0.0    Head
!   14  0.1050 0.073  0.105  0.0136 0.0000 0.0326  2  0  0  0.0    Head
!   26:30
    14  0.0001 0.001  0.001  0.0720 0.0000 0.0112  2  4  0  1.3E6  Face
+ Chin
!   14  0.0460 0.060  0.100  0.0720 0.0000 0.0112  2  4  0  1.3E6  Face
+ Chin
    15  0.080  0.110  0.060  -.0121 0.0944 0.0026  2  0  0  0.0    Left
Shoulder
    16  0.080  0.110  0.060  -.0121 -.0944 0.0026  2  0  0  0.0
Right Shoulder
    17  0.048  0.044  0.153  0.0000 0.0000 -.1130  2  0  0  0.0    Left
Upper Arm
    18  0.048  0.044  0.153  0.0000 0.0000 -.1130  2  0  0  0.0
Right Upper Arm
!   31:35
    19  0.044  0.044  0.146  0.0000 0.0000 -.1000  2  0  0  0.0    Left
Lower Arm
    20  0.044  0.044  0.146  0.0000 0.0000 -.1000  2  0  0  0.0
Right Lower Arm
    21  0.048  0.025  0.084  0.0000 0.0000 -.0690  2  0  0  0.0    Left
Hand
    22  0.048  0.025  0.084  0.0000 0.0000 -.0690  2  0  0  0.0
Right Hand
    23  0.234  0.088  0.083  0.2250 0.0050 0.0000  2  0  0  0.0    Left
Femur
!   36:40
    23  0.150  0.088  0.085  0.0700 -.0020 -.0189  2  8  0  0.0    Left
Hip
    24  0.234  0.088  0.083  0.2250 -.0050 0.0000  2  0  0  0.0
Right Femur
    24  0.150  0.088  0.085  0.0700 0.0020 -.0189  2  8  0  0.0
Right Hip
    25  0.068  0.065  0.068  0.1046 0.0000 0.0000  2 16 17  0.0    Left
Knee
    26  0.068  0.065  0.068  0.1046 0.0000 0.0000  2 16 17  0.0
Right Knee
!   41:45
    29  0.060  0.055  0.130  -.0150 0.0000 -.1200  2  9  0  0.0
Middle Tibia Left
    30  0.060  0.055  0.130  -.0150 0.0000 -.1200  2  9  0  0.0
Middle Tibia Right
    33  0.120  0.044  0.032  0.0600 0.0000 -.0470  2 13  0 -2.5E6  Left
Foot
    33  0.045  0.040  0.020 -0.0200 0.0000 -.0620  2 11 12 -6.0E6  Left
Heel
    36  0.090  0.060  0.015  0.1550 -.0100 0.0040  2 15  0  0.0    Frnt
Shoe SoleL
!   46:50
    36  0.050  0.050  0.025  -.0200 0.0000 -.0020  4 14  0  0.0    Heel
Shoe Left
    34  0.120  0.044  0.032  0.0600 0.0000 -.0470  2 13  0 -2.5E6
Right Foot
    34  0.045  0.040  0.020 -0.0200 0.0000 -.0620  2 11 12 -6.0E6
Right Heel
    37  0.090  0.060  0.015  0.1550 0.0100 0.0040  2 15  0  0.0    Frnt
Shoe SoleR
```

```
    37  0.050  0.050  0.025  -.0200 0.0000 -.0020  4 14  0  0.0    Heel
Shoe Right
!   51:55
    35  0.020  0.060  0.098  0.0150 0.0000 0.0000  2  7  0  0.0
Sternum
!   new detailed lower leg ellipsoids:
    27  0.055  0.060  0.070  0.0200 0.0000 -.0500  2  9  0  0.0
Upper Tibia Left
    28  0.055  0.060  0.070  0.0200 0.0000 -.0500  2  9  0  0.0
Upper Tibia Right
    29  0.065  0.055  0.075  -.0250 0.0000 -.0500  2  9  0  0.0    Mid
Tibia Left up
    30  0.065  0.055  0.075  -.0250 0.0000 -.0500  2  9  0  0.0    Mid
Tibia Right up
!   56:60
    29  0.055  0.045  0.050  0.0000 0.0000 -.2100  2  9  0  0.0    Mid
Tibia Left lower
    30  0.055  0.045  0.050  0.0000 0.0000 -.2100  2  9  0  0.0    Mid
Tibia Right lower
    31  0.055  0.045  0.070  0.0122 0.0000 -.0350  2  9  0  0.0
Lower Tibia Left
    32  0.055  0.045  0.070  0.0122 0.0000 -.0350  2  9  0  0.0
Lower Tibia Right
!   new detailed foot ellipsoids:
    33  0.085  0.049  0.020  0.1200 -.0040 -.0590  2 13  0  2.0E6  Left
Toes
!   61:65
    34  0.085  0.049  0.020  0.1200 0.0040 -.0590  2 13  0  2.0E6
Right Toes
    36  0.140  0.060  0.043  0.1100 -.0100 0.0300  2 15  0  0.0
Front Shoe Left
    37  0.140  0.060  0.043  0.1100 0.0100 0.0300  2 15  0  0.0
Front Shoe Right
!   only for 5-joint neck, Disk1 is defined above
    9   0.043  0.043  0.030  0.0000 0.0000 0.0141  2  0  0  0.0
Disk2
    10  0.043  0.043  0.030  0.0000 0.0000 0.0141  2  0  0  0.0
Disk3
    11  0.043  0.043  0.030  0.0000 0.0000 0.0141  2  0  0  0.0
Disk4
    12  0.043  0.043  0.030  0.0000 0.0000 0.0141  2  0  0  0.0
Disk5
*   1   0.015  0.015  0.015  -.0120 0.0530 -.0600  2  2  3  1.0E6  Left
Buttock
*   1   0.015  0.015  0.015  -.0120 -.0530 -.0600  2  2  3  1.0E6
Right Buttock
    38   .004   .004   .004  0      0      0       2  0  0  0.0
Goggle Hinge
  END
  ORIENTATIONS
!   Upper Torso Back ellipsoid backward 18 deg.
    7   0   1   2 -0.31416
!   Face pitch up 5 deg. relative to local frame
    26  0   1   2 -0.08727
!   Left Femur pitch up 7 deg., yaw right 1.64 deg. relative to local
frame
    35  0   1   2 -0.12217   3 -0.02862
```

```
!   Right Femur pitch up 7 deg., yaw left 1.64 deg. relative to local
frame
    37  0   1   2 -0.12217   3  0.02862
!   Left Hip pitch up 7 deg., yaw right 1.64 deg. relative to local
frame
    36  0   1   2 -0.12217   3 -0.02862
!   Right Hip pitch up 7 deg., yaw left 1.64 deg. relative to local
frame
    38  0   1   2 -0.12217   3  0.02862
!   Middle Tibia Left and Right
    41  0  1  2   -.170000
    42  0  1  2   -.170000
!   Left and Right Foot
    43  0  1  2   0.110000
    47  0  1  2   0.110000
!   Left and Right Heel Shoe
    46  0  1  2   -.070000
    50  0  1  2   -.070000
!   Front Shoe Sole Left and Right
    45  0  1  2   -.1720
    49  0  1  2   -.1720
!   Left and Right Upper Tibia
    52  0  1  2   -.180000
    53  0  1  2   -.180000
!   Middle Tibia Left and Right up
    54  0  1  2   0.17453
    55  0  1  2   0.17453
!   Lower Tibia Left and Right
    56  0  1  2   -.170000
    57  0  1  2   -.170000
!   Left and Right Toes
    60  0  1  2   -.090000  3  -.180000
    61  0  1  2   -.090000  3  0.180000
  END
  FUNCTIONS
!   1: foot to rigid flat plate contact, function for standard foot
(not used)
    5
    0.0 0.0  0.0021 126.9  0.0038 357.7  0.0084 1576.9  0.0114 2482.6
!   2: lower torso rear to rigid plate loading
    9
    0.0 0.0  0.0062  322.6  0.0131  903.2  0.0208  2064.5  0.0285
3419.4
    0.0320  4616.2  0.0350 6231.8  0.0370 8413.0  0.0390 11357.6
!   3: lower torso rear to rigid plate unloading
    8
    0.0 0.0  0.0123 0.0  0.0192 225.8  0.0285  774.2
    0.0320  1122.6  0.0350 1627.8  0.0370 2360.2  0.0390  3540.4
!   4: chin to flat plate contact
    6
    0.0 0.0  0.0017 94.7  0.0031 386.8  0.0041 718.4  0.0051 1365.8
    0.0069 3007.9
!   5: upper torso to half sphere contact
    5
    0.0 0.0  0.0145 76.5  0.0305 344.1  0.0512 910.0  0.0726 1621.2
!   6: jacket compression for half rib (un)loading, dynamic
```

```
!   (to be applied with:
)
!   (DAMPING ELASTIC FORCE for half ribs of 50% Hybrid III (with
DAMPING COEFFICIENT 1.0)                                    )
!   (6  0.0 0.0  272.1 60.8  567.9 177.6  1125.3 276.1  3157.1 803.0
6925.8 2648.5    )
    6
    0.0 0.0   0.013 272.1  0.020 567.9  0.024 1125.3  0.028 3157.1
0.031 6825.8
!   7: jacket compression for sternum (un)loading, dynamic
!   (to be applied with:
)
!   (DAMPING ELASTIC FORCE for sternum of 50% Hybrid III (with DAMPING
COEFFICIENT 1.0)                                    )
!   (6  0.0 0.0  816 182.4  1704 532.8  3376 828.3  9471 2409  20777
7945.5            )
    6
    0.0 0.0   0.013 816.0  0.020 1704.0  0.024 3376.0  0.028 9471.0
0.031 20777.0
!   8: lower torso bottom to rigid plate (un)loading, dynamic
!   (to be applied with:
)
!   (DAMPING ELASTIC FORCE for lower torso bottom of 50% Hybrid III to
rigid plate contact (with DAMPING COEFFICIENT 1.0)
!   (3  0.0 0.0  1190.0 1927.0  10088.0 10274
)
    7
    0.0 0.0  0.0062  322.6  0.0131  903.2
    0.0170 1990.0  0.020 3200.0  0.0230 5110.0  0.0260 10088.0
!   9: tibia to rigid flat plate contact, loading, static
*   6
*   0.0           0.0
*   0.01896      41.0
*   0.02475     100.0
*   0.02680     200.0
*   0.02900     371.0
*   0.03410    1390.0
!   9: tibia to rigid flat plate contact, loading, dynamic
    6
    0.0           0.0
    0.015       340.0
    0.018       600.0
    0.021      1300.0
    0.024      4000.0
    0.027     10000.0
!   10: tibia to rigid flat plate contact, unloading, static
    6
    0.0           0.0
    0.01896      22.0
    0.02680      41.0
    0.03210     129.0
    0.03280     200.0
    0.03410     371.0
!   11: new foot heel to rigid flat plate contact, loading
    8
    0.0             0.0
    2.51908E-003   89.0
```

```
    4.21946E-003  356.0
    6.04579E-003  890.0
    7.49426E-003 1510.24
    9.00571E-003 2588.9
    1.05801E-002 4585.0
    1.27843E-002  1.75069E+004
!   12: new foot heel to rigid flat plate contact, unloading
    3
    0.0             0.0
    7.49426E-003    0.0
    1.27843E-002    3.93437E+003
!   13: new foot front to rigid flat plate contact
    4
    0.0       0.0
    0.0071  2.49319E+003
    0.0128  4.41549E+003
    0.0207  8.57049E+003
!   14: heel shoe to ground contact
    3
    0.0             0.0
    0.003        1000.0
    0.006        4000.0
!   15: front shoe to ground contact
    4
    0.0             0.0
    0.003        1000.0
    0.005        3000.0
    0.006        5000.0
!   16:  knee to flat plate loading
    4
    0.0000       0.0
    0.001       96.8
    0.002      419.4
    0.0046    1548.4
!   17:  knee to flat plate unloading
    4
    0.0000       0.0
    0.0021      16.1
    0.0031     177.4
    0.0038     483.9
  END
!**********************************************************************
*
! FORCE MODELS HYBRID III 50th percentile male dummy
! these are now placed under SYSTEM instead of FORCE MODELS
!**********************************************************************
*
  POINT-RESTRAINTS
!   translational stiffness of the rib body:
!   1: ribs to upper torso
       5  0.1517 0.0   0.0762    6  0.000  0.000  0.000  +
    1  2  2.0E5  0.0   3  0  0.0  0.0   4  0  0.0  0.0  +
     600.0  9600.0  1200.0  Ribs
!   the effect of vertical abdomen compression on lumbar spine bending
!   has been incorporated with two point restraints:
!   2: Abdomen vertical compression left
       5  0.1988 0.1   -.07828    1  0.070  0.100  0.120  +
```

```
    0  0  0.0  0.0   0  0  0.0  0.0   5  6  1E5  0.0  +
    0.0  0.0  0.0  Abdomen-vert-left
!   3: Abdomen vertical compression right
       5  0.1988 -.1   -.07828    1  0.070  -.100  0.120  +
    0  0  0.0  0.0   0  0  0.0  0.0   5  6  1E5  0.0  +
    0.0  0.0  0.0  Abdomen-vert-right
!   4: Abdomen vertical compression middle
       4  0.14829  0.0  0.0001    1  0.067  0.000  0.140  +
    0  0  0.0  0.0   0  0  0.0  0.0   5  6  1E5  0.0  +
    0.0  0.0  0.0  Abdomen-vert-middle
!   5-8: translational stiffness of shoes wrt feet
      33  0.08   0.0   -.06     36  0.080  0.000  0.020  +
    7  8  3.0E5  0.0   9  10 2.0E5  0.0   11 12 2.0E5  0.0   +
       0.0     0.0     0.0  FrontLShoe
      33  -.02   0.0   -.06     36  -.020  0.000  0.020  +
    7  8  3.0E5  0.0   9  10 2.0E5  0.0   0  0  0.0    0.0   +
       0.0     0.0     0.0  RearLShoe
      34  0.08   0.0   -.06     37  0.080  0.000  0.020  +
    7  8  3.0E5  0.0   9  10 2.0E5  0.0   11 12 2.0E5  0.0   +
       0.0     0.0     0.0  FrontRShoe
      34  -.02   0.0   -.06     37  -.020  0.000  0.020  +
    7  8  3.0E5  0.0   9  10 2.0E5  0.0   0  0  0.0    0.0   +
       0.0     0.0     0.0  RearRShoe
  END
  ORIENTATIONS
! Ribs point restraint oriented just as the cardan restraint of the
Ribs
    1   0   1   2 -0.27053
! Abdomen-z point restraints left & right
    2   0   1   2 -0.25
    3   0   1   2 -0.25
! Abdomen-z point restraint middle
    4   0   1   2 -1.0
  END
  FUNCTIONS
!   1,2: ribs compression (negative), loading / unloading
    6
    -.0558  -8000.0  -.0437  -6000.0  -.0306  -4000.0  -.0165  -2000.0
                    0.0 0.0  0.0165  2000.0
    7
    -.0631  -8000.0  -.0510  -6000.0  -.0379  -4000.0  -.0232  -2000.0
    -.0085   -300.0  0.0 0.0  0.0085   300.0
!   3: ribs lateral displacement
    3
    -1.0  -9.60E5  0.0 0.0  1.0 9.60E5
!   4: ribs upward displacement
    4
    -.02 -5.00E3  -.01 -1.20E3  0.0 0.0  1.0 1.20E5
!   5: abdomen z-compression loading
    4
    -1.0  0.0  0.0 0.0  0.05 300  0.075  970    0.15 4100
!   6: abdomen z-compression unloading
    4
    -1.0  0.0  0.0 0.0  0.05   0  0.15 2050
!   7,8: shoes X loading / unloading
  5
  -.02  -1000
```

```
  -.01   -200
  0     0
  0.003   200
  0.01   2000
  3
  -.02    -50
  0     0
  0.01     50
!   9,10: Y loading / unloading
  5
  -.01   -500
  -.003  -100
  0     0
  0.003   100
  0.01    500
  3
  -.01    -50
  0     0
  0.01     50
!   11,12: Z loading / unloading
  4
  -.015 -1000
  -.005  -100
  0     0
  0.02    100
  3
  -.015  -100
  0     0
  0.02     10
  END
! ------------------------------------------------------------------
! lumbar spine cable for 1-pivot lumbar spine
! to be used in addition to PROTECTED JOINT model
! ------------------------------------------------------------------
  KELVIN
    3  -.0040 0.0000 0.0123  +
    4  -.0010 0.0000 0.0600  +
    ABSOLUTE   +
    1  0  0.0  0.0  0.0  0.12015  0  Spine Cable
  END
  FUNCTIONS
!   spine elongation minus 2850/0.0050
    6
    -1         0.0
    0.0000     0.0
    0.0002   100.0
    0.0010  1800.0
    0.0025  7000.0
    0.0050  20000.0
  END
  CONTACT INTERACTIONS
    ELLIPSOID-ELLIPSOID
!   SY1 EL1 SY2 EL2 CHO LO UNLO HYS   XEL DAMP1 FRIC FIN COR DAFR DAMP1
!     1,2: Chin to Left/Right Upper Torso
         26     9   3   0  0    0.0   0.  200.0 0.50      1  0    0
         26     10  3   0  0    0.0   0.  200.0 0.50      1  0    0
!     torso-leg contact
```

```
!     3,4: Left Lower Rib to Left Hip + femur
         16     35  4   1  0    0.0   0.   25.0 0.50      1  0    2
         16     36  4   1  0    0.0   0.   25.0 0.50      1  0    2
!     5,6: Right Lower Rib to Right Hip + femur
         22     37  4   1  0    0.0   0.   25.0 0.50      1  0    2
         22     38  4   1  0    0.0   0.   25.0 0.50      1  0    2
!     7: Face to Left Leg
*        25     36  4   1  0    0.0   0.   25.0 0.50      1  0    2
!     8: Face to Right Leg
*        25     38  4   1  0    0.0   0.   25.0 0.50      1  0    2
!     9: Knee to Knee contact
*        39     40  4   1  0    0.0   0.   25.0 0.50      1  0    2
    END
    FUNCTIONS
!   1: rib-hip loading
    3
    0.0      0.0
    0.020  200.0
    0.040  500.0
!   2: general DAMPING ELASTIC FORCE
    2
    0.0 0.0  1.0E4 1.0E4
    END
    PLANE-ELLIPSOID
!   SYS PLA SYS ELL CHO LO UNLO HYS   XEL DAMP1 FRIC FIN COR DAFR DAMP2
        1       44  4   1  0    0.0   0.  8.7E2 0.90 -1   0  0    2
heel-shoe-L
        1       60  4   3  0    0.0   0.  4.0E2 0.90 -1   0  0    2
toes-shoe-L
        2       48  4   1  0    0.0   0.  8.7E2 0.90 -1   0  0    2
heel-shoe-R
        2       61  4   3  0    0.0   0.  4.0E2 0.90 -1   0  0    2
toes-shoe-R
    END PLANE-ELLIPSOID
    FUNCTIONS
!   1: foot shoe compression
!   based on new foot heel to rigid flat plate contact, loading
    8
    0            0
    0.002        1.6042E+02
    0.00335      6.4167E+02
    0.0048       1.6042E+03
    0.00595      2.7221E+03
    0.00715      4.6663E+03
    0.0084       8.2642E+03
    0.01015      1.6041E+04
!   2: DAMPING ELASTIC FORCE function heel-plate (DAMP2)
         3
         0.0       0.0
         1.0E3     1.0
         1.0E4     2.0
!   3: new foot front to rigid flat plate contact
     4
    0.0       0.0
    0.0071  2.49319E+003
    0.0128  4.41549E+003
    0.0207  8.57049E+003
```

```
   END FUNCTIONS
END CONTACT INTERACTIONS
!************************************************************************
*
! end of FORCE MODELS HYBRID III 50th percentile male dummy
! these are now placed under SYSTEM instead of FORCE MODELS
!************************************************************************
*
FACET SURFACE 1
HybridIII 50% head
COORDINATES
      1   0.10007802   1.2213E-05   0.09572956
      … !(ABBREVIATED)
   622   -0.0515012   -0.0166696   -0.0077138
END COORDINATES
FACETS
1     TRIANG      356   357   379
… !(ABBREVIATED)
1210  TRIANG      253   239   256
END FACETS
GEOMETRIES
 ! Add the thickness of the counter object (specified in the contact
interaction) here.
  THICKNESS    0.1
  SET          1:622
END GEOMETRIES
SECTIONS
  BODY         14  ! defines a facet surface "coating" the dummy head
  SET          1:622
  INITIAL CONDITIONS
!   origin in upper neck load cell measuring point
!   (0.0178 m above nodding joint)
    0   0.000000   0.000000   0.000000
  ORIENTATIONS
    1   0   1   2   0.0
  END  ORIENTATIONS
END SECTIONS
END FACET SURFACE
!************************************************************************
**
FACET SURFACE 2
Goggles
COORDINATES
! 75 vertices (nodes) total
       1  1.262224895E-01  5.377368806E-02  -1.71500000E-02
      … !(ABBREVIATED)
      91  1.847225000E-01  5.344695000E-02  5.524600000E-02
END COORDINATES
FACETS
      ! end caps
       1  TRIANG       1         3        17
      … !(ABBREVIATED)
      16  TRIANG      15        16        18
     ! cylindrical surface
      17  QUAD        52        59        10         2
     … !(ABBREVIATED)
      80  QUAD        88        83        84        90
```

```
     ! hinge element
      81  TRIANG      91        84        75
END FACETS
GEOMETRIES
  THICKNESS    0.001
  SET          1:18,35:91
END GEOMETRIES
SECTIONS
  BODY      38  ! attached to spring loaded ball hinge betw NVG and
helmet
  SET       1:18,35:91
 ! local coordinates, turn triads on to see, moves goggles wrt ball
hinge
  INITIAL CONDITIONS
    0   .053  -.185  -0.055
  ORIENTATIONS
    1   0   1   3   1.570796
  END  ORIENTATIONS
END SECTIONS
END FACET SURFACE
!
************************************************************
FACET SURFACE 3
Orbit
COORDINATES
! 104 total vertices (nodes)
     ! orbital walls
       1  5.210270792E-02  5.697431203E-02  5.001761514E-03
       … !(ABBREVIATED)
       8  0.900533304E-01  7.295969575E-02  -1.59982385E-02
     ! trochlea (pulley) for superior oblique muscle
       9  0.102053      4.389056799E-02     0.015925
       … !(ABBREVIATED)
      120   0.102486    4.442374260E-02    0.015398
END COORDINATES
FACETS
! 94 total facet elements
    ! orbital walls
       1  QUAD  1  2  8  7
       … !(ABBREVIATED)
       4  QUAD  3  1  7  5
    ! trochlea (hook) for superior oblique muscle
      5  QUAD   9 10    26    25
      … !(ABBREVIATED)
     94  QUAD   119     120   57    58
END FACETS
GEOMETRIES
  THICKNESS    0.001
  SET          1:72,89:120
  END GEOMETRIES
SECTIONS
  BODY         14 ! dummy head
  SET          1:72,89:120
  INITIAL CONDITIONS
    0   -.0045  -0.0267  0.0471
  ORIENTATIONS
    1   0   1   2   0.0
```

```
  END  ORIENTATIONS
END SECTIONS
END FACET SURFACE
!          ************************************************************
FACET SURFACE 4
Helmet
COORDINATES
! 139 total vertices (nodes)
       1  -5.59012618E-02  9.657368806E-02  1.003734320E-01
      … !(ABBREVIATED)
     143  3.963009836E-02  4.657368806E-02   0.00000000E+00
   ! extend out towards goggle's spring loading ball hinge
     144  .12422907592   -2.34263119E-02     .10257851827
     145  .12160844717   1.748215580E-02     .10257851827
END COORDINATES
FACETS
! 246 total facet elements
       1  TRIANG        14        22         1
    … !(ABBREVIATED)
    242  TRIANG        71       143        70
 ! elements which support the goggles/hinge, purely visual
    243  TRIANG       144        11        62
    … !(ABBREVIATED)
    246  TRIANG       145       144        72
END FACETS
GEOMETRIES
  THICKNESS    0.001
  SET          1:129,132:134,136,140:145
  END GEOMETRIES
SECTIONS
  BODY         14 ! dummy head
  SET          1:129,132:134,136,140:145
  INITIAL CONDITIONS
    0   .045  0.022  0.001
  ORIENTATIONS
    1   0   1   2   0.0
  END  ORIENTATIONS
END SECTIONS
END FACET SURFACE 4
!*******************************
  INITIAL CONDITIONS
!   leave this line open, position dummy with JOINT DOF of joint 1

  JOINT DOF
!   dummy orientation: (roll right; pitch down; yaw left;) 4 Euler
params.
!                                -0.21644
    1   FREE   0.97630   0.00000  -0.08644   0.00000  +
!   dummy position:     forward;  leftward;  upward
!   25 deg rotation backwards     ! initially -1.250
                        -1.450     0.350     0.320
!   abdomen: compression=backward
    2   FREE   0.00000
!   lower lumbar spine bracket: always locked
    3   LOCK
!   lumbar spine: rz, ry, rx + z, y, x  !0.0000
    4   FREEROTATIONS   1  0.0000     2  0.0000     3  0.0000    +
```

```
                        0.00000       0.00000       0.00000
!   upper lumbar spine bracket: always locked
    5   LOCK
!   ribs        : ry, -rx, rz + y, -x, z
    6   FREEROTATIONS   1  0.0000     2  0.0000     3  0.0000    +
                        0.00000       0.00000       0.00000
!   neck flexion angle adjustment bracket
!   insert the angle as read from the bracket in here
!   flexion=pitch down, always locked ***made dummy look down, was
zero***
    7   LOCK   0.3000
             !.33
!   lower neck sensor: always locked
    8   LOCK
!   neck pivots: (roll right; pitch down; yaw left)
    9   FREEROTATIONS   1  0.0000     2  0.0000     3  0.0000
    10  FREEROTATIONS   1  0.0000     2  0.0000     3  0.0000
    11  FREEROTATIONS   1  0.0000     2  0.0000     3  0.0000
    12  FREEROTATIONS   1  0.0000     2  0.0000     3  0.0000
!   nodding joint, flexion
    13  FREE   0.0000
!   upper neck sensor: always locked
    14  LOCK
!   left clavicle: elevation=roll right; posterior rotation=yaw left
    15  FREE   0.00000   0.00000
!   right clavicle: depression=roll left, anterior rotation=yaw left
    16  FREE   0.00000   0.00000
!
!   shoulder degrees of freedom are not exactly the same as in previous
versions of the database;
!   in order to get about the same arm position the following
correction should be made :
!   .15708 has to be added to the second DOF of joint 14,
!   the same amount has to be subtracted from the second DOF of joint
15
!
!   left shoulder: extension=pitch down; abduction=roll right
!   50 deg flexion, 15 deg abduction
    17  FREE  0.07270   0.26180
!   right shoulder: extension=pitch down; adduction=roll right
!   50 deg flexion, 15 deg abduction
    18  FREE  -0.67270  -0.26180
!
!   left elbow: lateral rotation=yaw left; hyper-extension=pitch down
up
!   50 deg extension, 30 deg medial rotation
    19  FREE   -0.22360  -0.17270
!   right elbow: medial rotation=yaw left; hyper-extension=pitch down
up
!   50 deg extension, 30 deg medial rotation
    20  FREE   1.42360  -0.999270
!
!   left wrist: lateral axial rotation=yaw left; extension=roll right
    21  FREE   0.00000   0.00000
!   right wrist: medial axial rotation=yaw left; flexion=roll right
    22  FREE   2.00000   0.00000
!   previous models:
```

```
!   left hip: (extension=pitch down; medial rotation=roll left;
!              abduction=yaw left) 4 Euler params.
!   5 deg extension
    23  FREE   1.89905  0.00000  0.04362   0.00000
!   right hip: (extension=pitch down; lateral rotation=roll left;
!               adduction=yaw left) 4 Euler params.
!   5 deg extension
    24  FREE   1.89905  0.00000  0.04362   0.00000
!   femur load cells: allways locked
    25  LOCK
    26  LOCK
!   knees: flexion, compression of knee slider
!   25 deg extension
    27  FREE  -0.83633  0.0
    28  FREE  -0.83633  0.0
!   upper tibia load cells: allways locked
    29  LOCK
    30  LOCK
!   lower tibia load cells: allways locked
    31  LOCK
    32  LOCK
!   new ankles: compared to the previous model about
!   -.06 rad has to be added for rotation 3
! left : (1=lateral rotation=-z; 2=eversion =-x; 3=plantarflexion=y)
    33  FREEROTATIONS   1  0.0000     2  0.0000     3  -.0600
! right: (1=medial rotation =-z; 2=inversion=-x; 3=plantarflexion=y)
    34  FREEROTATIONS   1  0.0000     2  0.0000     3  -.0600
!   sternum -compression
    35  FREE   0.00000
!   shoes
    36  FREEROTATIONS   1  0.0000     2  0.0000     3  0.0000
    37  FREEROTATIONS   1  0.0000     2  0.0000     3  0.0000
!   goggles hinge
    38  FREE   0.0
  END
!************************************************************************
*
! END HYBRID III 50th percentile male dummy with 5-joint neck
!************************************************************************
*
END SYSTEM 2
FORCE MODELS
  CONTACT INTERACTIONS
    PLANE-ELLIPSOID
      1  3  2  45 1   0  0    0.0   0.01   200.00  0.6  0.0   0  0
      1  4  2  45 1   0  0    0.0   0.01   200.00  0.6  0.0   0  0
      1  3  2  46 1   0  0    0.0   0.01   200.00  0.6  0.0   0  0
      1  4  2  46 1   0  0    0.0   0.01   200.00  0.6  0.0   0  0
      1  3  2  49 1   0  0    0.0   0.01   200.00  0.6  0.0   0  0
      1  4  2  49 1   0  0    0.0   0.01   200.00  0.6  0.0   0  0
      1  3  2  50 1   0  0    0.0   0.01   200.00  0.6  0.0   0  0
      1  4  2  50 1   0  0    0.0   0.01   200.00  0.6  0.0   0  0
      1  5  2  39 2   0  0    0.0   0.025  100.00  0.3  0.005 0  0
      1  7  2  39 2   0  0    0.0   0.025  100.00  0.3  0.005 0  0
      1  6  2  40 2   0  0    0.0   0.025  100.00  0.3  0.005 0  0
      1  8  2  40 2   0  0    0.0   0.025  100.00  0.3  0.005 0  0
      1  1  2  36 2   0  0    0.0   0.025  100.00  0.3  0.005 1  0
```

```
    1  1  2  38 2   0  0    0.0   0.025  100.00  0.3  0.005 1  0
    1  1  2  1  2   0  0    0.0   0.025  100.00  0.3  0.005 1  0
    1  2  2  1  2   0  0    0.0   0.025  100.00  0.3  0.005 0  0
    1  2  2  7  2   0  0    0.0   0.025  100.00  0.3  0.005 0  0
    1  3  1  23 4   1  0   5.E5   0.01   100.00  0.3  0.0   1  0
    1  3  1  22 4   1  0   5.E5   0.01   100.00  0.3  0.0   1  0
  END
  FUNCTIONS
!   1: pedals to floor
    4
  0.000        0   0.002      125   0.004      400   0.010     2000
  END
  ELLIPSOID-ELLIPSOID
    1  19 2  26 4   2  0    0.0   0.01  100.0 0.3   0  0
    1  10 2  26 4   1  0    0.0   0.01  100.0 0.3   0  0
    1  11 2  26 4   1  0    0.0   0.01  100.0 0.3   0  0
    1  12 2  26 4   1  0    0.0   0.01  100.0 0.3   0  0
    1  19 2  9  4   2  0    0.0   0.01  100.0 0.3   0  0
    1  19 2  10 4   2  0    0.0   0.01  100.0 0.3   0  0
    1  18 2  51 4   1  0    0.0   0.01  100.0 0.3   0  0
    1  3  2  51 4   1  0    0.0   0.01  100.0 0.3   0  0
    1  4  2  51 4   1  0    0.0   0.01  100.0 0.3   0  0
    1  18 2  11 4   1  0    0.0   0.01  100.0 0.3   0  0
    1  3  2  11 4   1  0    0.0   0.01  100.0 0.3   0  0
    1  18 2  12 4   1  0    0.0   0.01  100.0 0.3   0  0
    1  3  2  12 4   1  0    0.0   0.01  100.0 0.3   0  0
    1  18 2  13 4   1  0    0.0   0.01  100.0 0.3   0  0
    1  3  2  13 4   1  0    0.0   0.01  100.0 0.3   0  0
    1  18 2  14 4   1  0    0.0   0.01  100.0 0.3   0  0
    1  3  2  14 4   1  0    0.0   0.01  100.0 0.3   0  0
    1  18 2  15 4   1  0    0.0   0.01  100.0 0.3   0  0
    1  3  2  15 4   1  0    0.0   0.01  100.0 0.3   0  0
    1  18 2  16 4   1  0    0.0   0.01  100.0 0.3   0  0
    1  3  2  16 4   1  0    0.0   0.01  100.0 0.3   0  0
    1  4  2  17 4   1  0    0.0   0.01  100.0 0.3   0  0
    1  3  2  17 4   1  0    0.0   0.01  100.0 0.3   0  0
    1  4  2  18 4   1  0    0.0   0.01  100.0 0.3   0  0
    1  3  2  18 4   1  0    0.0   0.01  100.0 0.3   0  0
    1  4  2  19 4   1  0    0.0   0.01  100.0 0.3   0  0
    1  3  2  19 4   1  0    0.0   0.01  100.0 0.3   0  0
    1  4  2  20 4   1  0    0.0   0.01  100.0 0.3   0  0
    1  3  2  20 4   1  0    0.0   0.01  100.0 0.3   0  0
    1  4  2  21 4   1  0    0.0   0.01  100.0 0.3   0  0
    1  3  2  21 4   1  0    0.0   0.01  100.0 0.3   0  0
    1  4  2  22 4   1  0    0.0   0.01  100.0 0.3   0  0
    1  3  2  22 4   1  0    0.0   0.01  100.0 0.3   0  0
    1  2  2  1  1   0  0    0.    0.    100.0 0.3   0  0
    1  23 2  49 2   0  0    0.0   0.01  100.0 0.7   0  0
    1  22 2  45 2   0  0    0.0   0.01  100.0 0.7   0  0
    1  23 2  50 2   0  0    0.0   0.01  100.0 0.7   0  0
    1  22 2  46 2   0  0    0.0   0.01  100.0 0.7   0  0
  * 1  20 2  40 1   0  0    0.0   0.01  300.0 0.3   0  0
  END
  FUNCTIONS
!   1:  Steering Wheel Rim - Body Parts
    3
    0.000        0   0.005      500   0.050    15000
```

```
  !   1:  Steering Wheel Hub - Body Parts
      3
      0.000        0   0.005      500   0.050     5000
    END
    EVALUATIONS
  !   one of the Rim ellipsoids to the Head
      2002  2003  2004
  !   one of the Rim ellipsoids to the Sternum
      2007  2008  2009
  !   one of the Rim ellipsoids to the one of the Left Rib ellipsoids
      2010  2011  2012  2013  2014  2015  2016  2017  2018  2019  2020
2021
  !   one of the Rim ellipsoids to the one of the Right Rib ellipsoids
      2022  2023  2024  2025  2026  2027  2028  2029  2030  2031  2032
2033
    END
  END CONTACT INTERACTIONS
END FORCE MODELS
!*********************************************************************
*
FEM MODEL 1
  Driver Airbag (600mm diameter)
  MODEL PARAMETERS
    ALPHA   50.0
    BAGV0   0.0001
  END
  REFERENCE COORDINATES
  ! ... NODES ON THE EDGES OF PATCHES
  ! ... ... SIDE 1
       1  3.000E-01  0.000E+00  1.000E-03
     … !(ABBREVIATED)
 !   node   1027 center inflator
    1027  0.000E-00  0.000E-00  0.000E-00
  END
  COORDINATES
       1  6.800E-02  0.000E+00  1.000E-03
    … !(ABBREVIATED)
    1027  0.000E-00  0.000E-00  0.000E-00
  END
  ELEMENTS
  ! ... ... SIDE 1
  ! ... ... ... PATCH NUMBER:   1
       1 MEM3   150    43    44
   … !(ABBREVIATED)
  !   ELEMENT   2048 IS A HOLE
    2048 MEM3   113   115   114
  END
  MATERIALS
! Patch number 1
    TYPE       ORTHOTEN
      E11       250.0E6
      E22       250.0E6
      NU12         0.00
      G12        25.0E6
      DAMPING      0.10
      MAT DIRECT    1.0  0.0  0.0
      DENSITY     750.0
```

```
     SET                   1:992
! Patch number 2
    TYPE       ORTHOTEN
      E11       250.0E6
      E22       250.0E6
      NU12         0.00
      G12        25.0E6
      DAMPING      0.10
      MAT DIRECT    1.0  0.0  0.0
      DENSITY     750.0
     SET                   993:1022
! Patch number 3
    TYPE       ORTHOTEN
      E11       250.0E6
      E22       250.0E6
      NU12         0.00
      G12        25.0E6
      DAMPING      0.10
      MAT DIRECT    1.0  0.0  0.0
      DENSITY     750.0
     SET                   1023:1024
! Patch number 4
    TYPE       ORTHOTEN
      E11       250.0E6
      E22       250.0E6
      NU12         0.00
      G12        25.0E6
      DAMPING      0.10
      MAT DIRECT    1.0  1.0  0.0
      DENSITY     750.0
     SET                   1025:2016
! Patch number 5
    TYPE       ORTHOTEN
      E11       250.0E6
      E22       250.0E6
      NU12         0.00
      G12        25.0E6
      DAMPING      0.10
      MAT DIRECT    1.0  1.0  0.0
      DENSITY     750.0
     SET                   2017:2046
! Patch number 6
    TYPE HOLE
  * !  correction for deviation from 30mm diameter
  *     CDEX   1.571E+00
  !  Cd 0.75 (40mm diameter)
     CDEX      2.09467
     SET                   2047:2048
  END MATERIALS
  GEOMETRIES
    TYPE  MEM3
       THICK   0.5E-3
    SET   1:2046
  END GEOMETRIES
  CONTACT INTERACTIONS
    ELLIPSOID-NODE
!   steering wheel Rim
```

```
      1   1  3  0.2   113:116  572:1018
      2   1  4  0.2   113:116  572:1018
      3   1  5  0.2   113:116  572:1018
      4   1  6  0.2   113:116  572:1018
      5   1  7  0.2   113:116  572:1018
      6   1  8  0.2   113:116  572:1018
      7   1  9  0.2   113:116  572:1018
      8   1  10 0.2   113:116  572:1018
      9   1  11 0.2   113:116  572:1018
      10  1  12 0.2   113:116  572:1018
      11  1  13 0.2   113:116  572:1018
      12  1  14 0.2   113:116  572:1018
      13  1  15 0.2   113:116  572:1018
      14  1  16 0.2   113:116  572:1018
      15  1  17 0.2   113:116  572:1018
      16  1  18 0.2   113:116  572:1018
!   vehicle A Pillar
      17  1  24 0.2   1:96  113:1018
!   dummy
      18  2  25 0.2  1:96  117:571
      19  2  26 0.2  1:96  117:571
      20  2  23 0.2  1:96  117:571
      21  2  8  0.2  1:96  117:571
      22  2  51 0.2  1:96  117:571
      23  2  9  0.2  1:96  117:571
      24  2  10 0.2  1:96  117:571
      25  2  11 0.2  1:96  117:571
      26  2  12 0.2  1:96  117:571
      27  2  13 0.2  1:96  117:571
      28  2  14 0.2  1:96  117:571
      29  2  15 0.2  1:96  117:571
      30  2  16 0.2  1:96  117:571
      31  2  17 0.2  1:96  117:571
      32  2  18 0.2  1:96  117:571
      33  2  19 0.2  1:96  117:571
      34  2  20 0.2  1:96  117:571
      35  2  21 0.2  1:96  117:571
      36  2  22 0.2  1:96  117:571
      37  2  27 0.2  1:96  117:571
      38  2  28 0.2  1:96  117:571
      39  2  29 0.2  1:96  117:571
      40  2  30 0.2  1:96  117:571
      41  2  64 0.2  1:96  117:571
      42  2  65 0.2  1:96  117:571
      43  2  66 0.2  1:96  117:571
      44  2  67 0.2  1:96  117:571
    END
    PLANE-NODE
!   airbag module
      45  1  9  0.001  0.0   1:96  113:1018
      46  1  10 0.001  0.0   1:96  113:1018
      47  1  11 0.001  0.0   1:96  113:1018
      48  1  12 0.001  0.0   1:96  113:1018
      49  1  13 0.001   0.0   1:96  113:1018
      50  1  14 0.1E-3  0.0   113:116  572:1018
      51  1  15 0.1E-3  0.0   113:116  572:1018
      52  1  16 0.1E-3  0.0   113:116  572:1018
```

```
      53  1  17 0.1E-3  0.0   113:116  572:1018
!   vehicle windscreen
      54  1  18 0.010  0.1   1:96  113:1018
    END
  END CONTACT INTERACTIONS
  SUPPORTS
    1   1  10 97:112  1019:1026
  END
  INITIAL CONDITIONS
    1027  0.015  0.000 -0.010   0.0  0.0  0.0   1   1  10
  ORIENTATIONS
    1   0   1   3   1.57080  1   1.57080
  END
  FEMHIS
    1  PRINT AIRBAG   PRESSURE.R   bag gage pressure (N/m^2)
    2  PRINT AIRBAG   TEMPERATURE
    3  PRINT AIRBAG   VOLUME.T     BAG VOLUME (m^3)
    4  PRINT AIRBAG   GAS          MASS OF GAS IN BAG (kg)
    5  PRINT AIRBAG   GAS.I        MASS OF GAS SUPPLIED (kg)
    6  PRINT AIRBAG   GAS.O        MASS OF GAS EXHAUSTED (kg)
!  leading edge velocity of airbag during deployment
!  node 564 is part of patch 2, the front rectangular patch
    7  PRINT NODE  564  VELOCITY.R  resultant velocity (m/s)
    8  PRINT NODE  564  VELOCITY.X  velocity in X-dir (m/s)
    9  PRINT NODE  564  VELOCITY.Y  velocity in Y-dir (m/s)
   10  PRINT NODE  564  VELOCITY.Z  velocity in Z-dir (m/s)
  END FEMHIS
  AIRBAG
    AMBIENT
      PRESSURE     101325.0
      TEMPERATURE     288.15
    END
    INFLATOR
      GASES
        N2   1.00
      END
      MASS FLOW
!      inflator (40gr gas)
        0.000    0.000   0.002    1.444   0.004    1.975   0.006
2.078
        0.008    2.040   0.010    1.970   0.012    1.916   0.014
1.829
        0.016    1.637   0.018    1.351   0.020    1.064   0.022
0.847
        0.024    0.678   0.026    0.508   0.028    0.332   0.030
0.181
        0.032    0.083   0.034    0.031   0.036    0.013   0.038
0.014
        0.040    0.020
      END
      TEMPERATURE
        0.000   500.00
        0.040   500.00
      END
      JET
        1   0.000  0.000  0.000   0.025  0.000   0.  0.  1.
      TRIGGER LOGIC  4
```

```
    END INFLATOR
  END AIRBAG
END FEM MODEL 1
!*****************************************************************
**********
FEM MODEL 2
shellensciliary
COORDINATES
     ! shell = cornea and sclera  ********************
     ! cornea = nodes 1-70, 41 total
       1  1.107946935E-01  5.377368806E-02   0.00000000E+00
      … !(ABBREVIATED)
      70  1.082945335E-01  5.895596910E-02  -2.14372947E-03
    ! sclera = nodes 71-458, 193 total
      71  1.063863935E-01  4.802366828E-02  -5.75001979E-03
      … !(ABBREVIATED)
     458  8.675469348E-02  5.377368806E-02   0.00000000E+00
! lens, 10 nodes *****************
       459  1.079946935E-01  5.377368806E-02   0.00000000E+00
     … !(ABBREVIATED)
       468  1.047546935E-01  5.377368806E-02   0.00000000E+00
! four straight muscles, 192 nodes ***********
     469    5.55E-02    5.74E-02    -2.80E-03
    … !(ABBREVIATED)
     699  9.462365203E-02  4.504862457E-02  -1.28E-02
! superior oblique muscle, 32 nodes
     700  5.892019627E-02  4.771848436E-02  1.905494498E-03
    … !(ABBREVIATED)
     731  9.819378696E-02  4.974328509E-02  1.096800464E-02
END COORDINATES
ELEMENTS
! shell **********************
! cornea, 64 elements
1     MEM3  1     2     3
… !(ABBREVIATED)
64    MEM3  36    35    22
! sclera, 400 elements ********************
65    MEM3  87    42    71
… !(ABBREVIATED)
464   MEM3  457   453   458
! lens, 16 elements  **************************
465   MEM3  459   460   461
… !(ABBREVIATED)
480   MEM3  467   462   468
! ciliary body muscles, 32 elements  ********************
481   MEM3  462   81  109
… !(ABBREVIATED)
504   MEM3  460  103   79
! replaced each mem4 with two mem3's to incr stability (Rob Marshall's
recom)
843   MEM3  460   79   94
… !(ABBREVIATED)
850   MEM3  462   97   81
! four straight eye muscles, 272 elements **********************
505   MEM3  469   470   486
… !(ABBREVIATED)
760   MEM3  212   248   671
```

```
! muscle to sclera attachment elements
761   MEM3  176   208   160
… !(ABBREVIATED)
776   MEM3  253   205   217
! inferior oblique muscle, 32 elements
777  MEM3    301  302   323
… !(ABBREVIATED)
808  MEM3    690  699   698
! superior oblique muscle, 34 elements
809   MEM3  700     701 716
… !(ABBREVIATED)
838   MEM3  220     195 730
! scleral attachment elements
839   MEM3  195  243  220
… !(ABBREVIATED)
842   MEM3  291  220  243
END ELEMENTS
MATERIALS
! non-linear cornea
  TYPE         HYSISO
   LOAD FUNC        1
   DENSITY       1400   ! water = 999 kg/m^3, collagen = 1800 kg/m^3
   SET           1:64   ! all corneal elements
! non-linear sclera
  TYPE         HYSISO
   LOAD FUNC        2
   DENSITY       1400   ! same as cornea
   SET         65:464   ! all scleral elements
! rigid lens
  TYPE          ISOLIN
   E               5E6   ! arbitrary value, later defined as rigid **
   NU              0.4   ! over-ruled after defined below as rigid **
   DENSITY         315   ! Kisielewicz et al., 1998
   SET         465:480
! ciliary body, 4 straight muscles, 2 obliques, *tension only*
  TYPE        ISOTEN
   E             11E6  ! passive strength of muscle collagen fibers...
   NU             0.4   ! Poisson's Ratio, 0.50 = incompressible
   DENSITY      1600   ! water = 999 kg/m^3, collagen = 1800 kg/m^3
   SET       481:504,843:850,505:776,777:842
END MATERIALS
FUNCTIONS
! these are points from the nonlinear stress-strain curves
7    ! cornea, taken from Uchio et al., 1999, strip tests
0 0 .026 3.24E6 .038 4.96E6 .051 6.54E6 .067 7.65E6 .112 8.81E6 .164
9.54E6
7    ! sclera, taken from Uchio et al., 1999, strip tests
0 0 .009 3.22E6 .015 4.94E6 .019 6.49E6 .026 7.65E6 .044 8.79E6 .064
9.49E6
END FUNCTIONS
GEOMETRIES
! shell with varying thickness
    TYPE  MEM3
       THICK   0.52E-3
    SET   1:8        ! corneal apex
    TYPE  MEM3
       THICK   0.59E-3
```

```
    SET   9:32
    TYPE  MEM3
       THICK   0.66E-3
    SET   33:64
    TYPE  MEM3
       THICK   0.80E-3
    SET   65:104     ! limbus
    TYPE  MEM3
       THICK   0.72E-3
    SET   105:152
    TYPE  MEM3
       THICK   0.63E-3
    SET   153:200
    TYPE  MEM3
       THICK   0.55E-3
    SET   201:296    ! scleral thinning
    TYPE  MEM3
       THICK   0.64E-3
    SET   297:344
    TYPE  MEM3
       THICK   0.73E-3
    SET   345:392
    TYPE  MEM3
       THICK   0.82E-3
    SET   393:432
    TYPE  MEM3
       THICK   0.91E-3
    SET   433:456
    TYPE  MEM3
       THICK   1.00E-3
    SET   457:464    ! posterior pole
! lens  ****************
    TYPE  MEM3
       THICK   0.2E-3
    SET   465:480
! ciliary body  ********
    TYPE  MEM3
       THICK   0.2E-3
    SET   481:504,843:850
 ! six eye muscles  ********
    TYPE  MEM3
       THICK   0.5E-3
    SET   505:842
END GEOMETRIES
INITIAL CONDITIONS
    0  -.006  -0.027  0.048   0.0  0.0  0.0  1  2  14
! moves with dummy head = body 14, system 2
ORIENTATIONS
  0  0  1  1  0.0  2  0.007  3  0.0
END ORIENTATIONS
 SUPPORTS
 ! attaches (fixes) nodes to the dummy head, body 14, system 2
  NUMBER     1
  SYSTEM     2
  BODY      14    ! dummy's head !
  DOF      ALL
! All extraocular muscle "free-ends" are supported by the head
```

```
! 443,444,448,451,452,453,456,457,458 are the nine posterior pole nodes
of sclera
! 469,486,503,520,537,554,571,588,605,622,639,656 are ends of 4
straight eye muscles
! 681,690,699 are end of inferior oblique,
! 700 and 716 are end of superior oblique
!SET    443,444,448,451,452,453,456,457,458,+
 SET     469,486,503,520,537,554,571,588,605,622,639,656,+
         681,690,699,+
         700,716
 END
 RIGID
  BODY
  ELEMENTS   465:480    ! lens, over-rules E defined above under
materials
  END BODY
 END RIGID
! element stress/strain data written to femani file for post processing
! contour plots viewed with altair's hypermesh
FEMANI
  ELEMENT
END FEMANI
END FEM MODEL 2
!*********************************************************************
***************
FEM MODEL 3
   aqueous
   COORDINATES
       ! 123 nodes total
       1  1.100523478E-01  5.377368806E-02  -2.82842712E-03
       … !(ABBREVIATED)
     191  1.078188823E-01  5.202480438E-02  -1.74889877E-03
END COORDINATES
ELEMENTS
   ! 72 elements total
       1  SOLID1         1         2         5         4        10
11        14        13
       … !(ABBREVIATED)
       72  SOLID1       176         5         2       132       191
6         3       147
END ELEMENTS
MATERIALS
  TYPE          ISOLIN
! approx as "soft" tissue (buttocks )= 47kPa (Todd & Thacker, 1994)
      E        0.037E6  ! MPa
      NU          0.49  ! nearly incompressible
      DENSITY      999  ! density of water, kg/m^3
      SET         1:72
END MATERIALS
 INITIAL CONDITIONS
    0  -.006  -0.027  0.048   0.0  0.0  0.0  1  2  14
 ORIENTATIONS
  0  0  1  1  0.0  2  0.007  3  0.0
 END ORIENTATIONS
END FEM MODEL 3
!*********************************************************************
*************
```

```
FEM MODEL 4
vitreous
COORDINATES
! 125 nodes total
1     8.73370006E-02    5.094526094E-02  0.000000000E+00
… !(ABBREVIATED)
221   8.98510261E-02    4.877973112E-02   -4.993902740E-03
END COORDINATES
ELEMENTS
! 80 elements total
1  SOLID1         1         2         7         6        16        17
22        21
… !(ABBREVIATED)
80  SOLID1       209        76        79       212       218        85
88       221
END ELEMENTS
MATERIALS
  TYPE          ISOLIN
! approx as "soft" tissue (buttocks)=47kPa (Todd & Thacker, 1994)
      E        0.042E6  ! Young's Modulus, MPa
      NU          0.49  ! nearly incompressible
      DENSITY      999  ! density of water, kg/m^3
      SET         1:80
END MATERIALS
 INITIAL CONDITIONS
    0  -.006  -0.027  0.048   0.0  0.0  0.0  1  2  14
 ORIENTATIONS
   0  0  1  1  0.0  2  0.007  3  0.0
 END ORIENTATIONS
END FEM MODEL 4
!*********************************************************************
**********
FEM MODEL 5
fatty
COORDINATES
    ! 294 nodes total
    ! anterior half of fat, more detail around eye
   1  8.935740174E-02  5.324670018E-02  -8.65999423E-03
   … !(ABBREVIATED)
  371 5.972806577E-02  5.821350989E-02  -6.33493698E-03
END COORDINATES
ELEMENTS
  ! 160 elements total
    ! anterior elements
     1  SOLID1         1         2         5         4        16
17        20        19
    … !(ABBREVIATED)
    160    SOLID1     340     341   346   345   365   366   371   370
END ELEMENTS
  MATERIALS
   TYPE          ISOLIN
! approx as "soft" tissue (buttocks) = 47 kPa (Todd & Thacker, 1994)
      E         0.047E6  ! Young's Modulus, MPa
      NU           0.49  ! nearly incompressible
      DENSITY       999  ! density of water = 999 kg/m^3
      SET         1:160  ! all fatty tissue elements
  END MATERIALS
```

```
 INITIAL CONDITIONS
 ! positioned same as the orbit, not eye components
    0  -.0055  -0.0267  0.0481   0.0  0.0  0.0  1  2  14
 ORIENTATIONS
   0  0  1  1  0.0  2  0.008  3  -0.002
 END ORIENTATIONS
    SUPPORTS
    NUMBER     1
    SYSTEM     2
    BODY      14    ! dummy's head !
    DOF      ALL
    ! outer nodes of five sides - posterior half of fatty tissue
    SET  297:301,322:326,347:351,+
         317:321,342:346,367:371,+
         356,361,366,331,336,341,306,311,316,+
         302,307,312,327,332,337,352,357,362,+
         353:355,358:360,363:365,+
    ! outer nodes of four sides - anterior half of fatty tissue
       140:142,136:138,132:134,190,195,200,189,194,199,+
       144:146,86:88,81:83,76:78,+
       197,198,249:251,245:247,192,193,187,188,+
       79,84,89,80,85,90,253:255
    END
END FEM MODEL 5
!  ********************************************************************
!SIMPLE CONSTRAINT EQUATIONS
! forces posterior pole of sclera to move with adjacent nodes of fat
! CONSTRAINT
!   MODEL     4                       ! posterior pole nodes
!   NODES     443,444,448,451,452,453,456,457,458
!   MODEL     7
!   NODES    37,40,52,22,34           ! nodes of fatty tissue
!   DOF        D1
! END CONSTRAINT
!END SIMPLE CONSTRAINT EQUATIONS
!           ************************************************************
! FE 1 = airbag                                  FS 1 = headform
! FE 2 = cornea, sclera, lens, 6 eye muscles...    FS 2 = goggles
! FE 3 = aqueous humor                         FS 3 = orbit
! FE 4 = vitreous                        FS 4 = helmet
! FE 5 = fatty tissue surrounding eye
CONTACT INTERACTIONS
!*1  airbag-goggles
  ELEMENTSET    esbag
   MODEL            1
   ELEMENTS    1:1024  ! front surface only, patches 1-3
  END
  VERTEXSET    vsgogl
   SYSTEM           2
   SURFACE          2
   VERTICES       ALL
  END
!*2  airbag-headform
  VERTEXSET    vshead
   SYSTEM           2
   SURFACE          1
   VERTICES       ALL
```

```
  END VERTEXSET
!*3a  goggle-cornea
  FACETSET    fsgogl
   SYSTEM          2
   SURFACE         2
   FACETS       1:16   ! end caps only
  END
  NODESET      nscorn
   MODEL            2
   NODES
1:7,10:13,17,20,21,22,25,26,28:37,40:42,46,49,52,53,57,60,+

62,64,65,67,70,71,72,76,79:81,84,85,87,88,91,92,94:97,100:103,+

105,106,109:112,116,119,120,121,124,125,127,128,133,134,137:140,+

145:148,151,152,157:160,164,167:169,172,173,175,176,181,182,+

185:188,193:196,199,200,205:208,212,215:217,220,221,223,224,+
               229,230,233:236,241:244,247,248,253:256
  END
!*3b  fsgogl-vshead
!*4a  aqueous-anterior chamber
   ELEMENTSET    esant
    MODEL           2
    ELEMENTS   1:104,465:480,481:504,843:850  ! cornea,lens,ciliary
body !
   END
   NODESET        nsaq
    MODEL           3
    NODES         ALL
   END
!*4b  aqueous-anterior chamber
   ELEMENTSET     esaq
    MODEL           3
    ELEMENTS      ALL
   END
   NODESET       nsant
    MODEL           2
    NODES         ALL
   END
!*5  posterior chamber - vitreous gel
   ELEMENTSET   espost
    MODEL           2
    ELEMENTS   105:464,465:480,481:504,843:850  ! sclera,lens,ciliary
body !
   END
   NODESET       nsvit
    MODEL           4
    NODES         ALL
   END
!*6  sclera-fatty tissue
   ELEMENTSET  esfat
    MODEL         5
    ELEMENTS    ALL
   END
   NODESET   nsclera
```

```
    MODEL          2
    ! posterior half of globe
    NODES
207,208,212,215:217,220,221,223,224,229,230,233:236,241:244,+

247,248,253:256,260,263:265,268,269,271,272,277,278,281:284,+

289:292,295,296,301,302,305,306,309:311,316:318,323,324,326,+

331,332,336:338,343:346,351:356,360,363:365,368,369,371,372,+

377,378,381:384,389:392,395,396,401:404,408,411:413,416,417,+
             419,424,427,428,433,434,437,442:444,448,451:453,456:458
   END
!*7  superior oblique muscle to trochlea (orbital pulley)
   ELEMENTSET    suproblq
    MODEL               2
    ELEMENTS      809:838
   END
   VERTEXSET  trochlea
    SYSTEM           2
    SURFACE          3
    VERTICES       ALL
   END
!*8  six muscles to four orbital walls
  FACETSET   fsorbit
   SYSTEM          2
   SURFACE         3
   FACETS        1:4   ! four outer walls
  END
  NODESET      nsmusc
   MODEL            2
   NODES      469:484,486:501,503:518,520:535,537:552,554:569,571:586,
+
              588:603,605:620,622:637,639:654,656:671,673:731
  END
!*9a  sclera - six muscles
   ELEMENTSET     elmusc
    MODEL              2
    ELEMENTS     505:760,777:838
   END
   NODESET   nsclera
    MODEL          2
    ! posterior half of globe
    NODES
207,208,212,215:217,220,221,223,224,229,230,233:236,241:244,+

247,248,253:256,260,263:265,268,269,271,272,277,278,281:284,+

289:292,295,296,301,302,305,306,309:311,316:318,323,324,326,+

331,332,336:338,343:346,351:356,360,363:365,368,369,371,372,+

377,378,381:384,389:392,395,396,401:404,408,411:413,416,417,+
             419,424,427,428,433,434,437,442:444,448,451:453,456:458
   END
!*9b  sclera - six muscles
```

```
   ELEMENTSET   elsclera
    MODEL              2
    ELEMENTS      65:464
   END
!             ************************************************************
!*1          ************************************************************
  ELEMENT-VERTEX
    ELEMENTSET             esbag
    VERTEXSET              vsgogl
    FRICTION               4
    CONTACT MODEL          STRESS
    LOADING FUNCTION       1
    UNLOADING FUNCTION     2
    HYSTERESIS MODEL       1
    HYSTERESIS SLOPE       250E6
    DAMPING COEFF          1.0E+05
    DAMP STRESS FUNC       3
    FUNCTIONS
!
! These contact functions belong to the headform skin and are suitable
! for contact with FE and a rigid facet surface.
!
! 1: loading
                  9
              0         0
              0.1       1.13945E+006
              0.2       3.52265E+006
              0.3       8.71314E+006
              0.35      1.21207E+007
              0.4       1.66505E+007
              0.45      2.22784E+007
              0.5       2.89159E+007
              0.55      3.63497E+007
! 2: unloading curve
             9
              0          0
              0.1        2.7871e+05
              0.2        7.3548e+05
              0.3        1.5019e+06
              0.35       2.0129e+06
              0.4        2.7484e+06
              0.45       3.6774e+06
              0.5        4.7729e+06
              0.55       6.0000e+06
! 3: damping-stress function.
            3
             0.0         0.0
             7.0E+06     3.14779E-001
             3.0E+07     1.02
! 4: friction coefficient as a function of relative velocity.
            3
              0.0        0.0
              0.05       0.3
              1.0        0.3
    END FUNCTIONS
  END ELEMENT-VERTEX
!*2           ************************************************
```

```
  ELEMENT-VERTEX
    ELEMENTSET            esbag
    VERTEXSET             vshead
    FRICTION              4
    CONTACT MODEL         STRESS
    LOADING FUNCTION      1
    UNLOADING FUNCTION    2
    HYSTERESIS MODEL      1
    HYSTERESIS SLOPE      250E6
    DAMPING COEFF         1.0E+05
    DAMP STRESS FUNC      3
    FUNCTIONS
!
! These contact functions belong to the headform skin and are suitable
! for contact with FE and a rigid facet surface.
!
! 1: loading
             9
          ! 100 times as stiff
            0        0
            0.1      113945000
            0.2      352265000
            0.3      871314000
            0.35     1212070000
            0.4      1665050000
            0.45     2227840000
            0.5      2891590000
            0.55     3634970000
           !   0          0
           !   0.1        1.13945E+006
           !   0.2        3.52265E+006
           !   0.3        8.71314E+006
           !   0.35       1.21207E+007
           !   0.4        1.66505E+007
           !   0.45       2.22784E+007
           !   0.5        2.89159E+007
           !   0.55       3.63497E+007
! 2: unloading curve
             9
              0          0
              0.1        2.7871e+05
              0.2        7.3548e+05
              0.3        1.5019e+06
              0.35       2.0129e+06
              0.4        2.7484e+06
              0.45       3.6774e+06
              0.5        4.7729e+06
              0.55       6.0000e+06
! 3: damping-stress function.
            3
             0.0         0.0
             7.0E+06     3.14779E-001
             3.0E+07     1.02
! 4: friction coefficient as a function of relative velocity.
            3
              0.0        0.0
              0.05       0.3
```

```
            1.0        0.3
    END FUNCTIONS
  END ELEMENT-VERTEX
!*3a              ****************************************************
  FACET-NODE
    FACETSET               fsgogl
    NODESET                nscorn
    FRICTION               3
    CONTACT MODEL          STRESS
    LOADING FUNCTION       1
    DAMPING COEFF          1.0E+05
    DAMP STRESS FUNC       2
    FUNCTIONS
!
! These contact functions belong to the headform skin and are suitable
! for contact with FE and a rigid facet surface.
!
! 1: loading
           9
           0          0
           0.1        1.13945E+006
           0.2        3.52265E+006
           0.3        8.71314E+006
           0.35       1.21207E+007
           0.4        1.66505E+007
           0.45       2.22784E+007
           0.5        2.89159E+007
           0.55       3.63497E+007
!  2: damping-stress function.
           3
            0.0         0.0
            7.0E+06     3.14779E-001
            3.0E+07     1.02
! 3: friction coefficient as a function of relative velocity.
           3
             0.0        0.0
             0.05       0.3
             1.0        0.3
    END FUNCTIONS
  END FACET-NODE
!*3b              ****************************************************
  FACET-VERTEX
    FACETSET               fsgogl
    VERTEXSET              vshead
    FRICTION               3
    CONTACT MODEL          STRESS
    LOADING FUNCTION       1
    DAMPING COEFF          1.0E+05
    DAMP STRESS FUNC       2
    FUNCTIONS
!
! These contact functions belong to the headform skin and are suitable
! for contact with FE and a rigid facet surface.
!
! 1: loading
          ! 100 times as stiff
           9
```

```
           0        0
           0.1      113945000
           0.2      352265000
           0.3      871314000
           0.35     1212070000
           0.4      1665050000
           0.45     2227840000
           0.5      2891590000
           0.55     3634970000
          !9
          !0          0
          !0.1        1.13945E+006
          !0.2        3.52265E+006
          !0.3        8.71314E+006
          !0.35       1.21207E+007
          !0.4        1.66505E+007
          !0.45       2.22784E+007
          !0.5        2.89159E+007
          !0.55       3.63497E+007
!  2: damping-stress function.
            3
            0.0         0.0
            7.0E+06     3.14779E-001
            3.0E+07     1.02
! 3: friction coefficient as a function of relative velocity.
           3
             0.0        0.0
             0.05       0.3
             1.0        0.3
    END FUNCTIONS
  END FACET-VERTEX
!*4a         ****************************************************
  ELEMENT-NODE
   ELEMENTSET   esant
   NODESET      nsaq
   PENALTY  0.1  ! 0.1 recommended
   MAXFRC   0.35  ! 1.0 recommended; decrease to make stable though
  END ELEMENT-NODE
!*4b        ****************************************************
  ELEMENT-NODE
   ELEMENTSET   esaq
   NODESET      nsant
   PENALTY  0.1     ! 0.1 recommended
   MAXFRC   0.35   ! 1.0 recommended; decrease to make stable though
  END ELEMENT-NODE
!*5          ****************************************************
 ELEMENT-NODE
   ELEMENTSET    espost
   NODESET        nsvit
   PENALTY  0.1
   MAXFRC   0.5
  END ELEMENT-NODE
!*6          ****************************************************
   ELEMENT-NODE
    ELEMENTSET    esfat
    NODESET     nsclera
    PENALTY  0.1
```

```
    MAXFRC   0.35
   END ELEMENT-NODE
!*7              ************************************************
  ELEMENT-VERTEX
    ELEMENTSET             suproblq
    VERTEXSET              trochlea
    FRICTION               4
    CONTACT MODEL          STRESS
    LOADING FUNCTION       1
    UNLOADING FUNCTION     2
    HYSTERESIS MODEL       1
    HYSTERESIS SLOPE       250E6
    DAMPING COEFF          1.0E+05
    DAMP STRESS FUNC       3
    FUNCTIONS
!
! These contact functions belong to the headform skin and are suitable
! for contact with FE and a rigid facet surface.
!
! 1: loading
            9
             0          0
             0.1        1.13945E+006
             0.2        3.52265E+006
             0.3        8.71314E+006
             0.35       1.21207E+007
             0.4        1.66505E+007
             0.45       2.22784E+007
             0.5        2.89159E+007
             0.55       3.63497E+007
! 2: unloading curve
            9
             0          0
             0.1        2.7871e+05
             0.2        7.3548e+05
             0.3        1.5019e+06
             0.35       2.0129e+06
             0.4        2.7484e+06
             0.45       3.6774e+06
             0.5        4.7729e+06
             0.55       6.0000e+06
! 3: damping-stress function.
           3
            0.0         0.0
            7.0E+06     3.14779E-001
            3.0E+07     1.02
! 4: friction coefficient as a function of relative velocity.
           3
             0.0        0.0
             0.05       0.3
             1.0        0.3
    END FUNCTIONS
  END ELEMENT-VERTEX
!*8            ***************************************************
  FACET-NODE
    FACETSET               fsorbit
    NODESET                nsmusc
```

```
    FRICTION              3
    CONTACT MODEL         STRESS
    LOADING FUNCTION      1
    DAMPING COEFF         1.0E+05
    DAMP STRESS FUNC      2
    FUNCTIONS
!
! These contact functions belong to the headform skin and are suitable
! for contact with FE and a rigid facet surface.
!
! 1: loading
            9
             0          0
             0.1        1.13945E+006
             0.2        3.52265E+006
             0.3        8.71314E+006
             0.35       1.21207E+007
             0.4        1.66505E+007
             0.45       2.22784E+007
             0.5        2.89159E+007
             0.55       3.63497E+007
!  2: damping-stress function.
           3
            0.0         0.0
            7.0E+06     3.14779E-001
            3.0E+07     1.02
! 3: friction coefficient as a function of relative velocity.
           3
             0.0        0.0
             0.05       0.3
             1.0        0.3
    END FUNCTIONS
  END FACET-NODE
!*9a
*****************************************************
   ELEMENT-NODE
    ELEMENTSET    elmusc
    NODESET      nsclera
    PENALTY          0.1
    MAXFRC           0.7
   END ELEMENT-NODE
!*9b
*****************************************************
   ELEMENT-NODE
    ELEMENTSET  elsclera
    NODESET       nsmusc
    PENALTY          0.1
    MAXFRC           0.7
   END ELEMENT-NODE
END CONTACT INTERACTIONS
!                   ***********************************************
TRIGGERING CONDITIONS
  NUMBER      1
  SIGNALTYPE  TIME
  LEVEL       0.001
  NUMBER      2
  SIGNALTYPE  TIME
```

```
  LEVEL       0.015
  NUMBER      3
  SIGNALTYPE  JOINT SENSOR
  SEQNUM      1
  LEVEL       0.001
  DELAY       0.001
  LEX         GE
  NUMBER      4
  SIGNALTYPE  TIME
  LEVEL       0.001
END TRIGGERING CONDITIONS
!
CONTROL MODULE
JOINT SENSOR
  1  JNTVEL  1  21  1
END JOINT SENSOR
END CONTROL MODULE
!************************************************************************
*
! CONTACT INTERACTIONS are still in MADYMO 5.2 syntax and can be found
within:
! FORCE MODELS
! FEM MODELS
!************************************************************************
*
OUTPUT CONTROL PARAMETERS
  TSKIN  0.0020
  KIN3   EXTENDED
  TSOUT  0.0001
FILTER PARAMETERS
IGNORE         NO
DEFAULT        CFC1000
PADDING        0.010
MOVECOMMAND    REMOVE
END FILTER PARAMETERS
  FORCES
!  contact force between goggle and eye
    8  3  0  goggle to cornea force
!  contact force between goggle and headform
    8  4  0  goggle to headform force
  END
!************************************************************************
*
! OUTPUT FOR HYBRID III 50th percentile male dummy with 5-joint neck
! NOTE: Replace all strings #1 by the appropriate system number of the
!       dummy in your MADYMO input file!
!************************************************************************
*
! Filtering according to SAE J211/1 March 95
! Coordinate-systems according to standardized dummy coordinate-systems
! for standing and seated postures
!************************************************************************
*
  RELDIS
   2  5   0.1517 0.0000 0.0762  2  35  0.0000 0.0000 0.0000  0  Sternum
  FILTERLIST  CFC600
  END
```

```
  DISVEL
   2  35  0.0000 0.0000 0.0000  2  5   0.1517 0.0000 0.0762  Sternum
  FILTERLIST  CFC600  CFC180
  END
  LINACC
!   acceleration corrected for pulse in x direction
   2  1  -0.0440 0.0000 0.0050  1  0  0  1   Lower Torso
   2  5   0.0155 0.0000 0.0647  1  0  0  1   Upper Torso
   2  14  0.0178 0.0000 0.0343  1  0  0  1   Head
  END
  ORIENTATIONS
!   1: lower torso accelerometer: x front, y right, z down
    1  0   1   1  3.14159
!   2: upper torso accelerometer: x front, y right, z down
    2  0   1   1  3.14159   2  0.1571
!   3: head accelerometer: x front, y right, z down
    3  0   1   1  3.14159
  END
  CONSTRAINT LOADS
!   WARNING: do not change the sequence of CONSTRAINT LOADS,
!   because there is refered to in INJURY PARAMETERS and LOAD CELLS
!   lower lumbar load cell
   2  3
!   upper lumbar load cell
   2  5
!   lower neck force (select CFC1000) and moment (select CFC600)
   2  8
  FILTERLIST  CFC1000  CFC600
!   upper neck force (select CFC1000) and moment (select CFC600)
   2  14
  FILTERLIST CFC1000  CFC600
!   left and right femur load cells
   2  25
  FILTERLIST CFC600
   2  26
  FILTERLIST CFC600
!   left and right upper tibia load cells
   2  29
  FILTERLIST CFC600
   2  30
  FILTERLIST CFC600
!   left and right lower tibia load cells
   2  31
  FILTERLIST CFC600
   2  32
  FILTERLIST CFC600
  END
  JNTPOS
! left and right knee, DOF1=extension, DOF2=knee slider displacement
   2  27
   2  28
  END
END OUTPUT CONTROL PARAMETERS
END INPUT DATA
!*********************************************************************
*
! END FRONTAL IMPACT APPLICATION
```

Vita

Erik D. Power

Erik Power was born in Guam, USA on March 28, 1977. He attended Benson Polytechnic High School in Portland, OR. At Benson, he was given the Portland Interscholastic League Scholar Athlete award in soccer four years in a row. He then attended Virginia Tech on an out of state scholarship, and received a Bachelors of Science degree in mechanical engineering in May of 2000, with *Magna Cum Laude* honors. At Virginia Tech, he was admitted to the five-year B.S./M.S. program and was awarded fellowships from both the department of mechanical engineering and the center for biomedical engineering. Remaining at Virginia Tech for his Masters of Science in mechanical engineering with a biomedical option, he completed his thesis studying ocular injuries from night vision goggles. He has published articles in the engineering and medical journals and conferences. In the summer of 2001, he will enter industry, conducting accident reconstruction and injury biomechanics investigations. He has plans to pursue a Ph.D. and Professional Engineering License shortly thereafter and become an expert witness in these areas. Erik also enjoys snowboarding, playing basketball, lifting weights, camping, hiking, and many other activities. He likes to travel around the world and snowboard in Lake Tahoe and Colorado.

Further information can be obtained by writing to his permanent address:

7033 N.E. Skidmore
Portland, OR 97218

_____

Erik D. Power